

Medical University of South Carolina

MEDICA

MUSC Theses and Dissertations

2015

The Pathogenesis of Noise-Induced Hearing Loss is Mediated by the Activation of AMPK via LKB1 and CaMKK β

Kayla Renee Hill

Medical University of South Carolina

Follow this and additional works at: <https://medica-musc.researchcommons.org/theses>

Recommended Citation

Hill, Kayla Renee, "The Pathogenesis of Noise-Induced Hearing Loss is Mediated by the Activation of AMPK via LKB1 and CaMKK β " (2015). *MUSC Theses and Dissertations*. 457.

<https://medica-musc.researchcommons.org/theses/457>

This Dissertation is brought to you for free and open access by MEDICA. It has been accepted for inclusion in MUSC Theses and Dissertations by an authorized administrator of MEDICA. For more information, please contact medica@musc.edu.

**The pathogenesis of noise-induced hearing loss is mediated by the activation of
AMPK via LKB1 and CaMKK β**

by

Kayla Renee Hill

A dissertation submitted to the faculty of the Medical University of South Carolina in
partial fulfillment of the requirements for the degree of Doctor of Philosophy in the
College of Graduate Studies

Department of Pathology and Laboratory Medicine

2015

Approved by:

Chairman, Advisory Committee:



Su-Hua Sha

Advisory Committee:



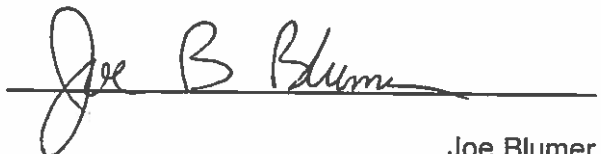
Bradley Schulte



Hainan Lang



John Lemasters



Joe Blumer



Jochen Schacht

TABLE OF CONTENTS

ABSTRACT	IV
LIST OF TABLES AND FIGURES	V
LIST OF ABBREVIATIONS	VIII
ACKNOWLEDGEMENTS	IX
CHAPTER ONE: INTRODUCTION	1
1. THE STRUCTURE AND FUNCTION OF THE EAR	2
1.1 <i>The outer and middle ear</i>	3
1.2 <i>The inner ear</i>	4
2. SENSORINEURAL HEARING LOSS	10
2.1 <i>Noise-induced hearing loss</i>	11
2.2 <i>Noise exposure</i>	11
2.3 <i>Noise-induced cochlear pathology</i>	12
2.4 <i>Noise-induced apoptosis and necrosis of hair cells</i>	15
3. MECHANISMS OF NOISE-INDUCED HEARING LOSS	17
3.1 <i>Evidence for noise-induced ATP reduction</i>	17
3.2 <i>Evidence for noise-induced ROS production</i>	18
3.3 <i>Evidence for noise-induced calcium influx</i>	20
3.4 <i>Interplay of calcium, ATP and ROS</i>	22
4. SIGNIFICANCE	25
CHAPTER TWO: MATERIALS AND METHODS	26
CHAPTER THREE: AMPK ACTIVATION IN NOISE-INDUCED HEARING LOSS	40
INTRODUCTION	41
RESULTS.....	43
DISCUSSION.....	64

CHAPTER FOUR: AMPK ACTIVATION BY LKB1 VIA CELLULAR ATP REDUCTION	71
INTRODUCTION	72
RESULTS.....	74
DISCUSSION.....	82
CHAPTER FIVE: AMPK ACTIVATION BY CAMKKB VIA INTRACELLULAR CALCIUM INFLUX.....	84
INTRODUCTION	85
RESULTS.....	88
DISCUSSION.....	102
CHAPTER SIX: SUMMARY AND FUTURE DIRECTIONS	106
SUMMARY AND FUTURE DIRECTIONS	107
REFERENCES.....	114

ABSTRACT

KAYLA RENEE HILL. The pathogenesis of noise-induced hearing loss is mediated by the activation of AMPK via LKB1 and CaMKK β . (Under the direction of SU-HUA SHA)

Noise-induced hearing loss (NIHL) is a major public health issue and an unresolved clinical problem. Here we investigate pathomechanisms of auditory sensory cell death and suggest a novel target pathway for intervention. Cellular survival from stress depends upon maintenance of energy homeostasis, largely by the adenosine monophosphate-activated protein kinase (AMPK) which coordinates metabolic pathways with the energy demands of the cell. In response to traumatic noise exposure which resulted in hair cell death, levels of p-AMPK α increased in hair cells in a noise intensity-dependent manner. Inhibition of AMPK via administration of siRNA or a pharmacological inhibitor attenuated noise-induced losses of hair cells and synaptic ribbons, and preserved auditory sensitivity. The phosphorylation of liver kinase B1 (p-LKB1), an AMPK kinase, was increased by noise exposure in cochlear tissues. Additionally, the phosphorylation of calcium-calmodulin kinases I and IV (p-CaMKI/IV), the targets of calcium-calmodulin kinase kinase beta (CaMKK β), an alternative AMPK kinase that is mediated by calcium, was increased in outer hair cells (OHCs) after the exposure. Inhibition of LKB1 or CaMKK β by siRNA or knockout mice reduced OHC loss and NIHL. Finally, the increased p-AMPK α in OHCs after noise exposure was attenuated by silencing LKB1 or using CaMKK β knockout mice. These results indicate that noise exposure leads to hair cell death by activating AMPK via LKB1- and CaMKK β -mediated pathways, facilitating the pathogenesis of NIHL.

LIST OF TABLES AND FIGURES

Chapter 1

Figure 1: The anatomical partitions of the ear.

Figure 2: Cross-section of the cochlea.

Figure 3: The organ of Corti.

Figure 4: Deflection of stereocilia in mechanotransduction.

Table 1: Characteristics of cell death pathways.

Chapter 2

Figure 5: Drug administration via intraperitoneal injection.

Figure 6: 3D reconstruction of CtBP2-immunolabeled synaptic ribbons.

Chapter 3

Figure 7: Noise exposure caused a base-to-apex gradient of outer hair cell loss.

Figure 8: Noise exposure induced permanent hearing loss and hair cell loss in adult CBA/J mice.

Figure 9: Noise exposure reduced the summed activity of auditory nerve fibers.

Figure 10: Noise exposure caused swelling of spiral ganglion neurons.

Figure 11: Noise exposure increased p-AMPK α in basal outer and inner hair cells in a noise intensity-dependent manner.

Figure 12: Noise exposure increased total AMPK α 1 and 2 in the organ of Corti.

Figure 13: Inhibition of AMPK α 1 via siRNA and Compound C protected against noise-induced hearing loss and outer hair cell loss.

Figure 14: Inhibition of AMPK attenuated noise-induced inner hair cell synaptic ribbon loss at 22 kHz one hour after 106-dB noise exposure.

Figure 15: Inhibition of AMPK protected noise-induced synaptopathy and noise-declined auditory nerve activity 14 days after 106-dB exposure.

Figure 16: AMPK α 1-knockout mice exacerbated noise induced hearing loss.

Figure 17: Noise-induced inner hair cell synaptic ribbon loss was not altered by AMPK α 1-knockout.

Chapter 4

Figure 18: LKB1 activates AMPK.

Figure 19: Noise exposure induced p-LKB1 in the organ of Corti, spiral ganglion neurons and spiral ligament.

Figure 20: Noise exposure increased the colocalization of LKB1-STRAD α in basal outer hair cells.

Figure 21: Inhibition of LKB1 reduced noise-induced p-LKB1, auditory sensitivity and outer hair cell loss.

Figure 22: Inhibition of LKB1 partially reduced noise-induced inner hair cell synaptic ribbon loss at 22 kHz and decline of ABR wave I amplitude.

Figure 23: Noise-induced phosphorylation of AMPK α is reduced in outer hair cells of siLKB1-pretreated mice.

Chapter 5

Figure 24: CaMKK signaling.

Figure 25: Verapamil treatment reduced noise-induced hearing loss and outer hair cell loss.

Figure 26: Verapamil treatment did not alter noise-induced inner hair cell synaptic ribbon loss.

Figure 27: Noise exposure increased CaMKK β in the organ of Corti, spiral ganglion neurons and spiral ligament.

Figure 28: Noise exposure induced p-CaMKI and p-CaMKIV in basal outer hair cells.

Figure 29: Inhibition of CaMKK β via siRNA reduced CaMKK β activity, noise-induced hearing loss and outer hair cell loss.

Figure 30: Noise-induced hearing loss and outer hair cell loss is reduced by CaMKK β -knockout.

Figure 31: Noise-attenuated inner hair cell synaptic ribbons were not altered by CaMKK β -knockout.

Figure 32: Noise-induced phosphorylation of AMPK α is reduced in outer hair cells of CaMKK β -knockout mice.

Chapter 6

Figure 33: Summary

List of Abbreviations

AMP	Adenosine Monophosphate
ATP	Adenosine Triphosphate
CaM	Calmodulin
CaMKI/IV	Calcium Calmodulin Kinase I and IV
CaMKK β	Calcium Calmodulin Kinase Kinase Beta
dB	decibels
IHC	Inner Hair Cell
LKB1	Liver Kinase B1
MO25	Mouse Protein 25
NIHL	Noise-Induced Hearing Loss
OHC	Outer Hair Cell
PTS	Permanent Threshold Shift
SGN	Spiral Ganglion Neuron
STRAD	Ste20 Related Adaptor Protein
TTS	Temporary Threshold Shift
VGCC	Voltage Gated Calcium Channel

ACKNOWLEDGEMENTS

First and foremost, I would like to thank my mentor, Su-Hua Sha (Shasha), for her unwavering dedication and support over the last 5 years. Shasha is an extraordinary mentor, who is always eager to stop whatever she is doing to assist in whatever I may need. The enormous amount of support I receive is unprecedented among the mentors of my fellow peers. Her influence has made a significant impact on my growth both personally and professionally and I owe a lot of my success to the skills and knowledge that I have learned from her. I am extremely grateful for her constant guidance in all of my endeavors.

I would also like to thank my committee members, Drs. Bradley Schulte, John Lemasters, Hainan Lang, Joe Blumer and Jochen Schacht. Each member was invaluable to the progression of this work. I am very grateful for their time and efforts on improving my dissertation research and providing critical and insightful comments on this project. I would like to especially thank Dr. John Lemasters for serving as a co-mentor for my F31 fellowship. I am certain that his expertise and track record made an impact in providing me with this opportunity to further my potential. Additionally, I would like to thank Dr. Joe Blumer for his constant support through his words of encouraging advice and for his endorsement of my fellowship and postdoctoral applications. I would also like to give special thanks to my “grand-mentor”, Jochen Schacht for his guidance throughout my research. I am thankful for the extra time and effort involved in traveling long distance to attend my committee meetings and for the insightful and encouraging discussions, both personal and professional, that we have shared.

Finally, I would like to thank my mother Yumiko Hill, my father Lester Hill, my sisters Kelly, Kathy and Diane Hill and my fiancé, Philip Sobolesky for their constant

encouragement, love and support. Thank you for always reminding me to focus on the important things in life.

CHAPTER ONE: INTRODUCTION

1. The structure and function of the ear

Hearing is our most sensitive organ and covers a great dynamic range. We are able to hear a small sound from a pin dropping onto the floor to the piercing sound of a gunshot. Hearing is also discriminative; we can distinguish the fine nuances during a concert. Hearing is a complex process that involves the collection of sound wave vibrational energy by the ear and the processing of these signals for interpretation by our brain. In order to understand the changes of the mammalian auditory organ after exposure to sound stimuli, I will take you on the journey through the three anatomical regions of the ear: the outer ear, middle ear, and inner ear (Fig. 1).

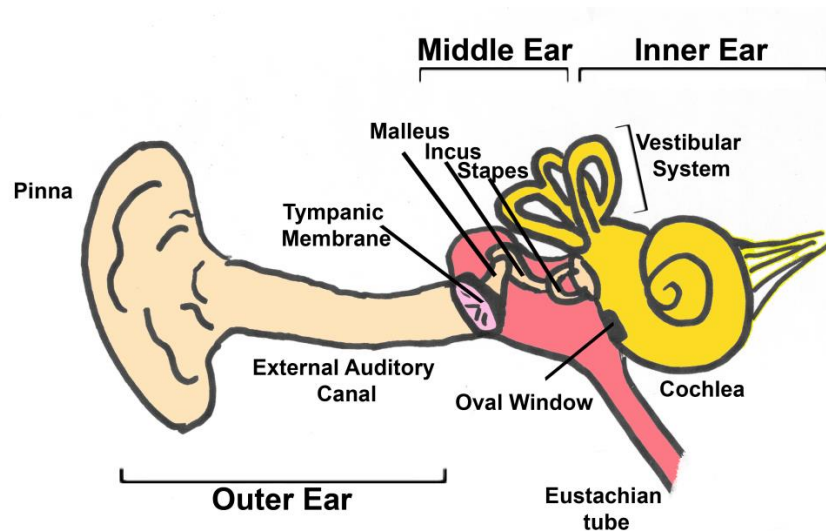


Figure 1. The anatomical partitions of the ear. The ear consists of 3 main regions: the outer, middle and inner ear. The outer ear consists of the pinna and external auditory canal, which function to collect sound vibrations, which are then transferred to the middle and inner ear. The middle ear begins at the tympanic membrane and consists of the 3 middle ear ossicles: the malleus, incus and stapes. The inner ear holds the cochlea and the vestibular system, which are responsible for hearing function and balance, respectively.

1.1 The outer and middle ear

The outer ear consists of two parts. The pinna, the only portion of the ear that is externally visible, is primarily made of cartilage and skin and serves as a complicated funnel to collect and enhance acoustic stimuli. Air-propagated sound waves are directed into the external auditory canal, which conducts sound waves along its length to the innermost limit of the canal, the tympanic membrane. The tympanic membrane, more commonly known as the ear drum, is the boundary between the outer and middle ear. It is a thin, cone-shaped membrane composed of radial fibers that have elastic properties, which allow the structure to vibrate in response to acoustic waves. This transfers the sound wave energy into vibrational energy, which is transferred to the middle ear via the middle ear ossicles. The malleus, the first of the three ossicles, is attached to the medial surface of the tympanic membrane and transfers acoustic vibrations to the incus, which, in turn, connects to the stapes, forming a chain of ossicles for vibrational energy to pass through towards the inner ear. The stapes sits on the oval window, an opening in the bony wall of the cochlea that separates the middle ear from the inner ear. The fluid-filled labyrinth of the cochlea is located on the medial side of the oval window. The impedance mismatch between the air-filled middle ear and fluid-filled inner ear necessitates the amplification of sound vibrations to effectively transfer the stimuli between the two media. This amplification is achieved by concentrating vibrational energy from the surface area of the tympanic membrane to the oval window, which is only $1/20^{\text{th}}$ of its size, thus increasing the energy per area by 22 times.

1.2 The inner ear

The inner ear is composed of 2 functionally distinct organs: the vestibular system and the cochlea. The vestibular system is responsible for balance and orientation in three-dimensional space. The cochlea is dedicated to the detection of sound and will be the focus of this dissertation. The cochlea is a bony, spiral shaped structure (Fig. 2). At its core is the spongy bone of the modiolus from which the bony osseous spiral lamina winds like a screw for 2.5 turns in humans. The cochlea is separated into three fluid-filled cavities by the Reissner's and basilar membrane: the scala vestibuli, scala media, and scala tympani. The scala vestibuli and scala tympani make up the upper and lower labyrinths and are filled with perilymph fluid which is composed of sodium (~145 mM), chloride (~120 mM), bicarbonate (~20 mM), potassium (~5 mM) and calcium (~1 mM) ions, comparable to cerebrospinal fluid.

The scala media, also known as the cochlear duct, is located in the middle of these two canals. It is enclosed superiorly by the Reissner's membrane, which forms a barrier from the scala vestibule. Inferiorly, the scala media is enclosed by the basilar membrane, which borders the scala tympani. The stria vascularis, the specialized capillary-rich tissue which adheres to the spiral ligament, adjacent to the outer wall of the bony cochlea and forms a lateral barrier. It is the specialized cells of stria vascularis that are responsible for the potassium-rich characteristics of the endolymph fluid within the scala media (1). The endolymph contrasts with perilymph composition primarily due to its low sodium (~1 mM) and calcium (~0.02 mM), and high potassium (~160 mM) concentrations. This specialized fluid maintains a high resting endocochlear potential (EP) of 70-100 mV in comparison with the low 0-5 mV potential of the perilymph and the -70 mV potential of hair cells. This potential difference between the endolymph and the

hair cell is the largest electrical potential difference in the body and is essential to the formation of an electrochemical gradient for the transduction current.

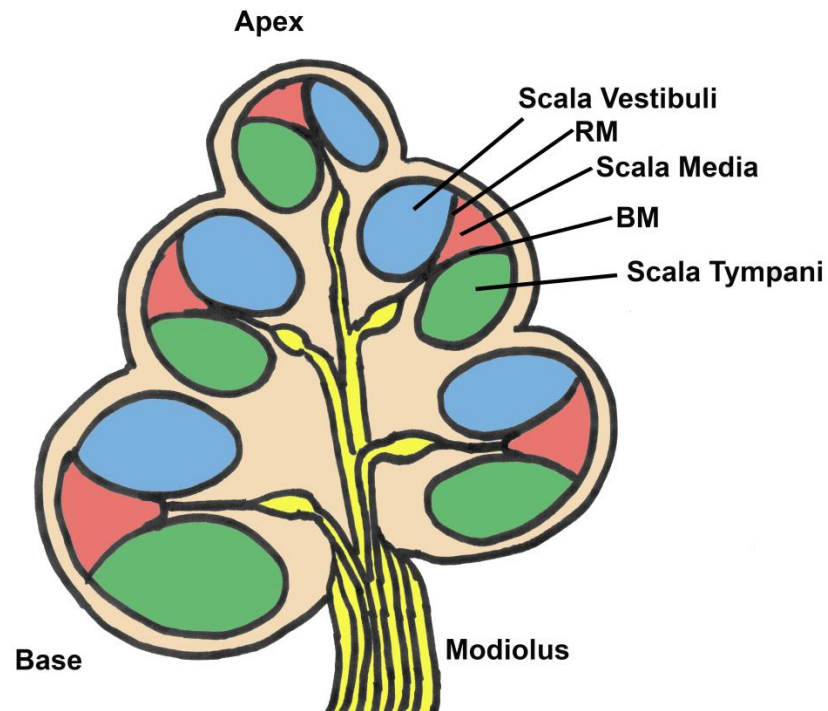


Figure 2. Cross-section of the cochlea. A cross section through the bony cochlea reveals 3 fluid filled cavities: scala vestibuli (blue), scala media (red) and scala tympani (green). The scala media is filled with endolymph and contains the organ of Corti, the sensory organ of the inner ear. The scala tympani and scala vestibuli are filled with perilymph. The Reissner's membrane (RM) separates the scala media from the scala vestibuli, while the basilar membrane (BM) provides a barrier for the scala tympani. The spiral ganglion neurons of the cochlear nerve (yellow) are situated within the modiolus, the central axis of the cochlea.

The stapes sends vibrations through the oval window to the perilymph of the scala vestibuli. The vibrational energy is transferred through the apical most point of the cochlea where the perilymph of the scala vestibuli meets the scala tympani at the helicotrema. The resulting pressure from the vibrations of the incompressible perilymph fluid is released at the round window, where it pulses within the bony, inflexible structure of the cochlea. The vibration of the fluids causes mechanical movement of the basilar membrane. This vibratory pattern, also known as the traveling wave, depends upon the characteristics of the basilar membrane, such as width and elasticity. As the basilar membrane progresses apically from the base of the cochlea, its thickness increases and alters its mechanical properties such as stiffness. Depending on the frequency of the auditory stimulus, the site of maximal amplitude of the basilar membrane traveling wave varies. Stimulation by high frequencies causes maximal amplitude of the traveling wave toward the stapedial or basal end of the basilar membrane, which presents narrow and stiff features. On the other hand, low-frequency stimuli causes maximal amplitude of the traveling wave near the apical end, where the basilar membrane is more wide and flaccid. These progressive changes create a tonotopic gradient that permits humans to detect sound frequencies that range from 20 Hz – 20 kHz. On the other hand, the range of mouse hearing, the model of focus in this study, extends from 2 – 90 kHz.

The organ of Corti rests on the basilar membrane within the scala media and contains the sensory cells of the cochlea (Fig. 3). It is composed of one row of inner hair cells (IHCs) located medially and three rows of outer hair cells (OHCs) located laterally. In the human, there are 3,500 IHCs and 12,000 OHCs in the cochlea. The mouse sensory epithelium contains 700 IHCs and 2,400 OHCs. The tunnel of Corti is formed by the inner and outer pillar cells that separate the two sensory cell groups. Stereocilia bundles are embedded at the cuticular plate, the uppermost region of hair cells. These

bundles are formed from three rows of stereocilia of graded length that are connected to each other via tip links and lateral links. The stereociliary bundles of IHCs and OHCs differ in their pattern; the former are in a lateral arrangement and the latter forms a “W” pattern. The OHC stereocilia bundles embed themselves firmly into the gelatinous tectorial membrane, while IHC stereocilia are weakly connected.

The stereocilia at the top of the hair cell play a fundamental role in converting the mechanical energy of the basilar membrane into electrical energy of hair cells for conversion to neuronal signals. The key step in this process is the deflection of stereocilia bundles, which causes the opening of mechanotransduction (MET) channels at the tips of the stereocilia of hair cells. The displacement of the basilar membrane forms shearing forces against the stereocilia bundles as they move up and down against the tectorial membrane. The resulting bend of the stereocilia bundles increases the tension of stereocilia tip links, which pulls the MET channels open (Fig. 4). A depolarizing current of potassium and calcium ions from the endolymph (-70 mV) flows through the MET channels and enters the hair cells (+80 mV). This depolarization opens L-type voltage-gated calcium channels (VGCC) in the basolateral region of hair cells that subsequently stimulate the influx of calcium proximal to the synaptic cleft, an active region that contains synaptic ribbons surrounded by glutamate-filled synaptic vesicles. These synaptic ribbons play a key role in the second half of this process by converting the changes in hair cell membrane potential to chemical neuronal signals that are sent to the brain. The secondary influx of calcium promotes the release of glutamate neurotransmitter from synaptic vesicles into the synaptic cleft, which then activates α -amino-3-hydroxy-5-methyl-4-isoxazolepropionic acid receptors (AMPA) in afferent nerve fibers that innervate the hair cells. The resulting action potential is carried by afferent nerve fibers into the central nervous system.

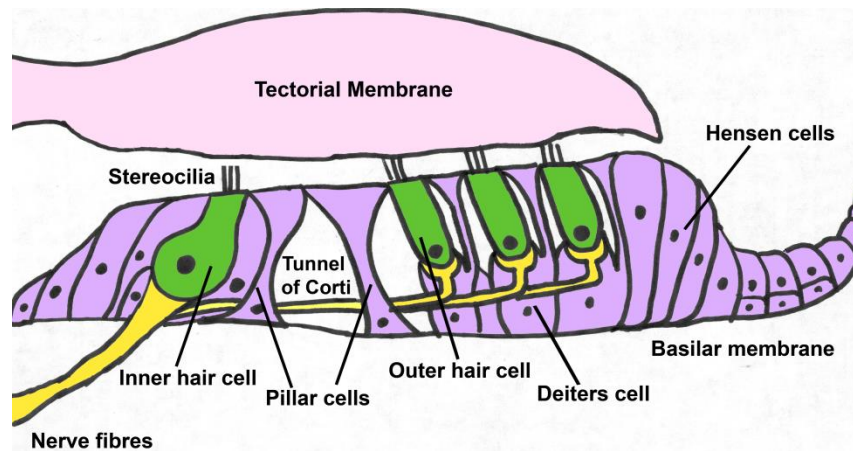


Figure 3. The organ of Corti. The organ of Corti sits above the basilar membrane. The stereocilia of the hair cells extend toward the tectorial membrane (pink). The IHCs (green) form a single row on the modiolar side and are separated from the 3 rows of OHCs (green) by 2 rows of pillar cells (purple) and the tunnel of Corti.

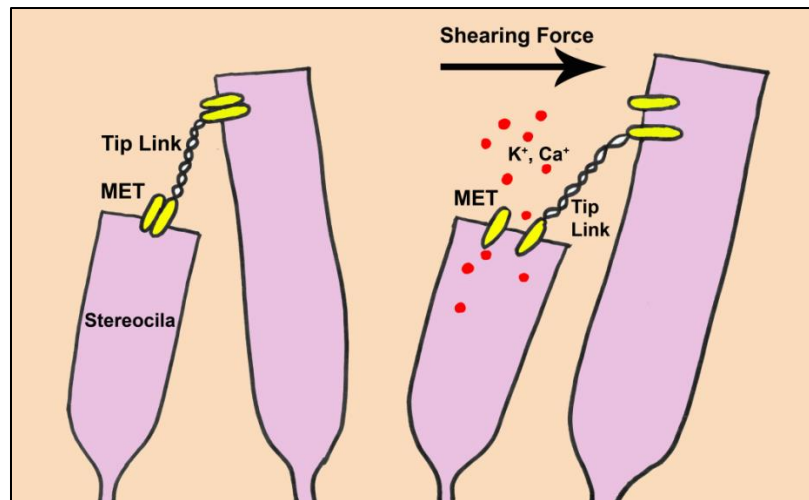


Figure 4. Deflection of stereocilia in mechanotransduction. The shearing force of the tectorial membrane deflects the stereocilia (pink) of hair cells. This increases tension in tip links (helix), which tugs the mechanotransduction (MET) channels (yellow) open to allow potassium and calcium ions (red) to enter.

The displacement of the basilar membrane is further amplified by the electromotility of OHCs, which allows them to change in length when stimulated. These electromotile responses are driven by the voltage-dependent changes in OHCs following the opening of mechanotransduction channels. The depolarization of OHCs changes the conformation of voltage-sensitive prestin, an OHC specific motor protein. Prestin is localized in the lateral plasma membranes of OHCs and alters its shape by binding intracellular chloride. In a non-depolarized state, chloride ions allosterically bind to prestin, resulting in an elongated shape. Upon basilar membrane displacement and subsequent depolarization, chloride ions are dissociated from the prestin binding sites, causing OHC contraction. The shape changes of prestin contracts and elongates the length of OHCs, and serves to augment the amplitude of the traveling wave at a particular frequency, and importantly, increases frequency sensitivity (2). This mechanical feedback characteristic has led to the description of OHCs as the cochlear amplifier to enhance mechanical stimulation of IHCs. Meanwhile, the IHCs are primarily responsible for transducing electrical signals that are sent to the brain.

The contrasting functions of OHC and IHCs explain the variations in hair cell innervation by the two subtypes of spiral ganglion neurons (SGN): Type I and Type II SGNs. Type I SGNs make up the majority (95%) of SGNs. This subset is myelinated and exclusively innervates IHCs. Each IHC is innervated by as many as 20 different afferents from type I SGN which can be divided into three types in the murine model: low threshold-high spontaneous rate (SR), high threshold-low SR, and average threshold-average SR. The low threshold-high SR fibers are the most sensitive to noise exposure and have small synaptic ribbons, but wide post-synaptic densities. The high threshold-low SR fibers have large synaptic ribbons and small post-synaptic densities. In contrast,

OHCs are only innervated by a single auditory afferent from Type II SGNs, each of which innervate multiple OHCs and make up only 5% of auditory afferents.

2. Sensorineural hearing loss

According to the World Health Organization, 360 million people or 5.3% of the world population have a disabling hearing loss and 15% are hearing impaired (3). Hearing loss is divided into two main types: genetic hearing loss and acquired hearing loss. As the name points out, genetic hearing loss is associated with inherited hearing loss. Acquired hearing loss will be the focus of this dissertation. Acquired hearing loss describes the loss of hearing function that develops during an individual's lifetime as one is exposed to various stresses, including viral or bacterial infections, aging, exposure to ototoxic drugs, such as the chemotherapeutic cisplatin and aminoglycoside antibiotics, and exposure to noise insults. The loss of hearing is mostly due to the fact that, unlike non-mammalian vertebrates, mammalian cochlear sensory hair cells lack the ability to regenerate; therefore, the loss or damage of mammalian hair cells in the cochlea is permanent and results in a permanent sensorineural hearing loss.

Additionally, other inner ear disorders may also occur as a result of acquired hearing loss. Tinnitus, commonly known as ringing in the ear, affects nearly 15% of the world population and can severely affect quality of life. Meniere's disease affects roughly 1-2% of the world population and causes spontaneous episodes of vertigo and hearing loss. Among the numerous reasons of acquired hearing loss, noise exposure, the aging process and treatment with ototoxic drugs are the three major causes. For my dissertation, I will focus on the damage elicited on the cochlea by noise exposure.

2.1 Noise-induced hearing loss

Exposure to loud sounds can cause damage to or death of cochlear hair cells, leading to noise-induced hearing loss (NIHL). NIHL is one of the most common causes of acquired hearing deficits and is one of the most frequent work-related disabilities in industrialized countries (4). Worldwide, 250 million people suffer from NIHL (5). According to the National Institute of Occupational Safety and Health (NIOSH), an estimated 30 million workers are exposed to potentially hazardous noise from factories, construction sites, and airports, in the U.S. alone (6). NIHL has become the most predominant disability in war veterans, with an economic impact of \$660 million in compensation payments annually (7-9). Furthermore, exposure to recreational noise, such as listening to loud music on personal listening devices, can also lead to NIHL (10).

2.2 Noise exposure

The magnitude of hearing loss depends upon the characteristics of noise, including the intensity, duration, and temporal characteristics such as continuous noise or impulse noise, a short-duration exposure to an intense sound (11). The greater the intensity (perceived as loudness) of a sound stimulus, the greater the amount of damage can occur to cochlear cells. Sound intensity is measured in decibels (dB), a logarithmic unit of sound pressure level (SPL). Typically, normal moderate human conversation occurs around 60 dB of intensity. Long or repeated exposures to sounds at 85 dB of intensity and above (~300 times the energy level of 60 dB) can result in hearing a loss, thus hearing protection is required by the Occupational Safety and Health Administration (OSHA) for occupational exposures of 85 dB SPL. This intensity levels includes some everyday sounds that many people may not consider harmful. The noises from a lawnmower, for example, can get up to 90 dB of intensity. At 120 dB of intensity and

above instant hearing damage can occur. Noises such as chain saws and other power tools have intensities of 110-120 dB. Around sixty million Americans own firearms, exposing themselves to potentially 140-170 dB of noise without the proper use of ear protectors.

Additionally, hearing loss can be induced with shorter exposure durations. According to the NIOSH, exposure levels should be controlled in order to limit hazardous levels of intensity and duration (12). To calculate the recommended exposure limit (REL), the NIOSH generated a formula to combine the damaging effects of intensity level (L) and duration (T): $T \text{ (min)} = 480/2^{(L-85)/3}$ (12). Using this formula, exposure durations of no more than 8 h, a typical work day, is recommended for noise exposure levels of 85 dB. On the other hand, shorter duration times of 15 minutes are endorsed for exposure intensities of 100 dB.

2.3 Noise-induced cochlear pathology

NIHL can be divided into two subtypes: temporary hearing loss and permanent hearing loss. The characteristic pathological feature of permanent hearing loss is the irreversible loss of sensory hair cells, resulting in a loss of hearing function that does not recover. On the other hand, lower levels of noise can cause a temporary hearing loss for minutes, hours, or days, depending on the parameters of the stimulus (13).

2.4 Noise-induced temporary hearing loss

At the lower limit of damaging noise, reversible changes can occur, resulting in a temporary auditory threshold shift (TTS), or temporary hearing loss that recovers within a few days. In TTS, sensory hair cells, including both IHCs and OHCs, are not lost. The pathological changes associated with TTS are not well understood.

Possible pathologies underlying TTS include swelling, fusion or distortion of stereocilia, resulting in detachment of stereocilia from the tectorial membrane or a reduction in the stiffness of stereocilia, both of which affect the deflection of stereocilia and the subsequent mechanotransduction necessary for hair cell depolarization (14, 15). Commonly, repairable excitotoxic effects are detected at the IHC synapses post TTS noise exposure. The presence of swollen afferent fibers at the base of IHCs was accompanied by vacuolization (16-18). More recently, studies have uncovered delayed manifestations of neural degeneration of IHC synaptic ribbons and SGN loss regardless of the reversibility of auditory threshold shifts and the absence sensory hair cell damage (19-22). Despite the reversible effects of TTS, TTS noise exposure at a young age can accelerate the synaptopathy of SGNs leading to age-related neuronal permanent hearing loss (23). This observation has challenged the traditional view that degeneration of SGNs occurs after sensory hair cell loss.

2.5 Noise-induced permanent hearing loss

Higher intensities of noise may result in a permanent auditory threshold shift (PTS), or permanent hearing loss. This deficit in hearing function is believed to be a result of metabolic and mechanical processes that damage the inner ear. Mechanical factors that result from extremely high forces of acoustic stimuli cause excessive movement of the cochlea, disrupting internal cellular structure, and typically inducing injuries rapidly after exposure to the insult. On the other hand, metabolic damage is considered to be a more gradual process that exhausts mitochondrial metabolism, alters homeostasis of cochlear cells and fluids, increases oxidative stress and induces changes in energy production, gene expression and protein synthesis. These changes can have various pathological effects, including cell death, excitotoxicity, and structural damage.

PTS has several pathological correlates ranging from subtle defects to severe lesions. Similar to the histopathology of TTS, stereocilia damage, including collapse, breakage and fusion, can also occur under the PTS condition (24-27). Vacuolization in the IHC is also common in the PTS condition (28). Furthermore, the innervating afferent terminals of IHCs become swollen and degenerate, and at later times, are followed by the degeneration of the afferent fibers and SGNs. Additionally, SGNs display a subset of swollen satellite cells (28).

PTS is typically characterized by irreversible loss of sensory hair cells. OHCs are more vulnerable than IHCs in the cochlea, but IHCs can also be damaged with increased intensity of noise exposure (28). Noise-induced hair cell loss is a frequency-related damage in humans and in some animal models, such as guinea pig and chinchilla; however, in mice and rats, hair cell susceptibility follows a base-to-apex pattern as a result of noise-induced tonotopic damage, with basal hair cells being much more easily damaged than the apically located cells. In contrast, supporting cell structures remain generally well-preserved, although reversible or permanent pathologies may occur. After higher intensity noise exposures, and particularly impulse noise, supporting cell structures can also be damaged by detachment from the basilar membrane or by separation of cell-cell junctions due to mechanical movement of the organ of Corti. This can change the impedance of the basilar membrane and affect the sensitivity of hearing in that region. These structural disturbances can occur before sensory hair cell death.

Severe exposures cause permanent degeneration of the fibrocytes of the spiral limbus and spiral ligament, of which type II and IV fibrocytes are the most vulnerable (28). Additionally, the stria vascularis might be acutely swollen, and may subsequently shrink due to loss of intermediate and marginal cells. Vasoconstriction and capillary loss

in the spiral ligament as well as a decreased stria blood flow has also been detected (29-31). These changes may transiently alter the EP, elevating auditory threshold shifts.

Noise insults caused by impulse noise, such as an explosion, can directly cause mechanical damage to the inner ear (32). The extreme impact of vibrations can forcefully cause the organ of Corti to detach from the basilar membrane, break the tympanic membrane or damage the middle ear ossicles. Furthermore, the rupture of the basilar and Reissner's membranes may cause large ionic and osmotic changes that further accelerate sensory hair cell death (33).

2.4 Noise-induced apoptosis and necrosis of hair cells

Noise-induced cochlear pathologies cause both apoptotic and necrotic hair cell death. Apoptotic cell death is a programmed cell death pathway commonly characterized by condensed nuclei with activation of multiple cell death pathways that are primarily regulated by caspases. Caspase 8 and 9 are initiator caspases that are frequently cleaved in extrinsic apoptotic pathways mediated by death receptors such as Fas cell surface death receptor. Intrinsic apoptosis is primarily induced in response to intracellular stress such as calcium overload or DNA damage. Intrinsic apoptosis is associated with the formation of a pore on the outer mitochondrial membrane by the pro-apoptotic Bcl-2 family mediators, such as Bax. The activation of Bax causes uncoupling of the mitochondrial membrane and mitochondrial membrane permeabilization, resulting in the release of mitochondrial proteins and apoptotic factors, such as endonuclease G and cytochrome C, into the cytosol (34). Endonuclease G can translocate into the nucleus where it is able to mediate DNA fragmentation. On the other hand, cytochrome C initiates a cell death cascade that triggers the cleavage of caspase 9. Both of the

extrinsic and intrinsic apoptotic pathways converge on caspase 3, the executioner caspase, involved in the final stages of apoptosis (35).

The pathological feature of necrotic cell death is characterized by swollen nuclei (36). The necrotic cell death pathways are not well understood, although recent studies have proven that a regulated form, termed necroptosis, commonly occurs. In necrosis, damage to the cell membrane causes a disruption of cell homeostasis as an influx of fluid and extracellular ions enter the cell and eventually cause swelling and rupture. Moreover, the membranes of internal organelles are also compromised, releasing lysosomal enzymes that exacerbate the damage. In necroptosis, the receptor-interacting protein (RIP) kinases 1 and 3 mediate necrotic cell death via the stimulation of death receptors (37, 38). RIP1 can directly interact with the death domains of death receptors, resulting in its activation and the subsequent cleavage of caspase 8. Additionally, RIP1 can also be activated through its interaction with RIP3.

Both apoptotic and necrotic cell death pathways have been detected in OHCs following noise exposure (39-41). Caspases 8, 9 and 3 have been expressed in OHCs with condensed nuclei after noise exposure (39, 42). Additionally, noise exposure caused the release of cytochrome C and the translocation of endonuclease G, which was detected in apoptotic OHCs (40, 41, 43, 44).

Mode of Death	Morphology	Biochemical Features
Intrinsic Apoptosis	<ul style="list-style-type: none"> • Cell shrinkage • Nuclear condensation and fragmentation 	<ul style="list-style-type: none"> • Intracellular stress (Ca²⁺, DNA damage) • Mitochondrial outer membrane permeabilization (Bax, Bak) • Cytochrome C release • Nuclear translocation of EndoG and AIF • Activation of caspase-9, -3
Extrinsic Apoptosis	<ul style="list-style-type: none"> • Cell shrinkage • Nuclear condensation and fragmentation 	<ul style="list-style-type: none"> • Death receptor signaling • Activation of caspase-8, -3
Necroptosis	<ul style="list-style-type: none"> • Cell swelling and vacuolization • Nuclear swelling 	<ul style="list-style-type: none"> • Death receptor signaling • RIP1/3 activation • Activation of caspase-8

Table 1. Characteristics of cell death pathways. Apoptotic cells are primarily characterized by nuclear condensation and induced by intracellular stress (intrinsic) or death receptors (extrinsic), while necrotic nuclei are and may be initiated by membrane permeabilization (necrosis) or death receptor signaling (necroptosis).

3. Mechanisms of noise-induced hearing loss

3.1 Evidence for noise-induced ATP reduction

Cochlear tissues use energy in the form of adenosine triphosphate (ATP) to maintain the steep ionic gradients across cell membranes. Energy reserves, as determined by levels of high energy phosphate, are primarily localized in the cells of the organ of Corti, followed by the stria vascularis, and lowest levels within the SGN, although the rate of energy metabolism is higher in the stria vascularis (45). Previous reports demonstrate the noise-induced cellular reduction of ATP levels in the cochlea associated with noise-induced permanent hearing loss, but no change with temporary hearing loss (40, 46-48). In the cochlea, high intensity of noise exposure decreases capillary blood flow and

caused local vasoconstriction (49, 50). The resulting ischemia decreases ATP levels within the inner ear, including the lateral wall structures (46, 47, 51). The maintenance of ATP levels via creatine, a compound that enhances cellular energy stores, attenuates temporary and permanent NIHL in guinea pigs, suggesting that conservation of ATP levels may prevent the initiation of subsequent pathological events such as free radical formation (52). Creatine kinase is abundant in the stria vascularis marginal cells, it is probable that the creatine treatment acts to maintain the endocochlear potential by supplying ATP for ionic pumps since the endocochlear potential is reduced by noise insults (53, 54).

Additionally, extracellular ATP can serve as a second messenger within the cochlea. Extracellular ATP concentrations are increased in the endolymph fluid of the guinea pig cochlea after noise insults, probably due to the release of ATP from vesicles in the stria vascularis or gap junctional hemichannels of supporting cells (55-57). This increase in extracellular ATP levels is implicated in both the pathogenesis and mitigation of NIHL (58, 59). An exogenous delivery of ATP provides a protective response and accelerates recovery from temporary threshold shifts in a guinea pig model possibly through its effect in reducing the endocochlear potential to desensitize the sensory cell response to noise insults (60). Extracellular ATP can initiate a variety of pathological signaling pathways through the purinergic receptors in the inner ear including OHC electromotility and calcium signaling, which may ultimately alter cochlear sensitivity (57, 61-63).

3.2 Evidence for noise-induced ROS production

The mitochondrial electron transport chain is implicated as a major source for reactive oxygen species (ROS) produced by cochlear tissues. Due to the high energy demands

of the cochlea, and particularly the stria vascularis in the maintenance of endolymph ionic balance, ROS are often produced as a product of the mitochondrial metabolism. During oxidative respiration, 98% of molecular oxygen is used by mitochondria to generate ATP. Under normal physiological conditions, 1-2% of the molecular oxygen is reduced to free radicals such as superoxide which can be oxidized to less toxic hydrogen peroxide by mitochondrial superoxide dismutase (SOD). This level of ROS can dramatically increase under pathological conditions (64, 65).

Increased ROS generation in cochlear tissues, including in OHCs, stria vascularis, and fluids, by traumatic noise exposure is well documented and persists for days after the exposure (66-71). Treatment with the superoxide generator paraquat induces a similar pattern of OHC death and permanent auditory threshold shifts as that induced by noise exposure, suggesting ROS as a cause for noise-induced cochlear pathology (72). The most intriguing evidence for the role of oxidative stress in NIHL is that treatment with a variety of antioxidants, such as Coenzyme Q, glutathione, D-methionine, N-acetyl-cysteine, salicylate and trolox, reduces the extent of noise-induced auditory deficits (71, 73-77). In line with this notion, basal OHCs, which are more susceptible to noise damage, contain a lower level of the antioxidant glutathione compared with their more resistant apical counterparts (78). Defects in antioxidant genes, such as a single nucleotide polymorphism in the mitochondrial manganese-superoxide dismutase gene in factor workers and glutathione peroxidase in mice increased susceptibility to noise-induced hearing loss (79-81).

While the source for this elevated ROS is still unclear, theories speculate that free radicals are triggered by the effects of ischemia-reperfusion or the influx of free calcium on mitochondria via dysregulation of the calcium-regulated enzyme α -ketoglutarate dehydrogenase within the Krebs cycle (82). Furthermore, targeting the

nicotinamide adenine dinucleotide phosphate (NADPH) oxidase complex, the major superoxide generator of the cell membrane, prior to noise exposure protects against hair cell death and the elevation of auditory threshold shifts by lowering the level of ROS generation (83). Supporting this concept, noise insults also induce the formation of the ROS by-product and vasoconstrictor 8-isoprostaglandin F(2alpha) in cochlear tissues and treatment with its antagonist block 8-isoprostaglandin F(2alpha)-induced reductions in cochlear blood flow (CBF) (50). The ischemia-reperfusion that results from a decrease in CBF may also contribute to increased oxidative stress.

3.3 Evidence for noise-induced calcium influx

Acoustic overstimulation has been shown to increase OHC cytoplasmic calcium concentration in guinea pig sensory cells (84-86). Evidence has demonstrated a sustained 60% increase in calcium-dependent fluorescence in guinea pig OHCs accompanied by a decrease in cochlear microphonics immediately following exposure to extremely high levels of noise at 130 dB. On the other hand, normal sound levels of 75 and 88 dB did not alter intracellular calcium levels of cochlear sensory cells (85). Moreover, in addition to increased fluorescence of free calcium in isolated OHCs of the guinea pig cochlea, hearing loss and OHC death was also significantly increased following high levels of noise exposure at 110 dB (85).

The role of calcium influx and signaling in the pathogenesis of NIHL is emphasized by inner ear studies investigating the plasma membrane calcium-ATPase (PMCA), the channel by which calcium is extruded to maintain the low intracellular calcium concentration of hair cells and prevent calcium overload (87). Mutant PMCA-null mice displayed deafness while heterozygotes exhibited significant hearing loss (88). Furthermore, the activation of calcium-dependent enzymes such as calcineurin increase

in the dying OHCs of guinea pigs exposed to noise trauma. Treatment with inhibitors of the calcium-dependent enzyme calcineurin, FK506 and cyclosporine A, reduce NIHL and hair cell death (89).

In addition to increased intracellular OHC calcium concentration, endolymph calcium levels increase by 50-fold in the noise-exposed guinea pig. This generates a high ionic concentration gradient that results in the entry of calcium into sensory cells through various channels, such as the VGCC and MET channels (90). At physiologic or resting membrane potential, VGCCs are normally closed. These channels open when excitable sensory cells are depolarized, allowing calcium entry into the cell. Several VGCC subunits are in the auditory organ of the chinchilla, guinea pig, and murine cochlea (91-93). The $\alpha 1$ subunit of VGCC is the pore forming component that is necessary for proper functioning of the channel. In fact, its critical role in hearing function is highlighted by evidence showing that $\alpha 1D$ -deficient mice are deaf (94, 95). Importantly, the VGCC $\alpha 1$ subunit is immunolocalized within IHCs and OHCs, but not supporting cells, of the chinchilla cochlea (91). The basolateral localization of VGCCs allow for the concentration of calcium influx at the synaptic ribbon active zone. The calcium concentration at this nanodomain functions to trigger neurotransmitter release at the ribbon synapse. However, an overloading of calcium influx can also cause synaptopathy by stimulating the excessive release of glutamate neurotransmitters at the synapse. The resulting overactivation of glutamate receptors on the post-synaptic terminals can cause excitotoxicity and swelling of the nerve terminals, resulting in functional deficits.

VGCCs are composed of several channel types that vary in their physiological roles. L-type and T-type VGCCs vary in their activation. L-type channels are high voltage-activated channels that require stronger than ~ 30 mV depolarization to open.

On the other hand, T-type channels are low voltage-activated channels that require only small changes in the resting membrane potential (~10 mV) to open (93, 96). L-type VGCCs are the predominant VGCC in IHCs and are also present in OHCs (97). Several L-type channel blockers diltiazem, verapamil, nicardipine, and nimodipine reduce the auditory threshold shift and decrease hair cell loss in female ddY mice at 8 weeks of age (98). Delivery of the L-type, high voltage-activated channel blocker diltiazem protects guinea pig OHCs from acute noise exposure (99). Furthermore, diltiazem treatment reduces the calcium content of guinea pig IHCs and OHCs under normal conditions (100). T-type channel blockers ethosuximide and trimethadione, delivered via drinking water, also protect against hearing loss and OHC death primarily in the basal turn of the C57BL/6 cochlea after noise exposure at 110 dB (101). Trimethadione protects against both TTS and PTS hearing loss and hair cell death, while ethosuximide significantly prevents only PTS (101).

3.4 Interplay of calcium, ATP and ROS

The previous sections review the three major metabolic events associated with NIHL: reduction of intracellular ATP levels, calcium influx and generation of ROS. However, a comprehensive mechanism of how these noise-induced metabolic stressors ultimately alter cell fate causing noise-induced cochlear pathologies is still unknown. It is likely that these changes in cellular energy, calcium and oxidative balance are interrelated in both normal and pathological cell function.

The relationship between these metabolic phenomena is particularly apparent in the mitochondrion. Under physiological conditions, calcium serves a beneficial function as a stimulus for ATP synthesis. Mitochondria serve as calcium sinks that rapidly uptake calcium via mitochondrial calcium uniporter (MCU) channels, providing buffering

capacity for cytosolic calcium overload. These channels are located within the inner mitochondrial membrane and transport calcium ions into the mitochondrial matrix through a process that is primarily driven by the negative charge of the mitochondrial membrane potential. This process is necessary for the stimulation of calcium-activated dehydrogenases located in the mitochondrial matrix: pyruvate dehydrogenase, α -ketoglutarate and isocitrate dehydrogenase. The sum of these activities enhances the aerobic respiration and the ATP output of the mitochondrion. The reduction of mitochondrial membrane potential in mitochondrial disease reduces the uptake of calcium into mitochondria and subsequent ATP production; treatment with a drug that restores mitochondrial matrix calcium content restores ATP production (102).

Alternatively, increases in matrix calcium content can trigger a pathological response. Calcium overloading of the mitochondrial matrix can reduce the mitochondrial membrane potential and subsequently reduce ATP production. This may be caused by a sustained opening of the mitochondrial permeability transition pore (mPTP) which is associated with cell death pathways. In contrast, a lower mitochondrial calcium content increases protective cellular functions such as autophagy, probably through increased kinase activity of AMPK, rather than driving a pro-apoptotic response (103). The physiological calcium stimulus typically changes into a pathological response when the cell is stressed due to accompanying insults which can include oxidative stress.

Calcium-mediated events can also directly affect ROS. For example, calcium can stimulate electron flow from the Krebs cycle to increase aerobic respiration and its associated ROS by-products. Additionally, calcium can stimulate the production of nitric oxide via nitric oxide synthase in the cytosol which can subsequently act to inhibit complex I or IV of the electron transport chain, enhancing ROS production (104). ROS can regulate calcium levels and mitochondrial activity. ROS can activate mitochondrial

uncoupling proteins to dissipate the mitochondrial membrane potential, which would probably be accompanied by reduced ATP output, reduced uptake of mitochondrial calcium and increased cytosolic calcium (105). On the other hand, ROS can also be regulated by mitochondrial activity, since mitochondrial uncouplers decrease ROS generation as well as ATP production (106, 107). This evidence highlights the multifaceted interactions among these three metabolic events (108).

The relationship between these metabolic stressors is further complicated by the often intertwining cross-talk and feedback loops that propagate the pathological stimulus. For example, the calcium or ROS-induced release of cytochrome C from the mPTP can disrupt the function of the inositol 1, 4, 5-triphosphate receptor (IP₃R) on the endoplasmic reticulum, another calcium store. A high cytosolic calcium level inhibits the opening of this calcium to prevent ER calcium release under physiological conditions; however, the cytochrome C-induced dysfunction prevents this autoinhibition, propagating the calcium overload (109). Extracellular ATP release by the marginal cells of the stria vascularis can also regulate ER calcium release through the P2Y metabotropic G-protein coupled receptors (GPCRs). The P2Y GPCRs activate phospholipase C (PLC), an enzyme which cleaves membrane phospholipids, releasing IP₃. IP₃ then binds to IP₃R in the ER, activating calcium release into the cytosol. Mitochondrial ROS also stimulate feedback loops that can cause mitochondrial dysfunction. ROS generation within the matrix via complex I is sensitive to the mitochondrial membrane potential and thus its dissipation can significantly reduce ROS levels (110). Since uncoupling can be stimulated by ROS, a resulting feedback loop may exist that further potentiates the dissipation of membrane potential. Meanwhile, it is likely that this mitochondrial dysfunction will be accompanied by a reduced ATP output and calcium uptake.

Finally, since ATP is necessary for many ion pumps within the many cellular membranes, any disruption of ATP levels will impact ionic balance across mitochondria, cytosol and endoplasmic reticulum. The exacerbation of ion transport across membranes will result in a disturbance in ion gradients that will worsen reduction in ATP levels and aggravate ROS generation as a consequence. Thus, the initial stimulus of intracellular calcium influx, ATP reduction or ROS generation can induce pathological responses through sustained propagation of these cyclical actions. Moreover, the complexities of these intertwining pathways challenge our understanding of the initiating pathological stimuli and the subsequent turn of events.

4. Significance

The investigation of NIHL can have a profound impact on public health as noise trauma is one of the most common causes of hearing loss in the adult population worldwide. In addition to the detrimental auditory defects of noise on war veterans and industrial workers, NIHL also poses negative economic consequences of \$242.4 million annually as NIHL has become one of the most common work-related disabilities (7). Since the underlying molecular mechanisms of NIHL and the clinical therapy for its prevention and treatment have not been established, detailed mechanisms of hair cell death in NIHL need to be elucidated in order to identify new targets for the development of a comprehensive therapy for translational research.

CHAPTER TWO: MATERIALS AND METHODS

Animals

Male CBA/J mice at the age of 11 weeks, breeding pairs of CaMKK β C57BL/6J heterozygous mice (B6.129X1-Camkk2^{tm1Tch}/J; stock #014172), AMPK α 1 C57BL/6 knockout mice (Prkaa1^{tm1.1Sim}/J; stock #014141) and wild type of C57BL/6J were purchased from The Jackson Laboratory. All mice had free access to water and a regular mouse diet (Purina 5025, St. Louis, MO) and were kept at 22 \pm 1 °C under a standard 12:12 hour light-dark cycle to acclimate for one week before the experiments. All experiments were conducted at the age of 12 weeks for male CBA/J mice. A younger age of seven weeks was used for CaMKK β C57BL/6J knockout and littermates and AMPK α 1 C57BL/6J knockout and wild type mice due to the *ahl* homozygous mutation on cadherin 23 which causes progressive age-related hearing loss in the C57BL/6J strain of mice. All research protocols were approved by the Institutional Animal Care & Use Committee at the Medical University of South Carolina (MUSC). Animal care was under the supervision of the Division of Laboratory Animal Resources at MUSC.

Noise exposure

CBA/J mice at 12 weeks of age were exposed to a broadband noise (BBN) with a frequency spectrum from 2–20 kHz for two hours at either 106 dB SPL to induce severe permanent threshold shifts that range from 50 – 65 dB at high frequencies or 98 dB SPL to induce moderate permanent threshold shifts (PTS) that range from 40 – 50 dB (71). All knockout and wild type C57B/6J mice at seven weeks of age were exposed to three different conditions of 94, 98 or 106 dB SPL BBN to induce PTS. Generally, four mice (one mouse per stainless steel wire cage) were placed in a sound exposure chamber and exposed at the same time. Age- and gender-matched control mice were kept within the same chamber and cages for two hours without noise exposure. The sound

exposure chamber was the same as we previously described (39, 40, 71). Briefly, it was fitted with a loudspeaker (model 2450H; JBL) driven by a power amplifier (model XLS 202D; Crown Audio) fed from a CD player (model CD-200; Tascam TEAC American) which played BBN. Audio CD sound files were created and equalized with audio editing software (Audition 3; Adobe System, Inc.). Sound levels were calibrated with a sound level meter (model 1200; Quest Technologies) at multiple locations within the chamber to ensure uniformity of the sound field among the four cages, and were measured before and after exposure to ensure stability.

Auditory brainstem responses (ABR)

Mice were anesthetized with an intra-peritoneal (IP) injection of xylazine (10 mg/kg) and ketamine (100 mg/kg), and then placed in a sound-isolated and electrically shielded booth (Acoustic Systems, Austin, TX). Body temperature was maintained near 37 °C with a heating pad. Acoustic stimuli were delivered monaurally to a Beyer earphone attached to a customized plastic speculum inserted into the ear canal. Sub-dermal electrodes were inserted at the vertex of the skull, under the left ear and under the right ear (ground). ABRs were measured at 8, 16, and 32 kHz. Tucker Davis Technology (TDT) System III hardware and SigGen/Biosig software were used to present the stimuli (15 ms duration tone bursts with 1 ms rise-fall time) and record the response. Up to 1200 responses were averaged for each stimulus level. Thresholds were determined for each frequency by reducing the intensity in 10 dB increments and then in 5 dB steps near threshold until no organized responses were detected. Thresholds were estimated between the lowest stimulus level where a response was observed and the highest level without response. All ABR measurements were conducted by the same experimenter.

Drug administration via intra-peritoneal (IP) route

The pharmacological AMPK inhibitor compound C (Sigma #P5499) was dissolved in dimethyl sulfoxide (DMSO) as a stock solution (31.25 mg/mL) and stored at -20 °C. The stock solution was diluted in 0.9% saline immediately before being injected into animals. Each animal received a total of three IP injections at a dose of 20 mg/kg or 10 mg/kg per injection. The three IP injections were administered 24 hours before, two hours before, and immediately after noise exposure. The animals were euthanized one hour after noise exposure and temporal bones were removed to dissect the cochlea for immunofluorescence assays. The mice used for experiments to observe the progression of ABR thresholds received an additional IP injection 24 hours after noise exposure.

Verapamil was dissolved in 0.9% saline solution as a stock solution (0.01 g/mL) and stored at -20 °C. The stock solution was diluted in saline immediately before being injected into animals. Each animal received a total of five IP injections of verapamil at a dose of 10 mg/kg per injection. The five IP injections were administered 24 and 1 hour before, immediately after, 24 and 36 hours after noise exposure. The ABR thresholds were measured two weeks after noise exposure (Fig. 5).

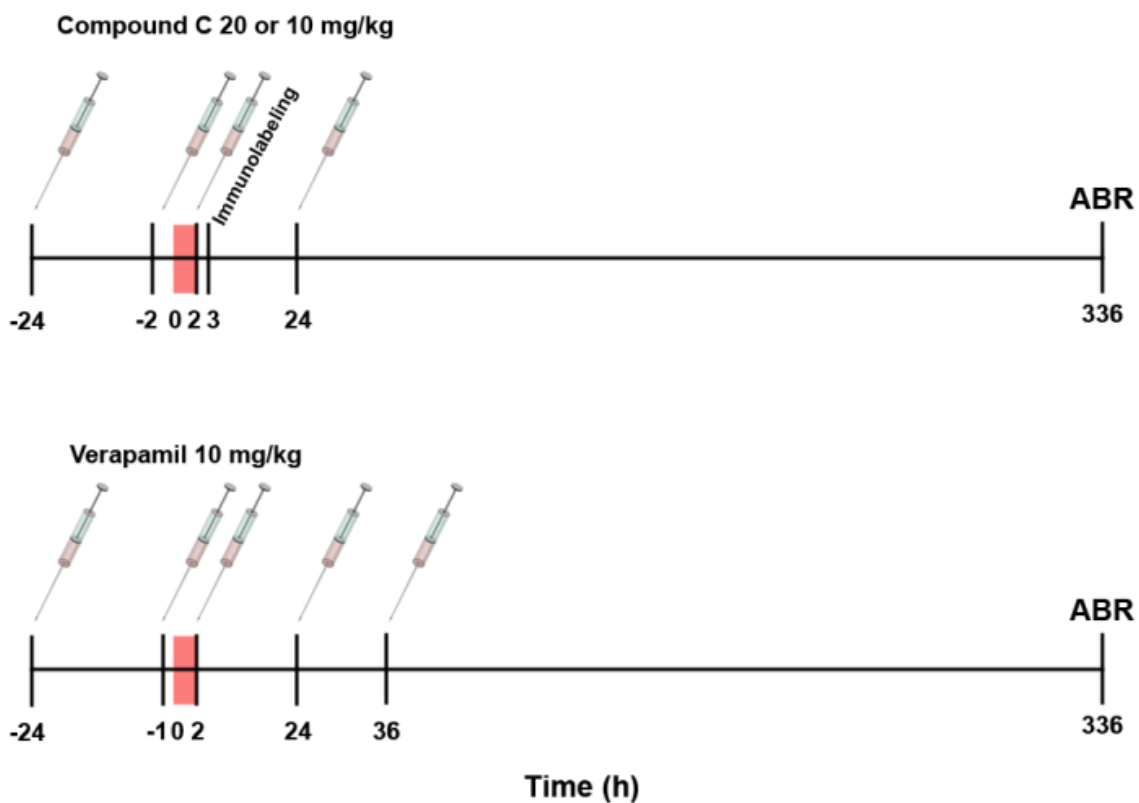


Figure 5. Drug administration via intraperitoneal injection. The doses of Compound C and verapamil are illustrated. Injections of each drug were delivered prior to and after a 2 h noise exposure (pink square). The time course (hours) shown is relative to noise exposure and begins with time 0 at the start of the 2 h noise exposure. Time points prior to noise exposure are noted with a negative sign (-).

Intra-tympanic delivery of siRNA

siAMPK α 1 (Invitrogen #s98535), siLKB1 (Invitrogen #s74497), siCaMKK β (Invitrogen #n437808) or scrambled siRNA (siControl) (Invitrogen) was locally delivered via intra-tympanic application, which allows the entry of siRNA specifically within sensory hair cells and minimal detection in other cochlear cell types (40, 111, 112). Briefly, after anesthesia, a retroauricular incision was made to approach the temporal bone. The otic bulla was identified ventral to the facial nerve and a shallow hole was made in the thin part of the otic bulla with a 30 G needle and enlarged with a dental drill to a diameter of 2 mm to visualize the round window. A syringe was inserted into one end of a customized sterile Micro Medical tube. The other end of the tube was inserted into the hole just above the round window to slowly deliver 10 μ L (0.3, 0.6 or 0.9 μ g) of a single siRNA species via syringe. After the siRNA delivery, the hole was covered with surrounding muscle and glued with tissue adhesive. Lastly, the skin incision was closed with tissue adhesive and the mouse was kept in the surgical position for one hour. Seventy-two hours after siRNA delivery, the animals were exposed to noise or kept in silence in the noise chamber for two hours.

Surface preparations and DAB staining of cochlear epithelia for hair cell counts

The procedures for surface preparations and diaminobenzidine (DAB) staining of cochlear epithelia were followed as previously described (40). Briefly, the temporal bones were removed immediately following euthanasia and perfused through the cochlear scala media with a solution of 4% paraformaldehyde in phosphate buffered saline, pH 7.4 (PBS) and kept in this fixative overnight at 4 °C. The cochleae were then rinsed in PBS. The cochlea were decalcification in a 4% solution of sodium EDTA (adjusted with HCl to pH 7.4) and the solution was changed daily for three days and

maintained at 4 °C. Following decalcification, the cochleae were placed in 3% hydrogen peroxide for 2.5 hours to quench endogenous peroxidases. After incubation in 10% normal goat serum to block non-specific antibody binding overnight at 4 °C, the tissues were incubated with a primary antibody (rabbit polyclonal anti-myosin VII, Proteus Bioscience # 25-6790) at a 1:100 dilution for 4 days at 4 °C on a Nutator mixer, washed in PBS, and then incubated overnight at 4 °C with secondary antibody (biotinylated goat anti-rabbit) at a 1:100 dilution. The specimens were rinsed again and then incubated in ABC solution (Vector Laboratories # PK-4001) overnight. Following another washing, the cochleae were incubated in DAB for three hours, as necessary for sufficient staining intensity, followed by washing to stop the DAB reaction. Finally, the cochleae were micro-dissected under a microscope into apical, middle, and basal segments and mounted on slides with Fluoromount-G mounting medium. Images were taken with Zeiss AxioCam MRc5 camera with Axioplan 2 imaging software with a Zeiss microscope for hair cell counts. Hair cells were counted from captured images using the 40x magnification lens on the Zeiss microscope. The lengths of the cochlear epithelia were measured and recorded in millimeters. Both OHCs and IHCs were counted from the apex to the base along the entire length of the mouse cochlear epithelium. Percentages of hair cell loss in each 0.5 mm length of epithelium were plotted as a function of the cochlear length as a cytochleogram.

Immunohistochemistry for cochlear paraffin sections

Following decalcification with 4% EDTA, each cochlea was embedded in paraffin for sections. The 5 µm formalin fixed paraffin embedded (FFPE) sections were routinely deparaffinized in xylene and rehydrated in alcohol. The sections were incubated with target retrieval solution (Dako S2367) in a steamer (Oster CKSTSTMD5-W) for 10

minutes and then 3% hydrogen peroxide for 10 minutes and protein block (Dako x0909) for 20 minutes at room temperature. Primary antibody was incubated overnight in a humid chamber at 4 °C, followed by biotinylated secondary antibody (Vector, CA USA) for 30 minutes and ABC reagent (Vector, CA USA) for 30 minutes. Immunocomplexes of horseradish peroxidase were visualized by DAB (Dako, Glostrup, Denmark) reaction, and sections were counterstained with hematoxylin before mounting.

Immunohistochemistry for cochlear surface preparations

Following decalcification with 4% EDTA, each cochlea for immunocytochemistry of surface preparations was dissected under a microscope by removing the softened otic capsule, stria vascularis, Reissner's membrane, and tectorial membrane. The remaining tissue, including the modiolus and cochlear sensory epithelium, was permeabilized in 3% Triton X-100 solution for 30 minutes at room temperature. The specimens were washed three times with PBS and blocked with 10% goat serum for 30 minutes at room temperature, followed by incubation in darkness at 4 °C for 72 hours with primary antibodies: monoclonal rabbit anti-p-AMPK α (Thr 177) at 1:50 (Cell Signaling Technology #2535S), monoclonal rabbit anti-AMPK α 1 at 1:50 (Abcam #ab32047), monoclonal rabbit anti-AMPK α 2 at 1:100 (Abcam ab3760), monoclonal rabbit anti-LKB1 at 1:100 (Cell Signaling Technology #13031), monoclonal rabbit anti-p-LKB1 at 1:50 (Cell Signaling Technology #3482), monoclonal mouse anti-LYK5 (STRAD α) at 1:100 (Sigma-Aldrich SAB1402648), monoclonal rabbit anti-CtBP2 at 1:100 (BD Biosciences #612044), polyclonal rabbit anti-CaMKK β at 1:100 (ThermoFisher #PA5-30399), monoclonal rabbit anti-CaMKI at 1:100 (abcam #ab68234), and polyclonal rabbit anti-CaMKIV at 1:100 (ProteinTech #13263-1-AP). After washing three times, the tissues

were incubated with the Alexa Fluor 594 or 488-conjugated secondary antibody at a concentration of 1:200 at 4 °C overnight in darkness. After washing, specimens were incubated with Alexa Fluor 488 phalloidin at a concentration of 1:100 for 1 hour in darkness. After the final wash with PBS, the tissue was dissected in PBS by removing the modiolus. The epithelia were divided into three segments (apex, middle, and base). Specimens were mounted on slides with Fluoro-gel with Tris buffer (Electron Microscopy Sciences # 17985-10). Control incubations were processed without primary antibody treatments. Images were taken using a Zeiss or Lecia laser confocal microscope (Zeiss LSM 510 or Leica TCS SP5).

Quantification of the immunolabeled signals from outer hair cells of surface preparations

Immunolabeled signals of OHCs on surface preparations was quantified from original confocal images, each taken with a 63× magnification lens under identical conditions and equal parameter settings for laser gains and PMT gains, using ImageJ software (National Institutes of Health, Bethesda, MD). The cochleae from the different groups were fixed and stained simultaneously with identical solutions and processed in parallel. All of the surface preparations were counter-stained with Alexa Fluor 488 phalloidin (green) to label hair cell structure. The borders of each individual OHC were outlined with the circle tool based on the phalloidin staining. The immunofluorescence of the target proteins were measured in the upper basal region of cochlear surface preparations in 0.12 mm segments, each containing about 60 OHCs. The intensity of the background fluorescence was subtracted and average fluorescence per cell was calculated. The fluorescence was quantified by normalizing the ratio of average fluorescence of noise-exposed hair cells to the average fluorescence of the unexposed

hair cells. The overlap coefficient for LKB1 and STRAD α in OHCs was determined using Zeiss Zen colocalization software. In these studies, there were no differences in the levels of p-AMPK α , LKB1, STRAD α , p-CaMKI and p-CaMKIV molecules in OHCs of the apical and middle turns between ears of control mice and those harvested one hour after noise.

Quantification of the immunolabeled ribbons from Z projections on surface preparations

Immunofluorescence of CtBP2 on surface preparations was quantified from original confocal images, each taken with a 63 \times magnification lens under identical Z-stack conditions with 0.25 intervals and equal parameter settings for laser gains and PMT gains. Three Z-stack images each in 0.12 mm segments (containing about 16 IHCs) were captured at the 22 kHz region (3 mm from the apex) of cochlear surface preparations. The number of synaptic ribbons were counted using ImageJ software (National Institutes of Health, Bethesda, MD). Briefly, the background of the images was subtracted, the noise was despeckled and the threshold was set to isolate the immunolabeling of ribbon signals from IHCs. The image was converted to a binary file and the number of ribbon particles was counted using the 3D Object Counter. The binary file was converted to a 3D zy projection to measure ribbon dispersion (Fig. 6).

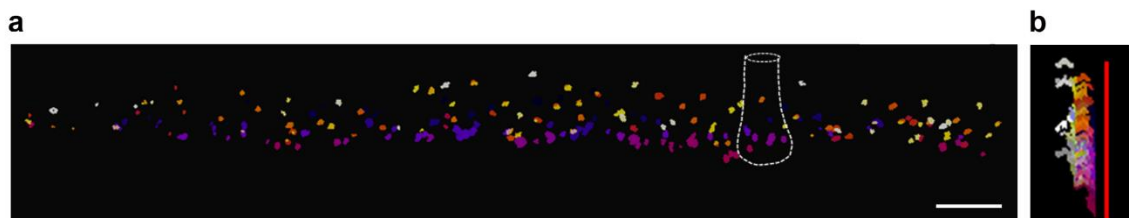


Figure 6. 3D reconstruction of CtBP2-immunolabeled synaptic ribbons. (a) ImageJ software was used to subtract background noise and isolate ribbon signals and convert

to the 3D image. Dotted line: representative outline of IHC. Scale bar = 5 μm . **(b)** The 3D image was rotated along the x-axis to visualize a zy projection of the ribbons for measurement of dispersion. Red line: representative line for measurement of dispersion in zy projection.

Extraction of total cochlear protein

Cochleae were rapidly removed and dissected in ice-cold PBS, pH 7.4, containing CompleteTM Mini EDTA-free protease inhibitor cocktail tablets (Roche Diagnostic GmbH # 11836170001). To extract total protein, tissues from the cochleae of a single mouse were homogenized in ice-cold RIPA lysis buffer containing RIPA lysis buffer (Sigma Aldrich #R0278) plus Phosphatase Inhibitor Cocktails II and III, and Roche protease inhibitor by using a glass/glass micro tissue grind pestle and vessel for 30 seconds. Tissue debris were removed by centrifugation at 10,000 \times g at 4 $^{\circ}\text{C}$ for 10 minutes and the supernatants were retained as the total protein fractions. Protein concentrations were determined using the Bio-Rad Protein Assay dye reagent (Bio-Rad) with bovine serum albumin as a protein standard. Two cochleae from the same mouse were pooled for each sample. Unless otherwise specified, all chemicals and reagents used were purchased from Sigma Aldrich.

Extraction of protein from formalin-fixed sensory epithelium

Cochleae were rapidly removed and perfused with 4% paraformaldehyde through the cochlea scala media for two hours at room temperature (25 $^{\circ}\text{C}$). The cochleae were then rinsed in PBS and decalcified in a 4% solution of sodium EDTA for three days at 4 $^{\circ}\text{C}$, with the EDTA solution changed daily. Following decalcification, the dissected sensory epithelium from three cochleae were placed in 1.5 mL collection tubes with 100 μL of

extraction buffer EXB plus (Qiagen Qproteome FFPE Tissue kit #37623) supplemented with β -mercaptoethanol. Glass micro grinder pestles were used to grind the tissue for three minutes. The tubes were sealed with a sealing clip and vortexed. The samples were incubated on ice for five minutes, followed by vortexing. The tubes were then incubated for 20 minutes at 100 °C on a heating block. After this incubation, the tubes were incubated for two hours at 80 °C with agitation at 750 rpm (Eppendorf) and then allowed to cool at 4 °C for 1 minute. Finally, the samples were centrifuged at 14,000 x g at 4 °C for 15 minutes. The supernatant containing the extracted proteins were transferred to a new tube. Protein concentrations were determined using the Bio-Rad RC DC protein assay (Invitrogen #500-0119) with bovine serum albumin as a protein standard.

Western blot analysis

Protein samples (30 μ g) were separated by SDS-PAGE. After electrophoresis, the proteins were transferred onto a nitrocellulose membrane (Pierce Rockford, IL) which was blocked with 5% nonfat dry milk in PBS-0.1% Tween 20 (PBS-T). The membranes were incubated with anti-p-AMPK α (1:1,000), anti-AMPK α 1 (1:1000), anti-p-LKB1 (1:1000), anti-LKB1 (1:1000), anti-CaMKK β (1:1000), anti-CaMKI (1:1000), anti-CaMKIV (1:1000) or anti-GAPDH (Millipore # ABS16, 1:10,000) at 4 °C overnight, and then washed three times (10 minutes each) with PBS-T buffer. Membranes were incubated with an appropriate secondary antibody at a concentration of 1:2,500 for one hour. Following extensive washing of the membrane, the immunoreactive bands were visualized by SuperSignal[®] West Dura Extended Duration Substrate or Pierce[®] ECL Western Blotting Substrate (Thermo Scientific). X-ray films of Western blots were scanned and analyzed using ImageJ software. The band densities were first normalized

to background. Next, the probing protein/GAPDH ratio was calculated from the band densities run on the same gel. Finally, the difference in the ratio of the control and experimental bands was tested for statistical significance.

Extraction of total cochlear RNA for qPCR

Cochleae were rapidly removed and isolated in RNAlater (Invitrogen). Cochleae from a single mouse were placed in a 2 mL tube with 100 μ L of RNAlater and immediately crushed with forceps. A 1 mL volume of TRIzol (Invitrogen) was added to each sample, followed by homogenization with an RNase-free Polytron tissue grinder (Kinematica). The samples were incubated for 5 minutes at room temperature prior to the addition of 0.2 mL of chloroform and vigorous shaking. After 2-3 minutes of incubation, the samples were centrifuged at 12,000 \times g at 4 $^{\circ}$ C for 15 minutes and the upper colorless aqueous phase was retained and transferred to Phase Lock Gel Heavy (Eppendorf) tubes. The 0.2 mL of chloroform was added to each sample and followed by centrifugation at 12,000 \times g at 4 $^{\circ}$ C for 10 minutes. The upper aqueous phase was transferred to a fresh RNase-free tube for RNA precipitation with 1.5 μ L of glycogen and 0.5 mL of isopropanol, followed by centrifugation at 12,000 \times g at 4 $^{\circ}$ C for 10 minutes. The RNA pellet was washed in 75% ethanol and dissolved in DEPC water. RNA concentrations were determined using the Nanodrop spectrophotometer. Absolute copy numbers were analyzed using the QX100 Droplet Digital PCR System (Bio-Rad). Unless otherwise specified, all chemicals and reagents used were purchased from Sigma Aldrich.

Statistical analysis

Data were analyzed using SYSTAT and GraphPad software for Windows. The group size (n) *in vivo* was determined by the variability of measurements and the magnitude of

the differences between groups. Based on our previous and current preliminary studies, we determined that six to eight animals per group provided sufficient statistical power ($p < 0.05$). Statistical methods used include one-way Analysis of Variance (ANOVA) with Tukey's multiple comparisons, repeated-measures ANOVA with post-hoc testing, unpaired t-tests, and one-sample t-tests. All tests were two-tailed and a p-value < 0.05 was considered statistically significant.

CHAPTER THREE: AMPK ACTIVATION IN NOISE-INDUCED HEARING LOSS

Introduction

The survival of essentially all organisms depends on the dynamic control of energy metabolism during acute or prolonged exposure to various stress (113). Adenosine monophosphate-activated protein kinase (AMPK) is a cellular energy sensor that is able to detect and react to the fluctuations of the AMP:ATP ratio of the cell (114). This kinase serves as a key regulator of energy homeostasis that coordinates metabolic pathways with the energy demands of the cell by directing the cell to switch off energy consuming activities and turn on energy-generating pathways (113, 115, 116). In response to an increase in AMP levels, the AMPK γ subunit allosterically binds AMP, resulting in a 2-5 fold increase in the activity of AMPK (117). In addition to this allosteric activation, the binding of AMP exposes the threonine 172 (T172) residue on the catalytic α -subunit to reversible phosphorylation by upstream kinases such as liver kinase B1 (LKB1). Moreover, the conformational change of the kinase domain induced by AMP binding protects AMPK from the activity of phosphatases (118). This combined activation via allosteric and phosphorylation mechanisms causes a 1000-fold increase in the kinase activity of AMPK, allowing high sensitivity in response to small changes in the intracellular energy status (119).

The regulation of cellular energy homeostasis by AMPK contributes to its role in the determinations of cell fate as energy is necessary for cellular survival. Initially, the activation of AMPK was considered an adaptive response to cellular stress; however, there are diverse outcomes of AMPK activity on cell death and survival. In neuronal cells, in particular, AMPK has a neuroprotective effect to glutamate excitotoxicity by elevating Glucose Transporter 3 trafficking in response to a decrease in cellular ATP levels (120). On the other hand, the sustained activation of AMPK has a hazardous

effect on the cell in some models of cellular stress, including ischemia-reperfusion, hypoxia and stroke (121, 122). The prolonged elevation of p-AMPK triggers the chronic activation of the c-Jun N-terminal kinase (JNK), upregulation of pro-apoptotic Bim and subsequent apoptosis in neuronal and pancreatic cells (120, 123, 124). AMPK is also able to inhibit JNK activity in neuronal cells, suggesting that the regulation of cell fate by AMPK is complex and may depend on the cell type and insult (120, 125, 126). Despite the central functions of AMPK in the regulation of cell death and survival, no studies thus far have elucidated the role of AMPK in noise-exposed sensory hair cells.

The small molecule Compound C (dorsomorphin) is a selective, potent, cell-permeable AMPK inhibitor through its ATP-competitive function (127). Many studies demonstrate the effectiveness of Compound C in inhibiting the activation of AMPK and its downstream activities. For example, treatment with Compound C *in vivo* protects against stroke-induced cerebral damage. Validating its pharmacological target, this neuroprotection is absent in AMPK α 2-knockout mice (122).

Total AMPK α 1 mRNA and protein expression is localized in murine cochlear tissue, with predominant expression in OHCs (128). The phosphorylation of AMPK α is detectable in OHCs and cochlear tissues, particularly after exposure to noise insults (40, 47). Furthermore, ROS-dependent robust activation of AMPK α is detected in the stria vascularis in a transgenic mouse mitochondrial disease model that exhibits hearing loss (129). In this chapter, our investigation focuses on the activation of AMPK by noise exposure in the inner ear using the mouse model that our lab has characterized in detail. We also explore the role of AMPK in the pathogenesis of NIHL using the pharmacological inhibitor Compound C, siRNA silencing and knockout mice.

Results

Noise conditions for temporary and permanent threshold shifts.

Based on our previously characterized parameters for CBA/ J mice, noise conditions for TTS (92 dB SPL) without OHC loss, PTS (98 dB SPL) with only OHC loss, and severe PTS (106 dB SPL) with both OHC and IHC loss were used (40, 71). Exposure of CBA/J mice at 12 weeks of age to broadband noise (BBN, 2-20 kHz) for 2 h at 92 dB SPL did not alter threshold shifts at 2 weeks after the exposure. On the other hand, a 98-dB exposure increased threshold shifts by 30, 50, and 55 dB at 8, 16, and 32 kHz, and a 106-dB exposure resulted in even larger threshold shifts at all three measured frequencies (Fig. 8a). Two weeks after noise exposure, the 98-dB exposure resulted in partial OHC loss beginning around 3.5 mm from the apex and increasing toward the base, while IHCs remained intact (Fig. 8c, d). The 106-dB noise exposure resulted in loss of both OHCs and IHCs (Fig. 7). OHC loss began around 2.5 mm from the apex (Fig. 8b) and IHC loss began around 4.5 mm from the apex (Fig. 8c), following a base-to-apex gradient with increased severity towards the base. The amount of OHC loss induced by 106 dB SPL was significantly higher than by 98 dB SPL. Age-matched sham-exposed control mice presented no elevation of auditory thresholds or hair cell loss 2 weeks after exposure. In agreement with the literature, synaptic ribbon number was also reduced in an intensity-dependent fashion (19, 130). Two weeks after a 106-dB noise exposure, the activity of auditory nerve fibers were decreased as determined by reduced ABR wave I amplitudes at 8, 16 and 32 kHz (Fig. 9). Additionally, 1 h after a 98-dB noise exposure, swelling of the spiral ganglion neuron bodies was apparent (Fig. 10).

AMPK α is activated in basal outer hair cells by noise in an intensity-dependent manner.

Using the above conditions, we first assessed the activation of the cellular metabolic sensor AMPK after noise exposure at 92, 98 and 106 dB SPL in OHCs of surface preparations. The expression of phosphorylated AMPK α (p-AMPK α) at threonine 172 in OHCs 1 h after 92-dB exposure was similar to age-matched controls without the exposure; however, immunolabeling for p-AMPK α in basal OHCs was increased by 60% after 98-dB and 230% after 106-dB exposure compared to controls (Fig. 11a, a'). Since changes in AMPK α phosphorylation were only detected under the PTS noise conditions, PTS noise exposures were used for the rest of the study. To evaluate the localization of this increased p-AMPK α in three key regions of the cochlea, the organ of Corti, spiral ganglion and stria vascularis, p-AMPK was immunolabeled in cochlear sections. In the control animal, immunolabeling for p-AMPK α in OHCs (arrow heads) and IHCs (arrow) was weak. One hour after 98-dB noise exposure, the expression of p-AMPK α was increased in IHCs and OHCs, but was only marginally increased and remained relatively weak within the SGNs and the stria vascularis (Fig. 11c). Western blot using formalin-fixed tissues of the sensory epithelium detected a single band for p-AMPK α at 63 kDa, indicating the specificity of the antibody, although the band density was not altered with noise exposure (Fig. 11b). Since noise increased the activation of AMPK α , we also examined the expression of total AMPK α in cochlear cell types. In the control animal, immunolabeling for AMPK α 1 was primarily localized to supporting cells, such as Deiters' and pillar cells of the organ of Corti. One hour after 98-dB noise exposure, the immunolabeled AMPK α 1 was increased in OHCs, IHCs and pillar cells in the organ of Corti, SGNs, the stria vascularis, including marginal and basal cells, and fibrocytes in the spiral ligament (Fig. 12a). Likewise, AMPK α 2 immunolabeling was also increased in the

nuclei and cytosol of IHCs, OHCs, supporting cells, SGNs, the stria vascularis, and fibrocytes (Fig. 12b)

Inhibition of AMPK α 1 by pretreatment with AMPK α 1 siRNA or pharmacological inhibitor compound C protected against noise-induced outer hair cell loss and permanent hearing loss.

To determine the contribution of AMPK α to NIHL, AMPK α 1 siRNA (siAMPK α 1) was used. First, three concentrations (0.3, 0.6 and 0.9 μ g) of siAMPK α 1 were tested in preliminary *in vivo* experiments; 0.6 μ g was selected for use in this study due to efficiency of siRNA entry into hair cells. As described in Chapter 2, the intratympanic delivery of siRNA resulted in the localization of siRNA specifically within OHCs and minor detection in other cochlear cell types. Surface preparations revealed a 20% reduction in AMPK α 1 levels specifically within OHCs 72 h after treatment with 0.6 μ g of siAMPK α 1, compared to OHCs of mice that received scrambled siRNA (siControl) treatment. We then assessed if silencing AMPK α 1 could diminish 98-dB noise-elevated p-AMPK α in OHCs. Pretreatment with siAMPK α 1 reduced 30% of noise-elevated p-AMPK α in OHCs (Fig. 13a, a'). Furthermore, pretreatment with siAMPK α 1 prevented noise-induced OHC loss to baseline levels at 3 – 3.5 mm and significantly reduced OHC loss by over 55% at 4 – 5.5 mm distances from the apex of the sensory epithelium two weeks after the 98-dB exposure (Fig. 13d). Consequently, auditory threshold shifts of the siAMPK α 1-treated group recovered to near baseline levels at 8 kHz and were attenuated from 50 to 10 dB at 16 and 32 kHz two weeks after 98-dB exposure (Fig. 13b). In addition, the siAMPK α 1 pretreatment significantly reduced auditory threshold shifts by 30 dB at 8 kHz and 20 dB at 16 and 32 kHz after exposure to 106-dB noise (Fig. 13c).

Since silencing AMPK α 1 protected against noise-induced hair cell loss and NIHL, next, the effects of compound C, a selective ATP-competitive inhibitor of AMPK were

examined on noise-induced OHC death and hearing loss. Based on the literature, we tested two concentrations (10 and 20 mg/kg) in adult CBA/J mice (131). Our preliminary results indicated that mice receiving five doses of either concentration have normal bodyweights and hearing thresholds. The fur of treated mice also appeared as shiny as that of control mice and the mice displayed no overt signs of illness. Treatment with either concentration of compound C significantly reduced the auditory threshold shifts at 8, 16 and 32 kHz two weeks after a 98-dB exposure in a dose-dependent fashion (Fig. 13e). Since the higher dose (20 mg/kg) of compound C elicited greater protection, OHC loss was examined in animals treated with this concentration. OHC loss remained lower than 10% throughout the basal region of the cochlea of compound C-treated mice two weeks after 98-dB exposure, in contrast to 40%, 90% and 100% OHC loss which occurred at 4, 5 and 5.5 mm from the apex in the vehicle (DMSO)-treated group (Fig. 13g). Furthermore, treatment with compound C also reduced OHC loss by 50-20% at 4 – 5.5 mm from the apex (Fig. 13h) and attenuated 106-dB noise-induced auditory threshold shifts by 30, 15 and 20 dB at 8, 16 and 32 kHz 2 weeks after the exposure (Fig. 13f). However, treatment with compound C did not alter 106-dB noise-induced IHC loss (Fig. 13i).

Inhibition of AMPK α 1 via AMPK α 1 siRNA or Compound C prevented noise-induced loss of inner hair cell synaptic ribbons and decline of wave I amplitudes.

In order to determine if blockade of AMPK α 1 activation by siRNA or compound C can attenuate noise-induced loss of IHC synaptic connections, ribbons were counted one hour after, or ABR wave I amplitude was measured two weeks after noise exposure. Exposure to 98-dB noise significantly reduced synaptic ribbon counts by 50% one hour after the exposure, but the loss recovered to a level comparable to that of unexposed

controls 14 days later (Fig. 15a). Due to the significant recovery at 14 days after exposures, the protection of synaptic ribbons was only examined after the 106 dB noise exposure. The 106-dB noise exposure decreased CtBP2-labeled synaptic ribbons on IHCs of surface preparations at 22 kHz (corresponding to a location 3 mm from the apex) by 70% one hour after the exposure compared to unexposed controls. Pretreatment with siAMPK α 1 prevented loss of synaptic ribbons by 50% (Fig. 14a, b). Additionally, noise exposure caused a wide dispersion of synaptic ribbons along the IHC longitudinal axis, which was prevented with siAMPK α 1 pretreatment (Fig. 14c). Although 106-dB noise exposure induced synaptic ribbon loss, this loss was also partially recovered by 14 days after the exposure, but remained significantly lower than unexposed controls (Fig. 15b). Pretreatment with siAMPK α 1 still significantly protected against the synaptic ribbon loss at 5, 8, 22 and 32 kHz, at a timepoint 14 days after the exposure (Fig. 15c). ABR wave I amplitudes were examined 14 days after exposures at 8 kHz (1 mm from apex) and 16 kHz (2.4 mm from apex) in order to avoid regions of hair cell loss (132). Fourteen days after exposure to 106 dB noise, the wave I amplitudes were significantly decreased at sound intensities of 70 – 100 dB at 8 and 16 kHz, compared to baseline controls. At 8 kHz, pretreatment with siAMPK α 1 elevated the amplitude at 100 dB by greater than 3-fold (Fig. 15d). The decline of wave I amplitudes was also prevented at 16 kHz at 100 dB (Fig. 15e). Furthermore, treatment with compound C reduced the noise-induced loss of synaptic ribbons per IHC by 50% one hour after 106-dB noise exposure (Fig. 14d, e) and increased wave I amplitudes by 2-fold at 8 kHz at intensities of 90 dB and 100 dB SPL compared to noise-exposed groups at 14 days (Fig. 15f).

Noise-induced hearing loss was exacerbated in AMPK α 1-KO mice, but not outer hair cell and synaptic ribbon loss.

To explore the pathological consequences of AMPK activation in NIHL, AMPK α 1-knockout (AMPK α 1-KO) mice were used (128). The knockout of AMPK α 1 resulted in an 80% reduction of p-AMPK α compared to WT littermates 1 hour after a 98-dB noise exposure (Fig. 16e). Despite the knockout of the α 1 isoform, AMPK α 1-KO mice had normal baseline auditory thresholds. Permanent threshold shifts were induced by 94, 98 and 106 dB SPL noise exposures as determined 2 weeks after the exposure. The 94-dB noise exposure induced permanent threshold shifts of 30 dB at 16 and 32 kHz in both AMPK α 1-KO and –WT mice 14 days after the exposure (Fig. 16a). Exposures to noise at both 98 and 106 dB SPL resulted in higher auditory threshold shifts for AMPK α 1-KO mice at 32 kHz compared to WT mice under the same conditions (Fig 16b, c). The 32 kHz threshold shifts of AMPK α 1-KO mice were increased against AMPK α 1-WT mice by 30 to 45 dB and 60 to 70 dB 14 days after 98 and 106 dB exposures, respectively. Despite the threshold shifts, OHC loss was not altered in the cochlea of AMPK α 1-KO mice compared to WT mice 2 weeks after 98 dB exposure (Fig. 16d). Furthermore, the number of synaptic ribbons at the middle turn (2.5 – 3.5 mm from the apex) did not differ between AMPK α 1-KO and –WT mice 1 h after a 106 dB exposure, even though the noise exposure decreased CtBP2-labeled synaptic ribbons of WT mice by 50% compared to unexposed WT controls (Fig. 17a, b).

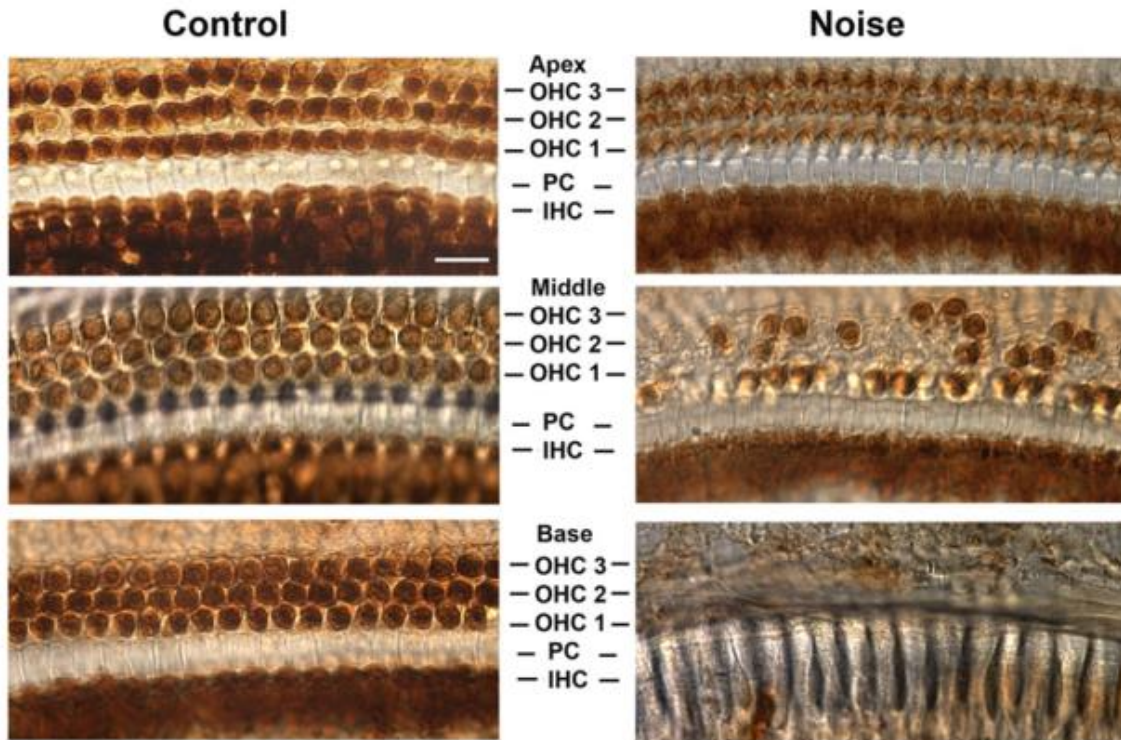


Figure 7. Noise exposure caused a base-to-apex gradient of outer hair cell loss. Representative images of DAB-stained myosin VIIa immunolabeled hair cells document that OHC losses increase as a function of distance from the apex 14 days after noise exposure at 106 dB SPL. Significant IHC losses also occurred in the base.

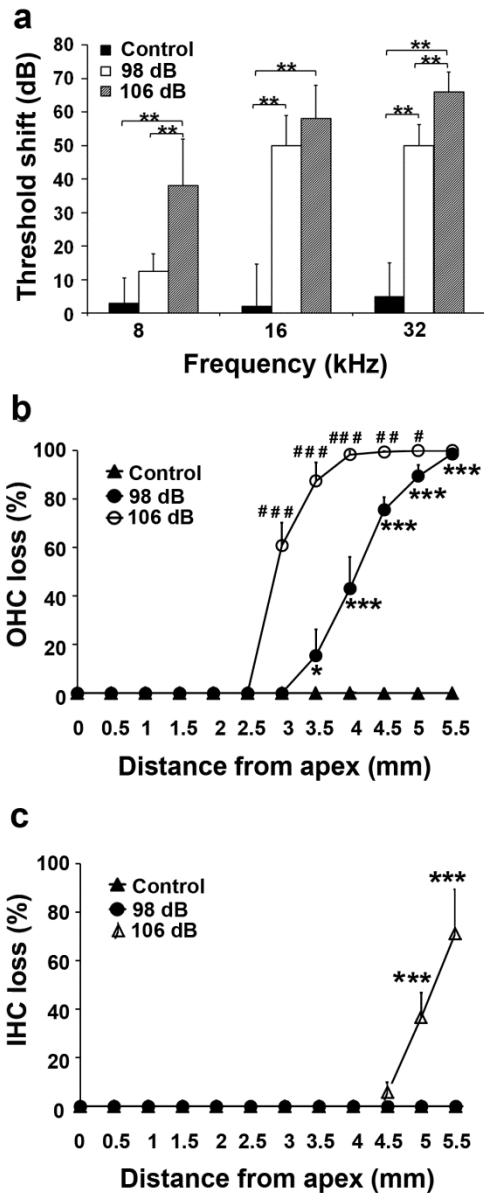


Figure 8. Noise exposure induced permanent hearing loss and hair cell loss in adult CBA/J mice. (a) 98 and 106 dB SPL noise exposure induced significant auditory threshold shifts at 8, 16, and 32 kHz as detected 14 days after the exposures. $n = 25$. **(b)** Quantification of OHC loss 14 days after the exposures confirmed significant OHC loss with 106 dB SPL versus 98 dB SPL. 98 dB: $n = 7$; 106 dB: $n = 3$. **(c)** 106 dB SPL noise results in IHC losses in the basal turn. $n = 5$. Data are presented as means + SD. $*/# p < 0.05$, $**/#\# p < 0.01$, $***/\#\#\# p < 0.001$.

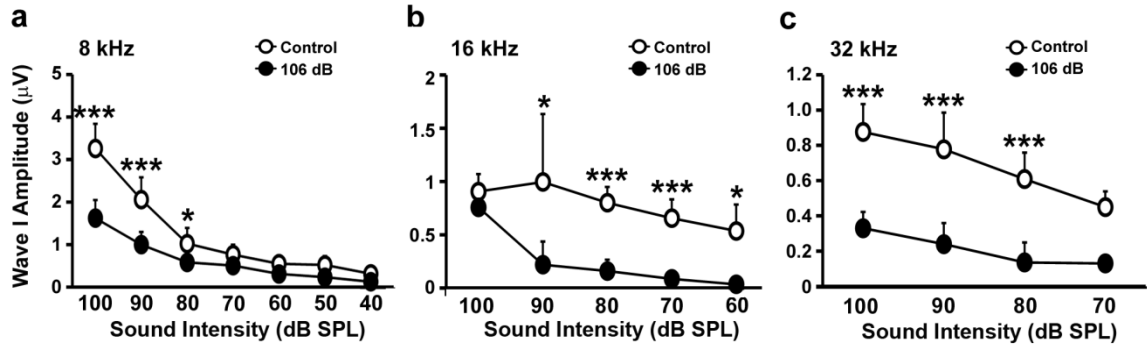


Figure 9. Noise exposure reduced the summed activity of auditory nerve fibers. (a, b, c) 106 dB SPL noise reduced the wave I amplitude at 8 kHz **(a)** at sound intensities of 100, 90 and 90 dB SPL, at 16 kHz **(b)** at sound intensities of 90, 80, 70 and 60 dB SPL, and at 32 kHz **(c)** at 100, 90, 80 and 70 dB SPL, 14 days after the exposure. Data **(a, b, c)** are presented as means + SD, *** $p < 0.001$, * $p < 0.05$.

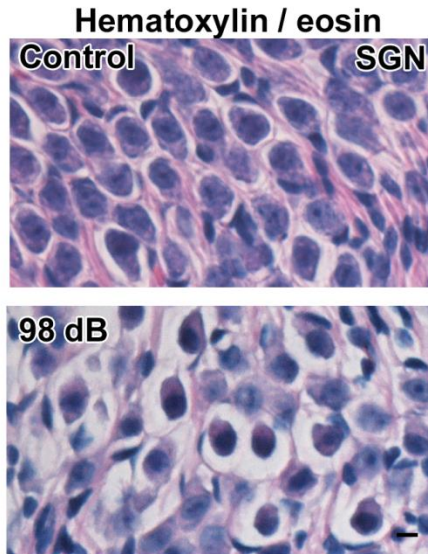


Figure 10. Noise exposure caused swelling of spiral ganglion neurons. Sections of the adult CBA/J mouse inner ear showed swelling of spiral ganglion neurons 1 h after 98 dB noise exposure. The swelling of noise-exposed spiral ganglion neurons is displayed by the non-stained (white) regions. The nuclei of the SGNs are labeled blue by hematoxylin and the cytoplasm can be viewed as pink by the eosin stain. Representative images were taken from the basal turn, scale bar = 10 μm .

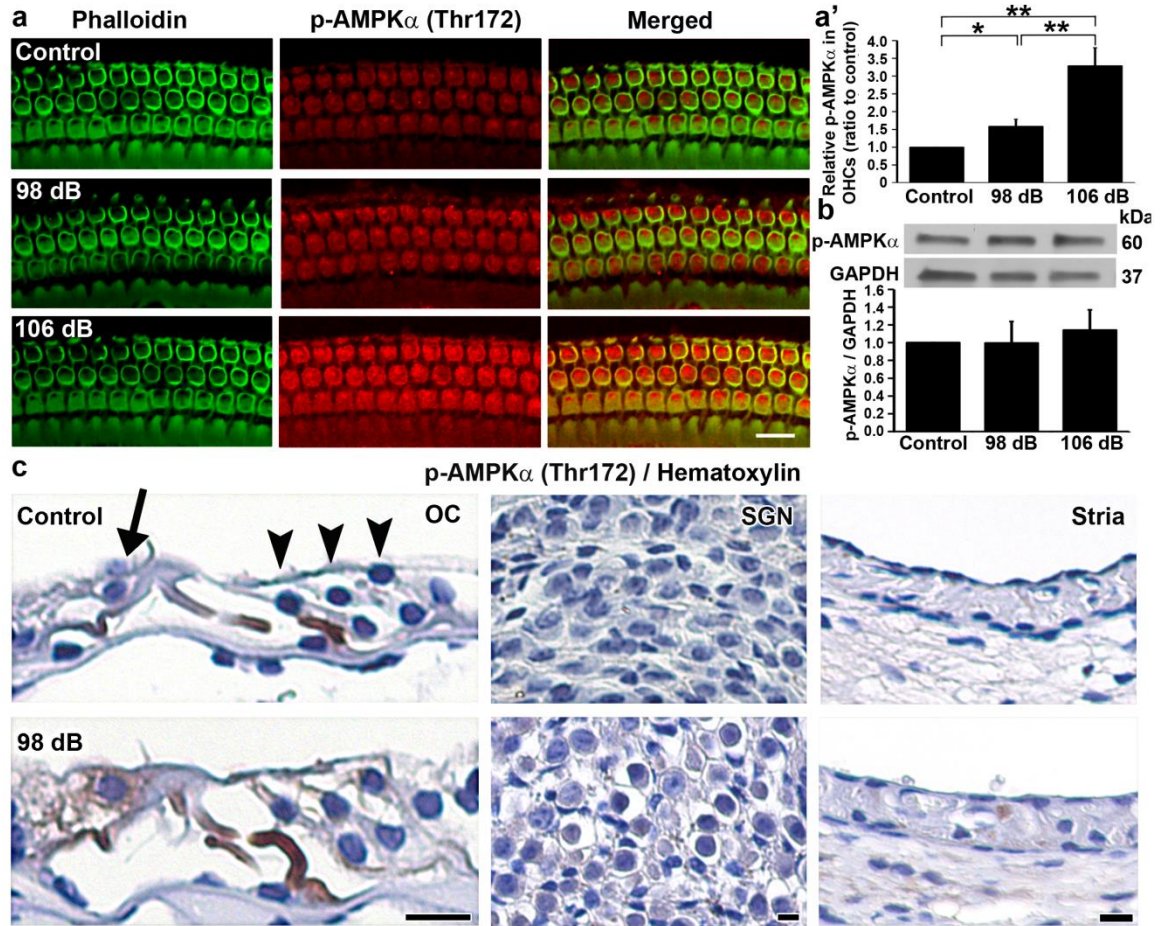


Figure 11. Noise exposure increased p-AMPK α in basal outer and inner hair cells intensity-dependent manner.

(a) The p-AMPK α (red) immunolabeling was stronger in basal OHCs with phalloidin staining (green) 1 h after exposure to 98 and 106 dB noises than unexposed controls.

(a') Immunolabeling of p-AMPK α in basal OHCs was significantly increased in a noise intensity-dependent fashion. Control: $n = 4$; 98 dB: $n = 3$, 106 dB: $n = 4$.

(b) Western blot using sensory epithelium tissues displayed no difference in band densities of p-AMPK α (60 kDa) 1 h after 98 and 106 dB exposures compared to controls. GAPDH served as the loading control. $n = 4$.

(c) Sections of the adult CBA/J mouse inner ear revealed increased DAB-stained immunolabeling of p-AMPK α (brown) in IHCs (arrow) OHCs

(arrowheads) of the organ of Corti, but no obvious changes were detected in spiral ganglion neurons and stria vascularis 1 h after 98 dB noise exposure. Representative images (**a**, **c**) were taken from the basal turn, scale bar = 10 μm . Data (**a'**, **b**) are presented as means + SD, ** $p < 0.01$, * $p < 0.05$.

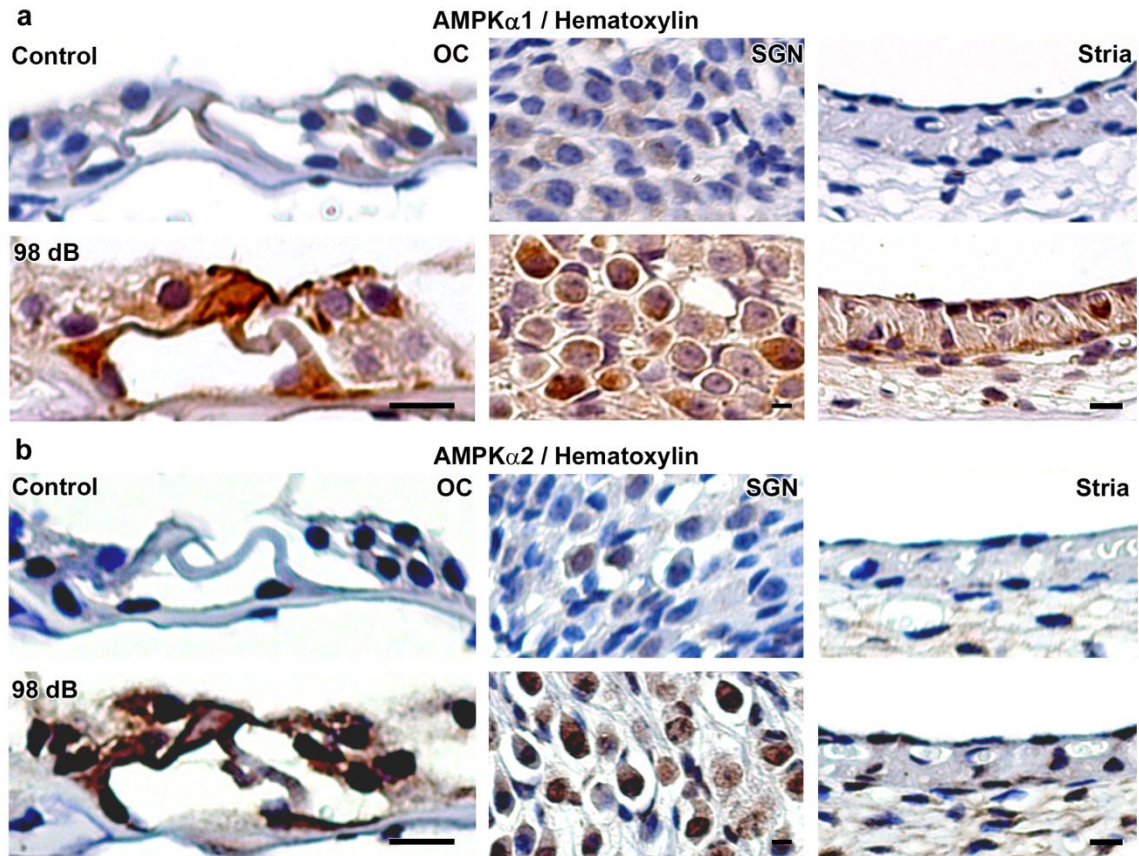


Figure 12. Noise exposure increased total AMPK α 1 and 2 in the organ of Corti. (a, b) Sections of the normal adult CBA/J mouse inner ear revealed increase in DAB-stained immunolabeling of total AMPK α 1 (**a**) or AMPK α 2 (**b**) (brown) in the organ of Corti, including in OHCs, IHCs, inner and outer pillar cells, spiral ganglion neurons, marginal and basal cells of stria vascularis, and fibrocytes of spiral ligament 1 h after 98 dB noise exposure. AMPK α 1 was mainly localized in cytosol, while AMPK α 2 was predominantly localized in the nuclei. Representative images were taken from the basal turn, scale bar = 10 μ m.

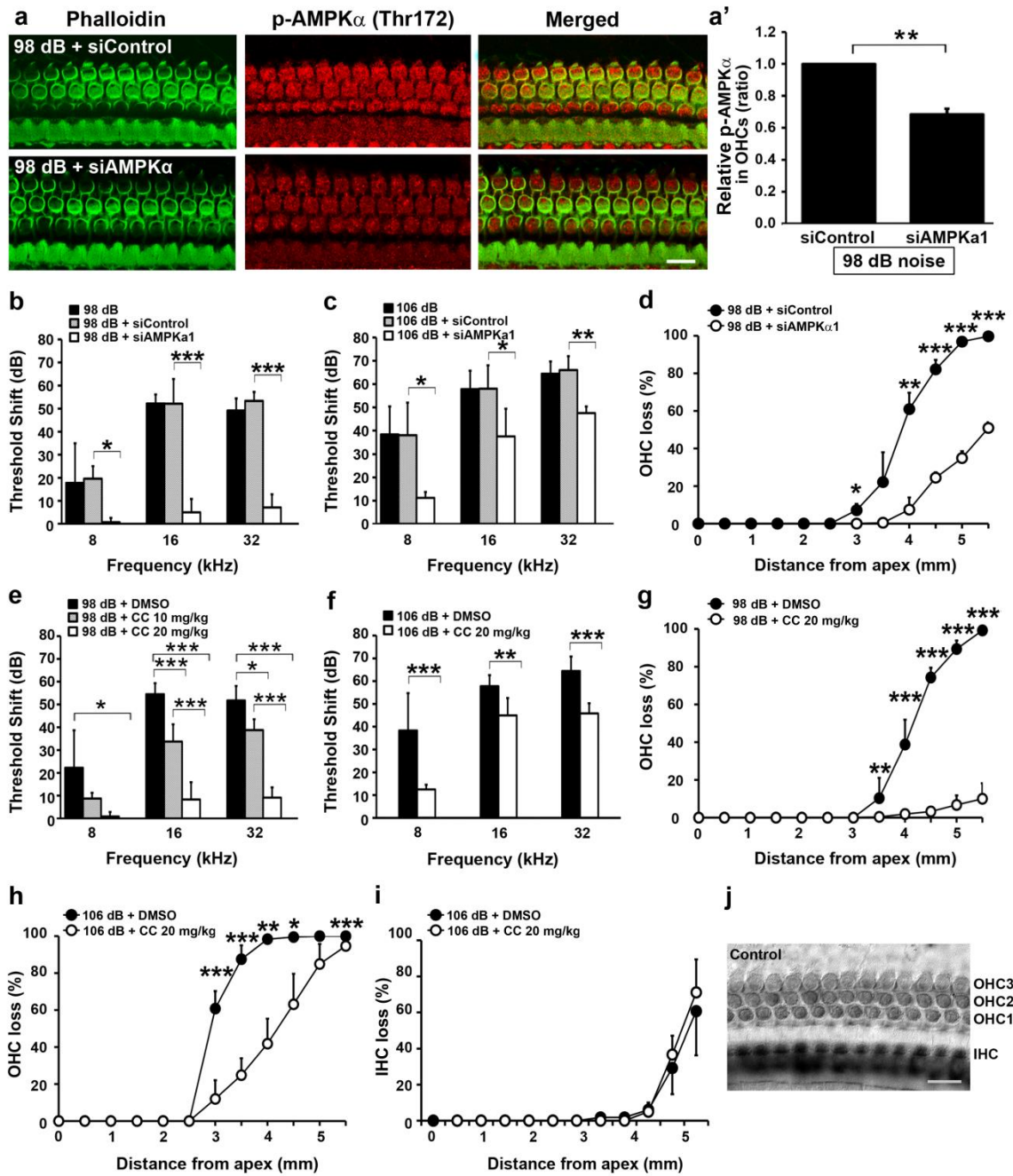


Figure 13. Inhibition of AMPK α 1 by siRNA and compound C protected against noise-induced hearing loss and outer hair cell loss. (a) Treatment with siAMPK α 1 decreased noise-induced immunolabeled AMPK α 1 (red) in OHCs (labeled with phalloidin staining in green) compared to siControl treatment 1 h after 98-dB exposure. .

Representative images were taken from the basal turn, scale bar = 10 μ m. **(a')** Quantification of AMPK α 1 in OHCs confirmed a significant decrease. $n = 3$. **(b, c)** siAMPK α 1 pretreatment reduced 98 and 106 dB noise-induced permanent threshold shifts. 98 dB: $n = 18$; 98 dB + siControl: $n = 8$; 98 dB + siAMPK α 1: $n = 7$; 106 dB: $n = 6$; 106 dB + siControl: $n = 3$; 106 dB + siAMPK α 1: $n = 4$. **(d)** Noise-induced (98 dB) OHC loss was reduced by siAMPK α 1 pretreatment. $n = 3$. **(e)** Compound C treatment reduced 98 dB noise-induced permanent threshold shifts in a dose-dependent fashion. 98 dB + DMSO: $n = 20$; 98 dB + CC 10 mg/kg: $n = 4$; 98 dB + CC 20 mg/kg: $n = 6$. **(f)** Compound C (20 mg/kg) treatment reduced 106 dB noise-induced permanent threshold shifts. $n = 6$. **(g)** Compound C (20 mg/kg) treatment decreased 98 dB noise-induced OHC loss. 98 dB + DMSO: $n = 7$; 98 dB + CC 20 mg/kg: $n = 6$. **(h)** Compound C (20 mg/kg) treatment decreased the extent of 106 dB noise-induced OHC loss. 106 dB + DMSO: $n = 3$; 106 dB + CC 20 mg/kg: $n = 9$. **(i)** Treatment with compound C (20 mg/kg) did not alter 106 dB noise-induced IHC losses. $n = 4$. **(j)** Representative image displays DAB-stained myosin VIIa immunolabeling of sensory hair cells in the basal region of the control CBA/J mouse. Data **(a', b, c, d, e, f, g, h, i)** are presented as means + SD, 14 days after the exposures, *****/###** $p < 0.001$, ****/##** $p < 0.01$, ***/#** $p < 0.05$.

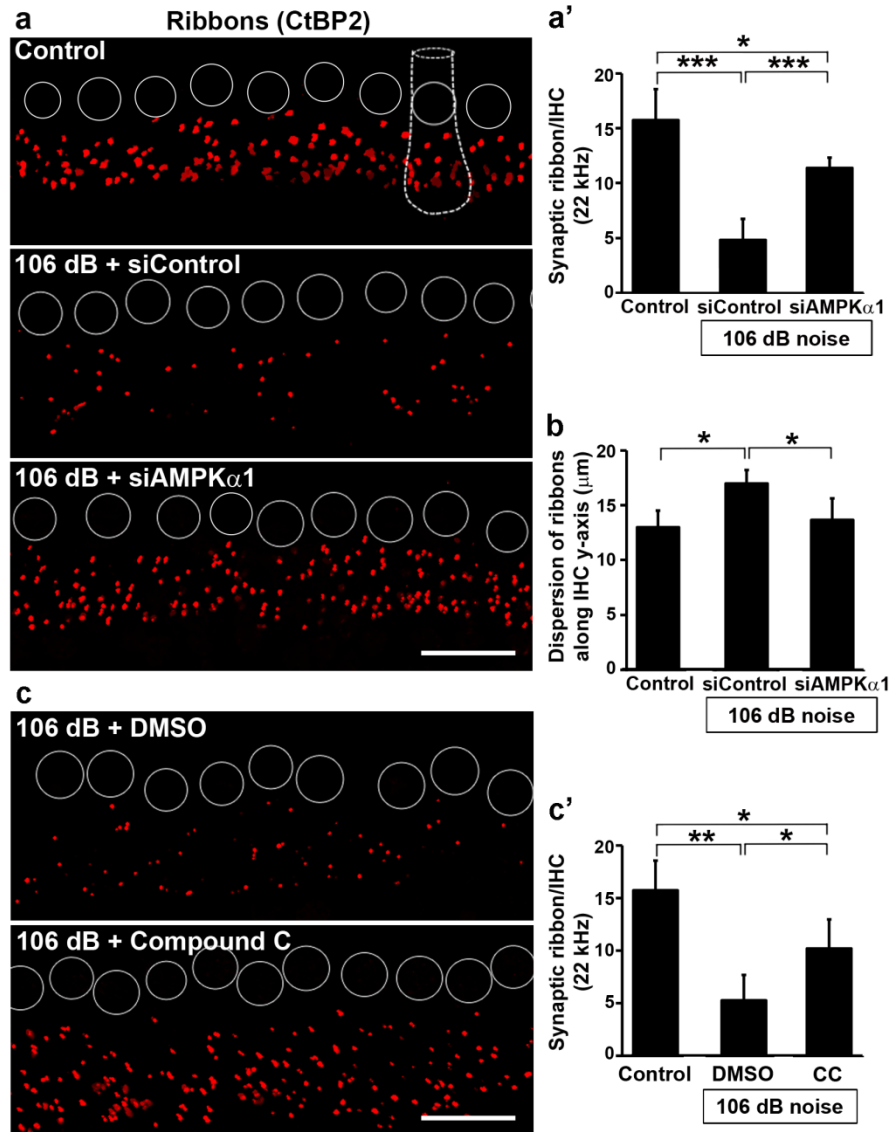


Figure 14. Inhibition of AMPK attenuated noise-induced inner hair cell synaptic ribbon loss at 22 kHz one hour after 106-dB noise exposure. (a) Noise-induced loss of immunolabeled CtBP2 (red) in IHCs was prevented by pretreatment with siAMPK α 1. **(a')** Quantification of CtBP2 immunolabeled ribbon particles in IHCs confirmed that noise-induced reduction of ribbons was partially prevented with siAMPK α 1 pretreatment. $n = 4$. **(b)** Noise-induced dispersion of CtBP2 immunolabeled ribbon particles along the

IHC y-axis returned to baseline levels with siAMPK α 1 pretreatment. $n = 4$. **(c)** Compound C (20 mg/kg) treatment prevented the noise-induced loss of CtBP2 (red) immunolabeled synaptic ribbons in IHCs. **(c')** Quantification of CtBP2 immunolabeled ribbon particles in IHCs confirmed significant increases with compound C (20 mg/kg) treatment. $n = 4$. Representative images **(a, c)** were taken from the 22 kHz region, $n = 4$, scale bar = 10 μ m. Dashed circles represent the outline of IHC nuclei. Data **(a', b, c')** are presented as means + SD, *** $p < 0.001$, ** $p < 0.01$, * $p < 0.05$.

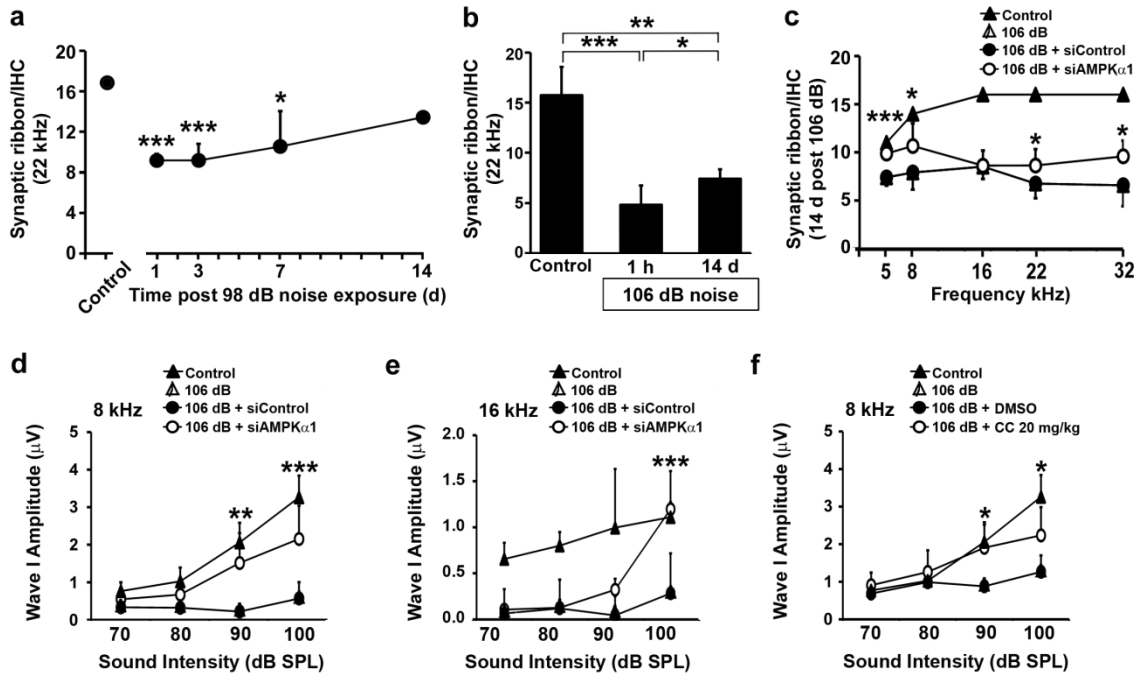


Figure 15. Inhibition of AMPK protected noise-induced synaptopathy and noise-declined auditory nerve activity 14 days after 106-dB exposure. (a) CtBP2 immunolabeled ribbon particles in IHCs at 22 kHz were significantly decreased 1 d after 98-dB noise exposure, but slowly recovered by 14 days after the exposure. $n = 3$. **(b)** CtBP2 immunolabeled ribbon particles in IHCs at 22 kHz were significantly decreased 1 h after 106 dB noise exposure, but the loss partially recovered by 14 d after the exposure. $n = 10$. **(c)** The noise-induced loss of CtBP2 immunolabeled ribbon particles in IHCs were significantly reduced 14 days after 106 dB noise exposure. Pretreatment with siAMPK α 1 increased the number of synaptic ribbon particles at 5, 8, 22 and 32 kHz regions of the sensory epithelium. Control: $n = 4$, 106 dB: $n = 5$, 106 dB + siControl: $n = 5$; 106 dB + siAMPK α 1: $n = 5$. **(d)** Wave I amplitudes were reduced by 106 dB noise exposure at sound intensities of 70 – 100 dB at 8 kHz. Pretreatment with siAMPK α 1 elevated the wave I amplitude at sound intensities of 90 and 100 dB SPL. Control: $n = 10$; 106 dB + siControl: $n = 8$; 106 dB + siAMPK α 1: $n = 4$. **(e)** The reduction of wave I

amplitude by 106 dB noise was decreased by pretreatment with siAMPK α 1 at sound intensities of 90 and 100 dB SPL at 16 kHz. Control: $n = 10$; 106 dB + siControl: $n = 6$; 106 dB + siAMPK α 1: $n = 4$. **(f)** The decrease of wave I amplitudes by 106 dB noise was reduced by compound C (20 mg/kg) treatment at sound intensities of 90 and 100 dB SPL at 8 kHz. Control: $n = 10$; 106 dB + DMSO: $n = 14$; 106 dB + CC 20 mg/kg: $n = 4$. Data are presented as means + SD, *** $p < 0.001$, ** $p < 0.01$, * $p < 0.05$. For Data (c, d, e, f), *: 106 dB + siControl vs 106 dB + siAMPK α 1.

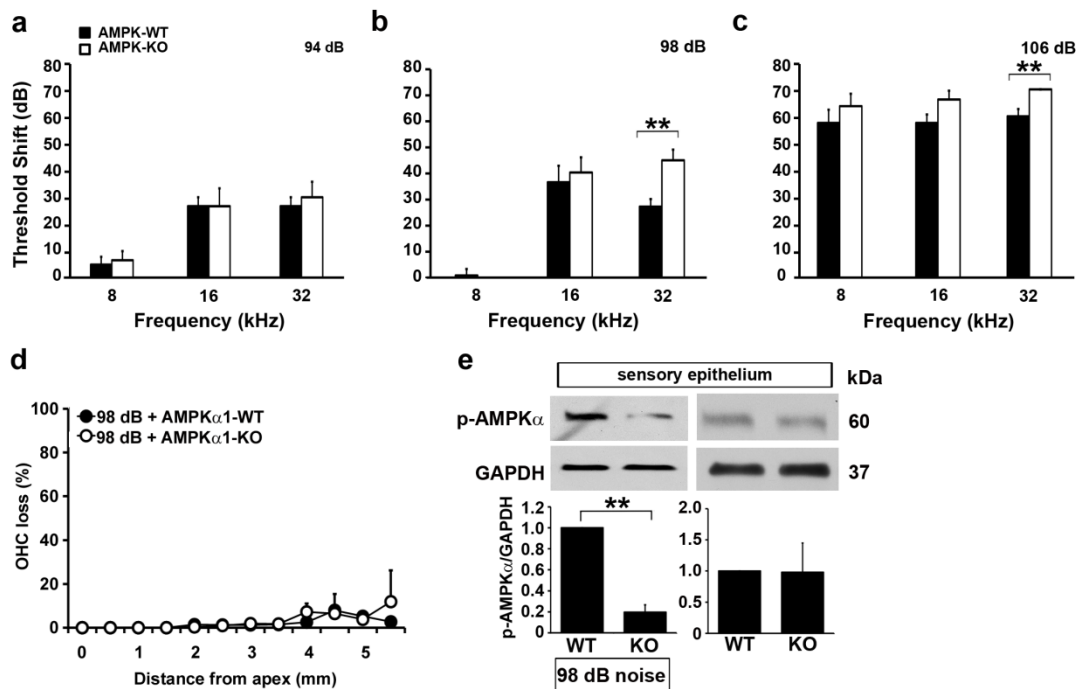


Figure 16. AMPK α 1-KO mice exacerbated noise-induced hearing loss. (a) The 94 dB SPL noise-induced permanent threshold shifts remained unchanged between AMPK α 1-KO and -WT mice 14 days after the exposure. $n = 3$. **(b)** The 98 dB SPL noise-induced threshold shifts were increased at 32 kHz in AMPK α 1-KO mice compared to WT counterparts as determined 14 days after the exposure. $n = 5$. **(c)** The 106 dB SPL noise-induced threshold shifts were increased at 32 kHz in AMPK α 1-KO mice as determined 14 days after the exposure. $n = 8$. **(d)** Noise-induced (98 dB) OHC loss was not altered by AMPK α 1-KO. $n = 6$. **(e)** The levels of p-AMPK α protein were reduced in sensory epithelium tissues of AMPK α 1-KO mice compared to WT counterparts exposed to 98 dB SPL, but remained unchanged between unexposed AMPK α 1-KO and -WT mice. $n = 4$. Data are presented as means + SD, ** $p < 0.01$, * $p < 0.05$.

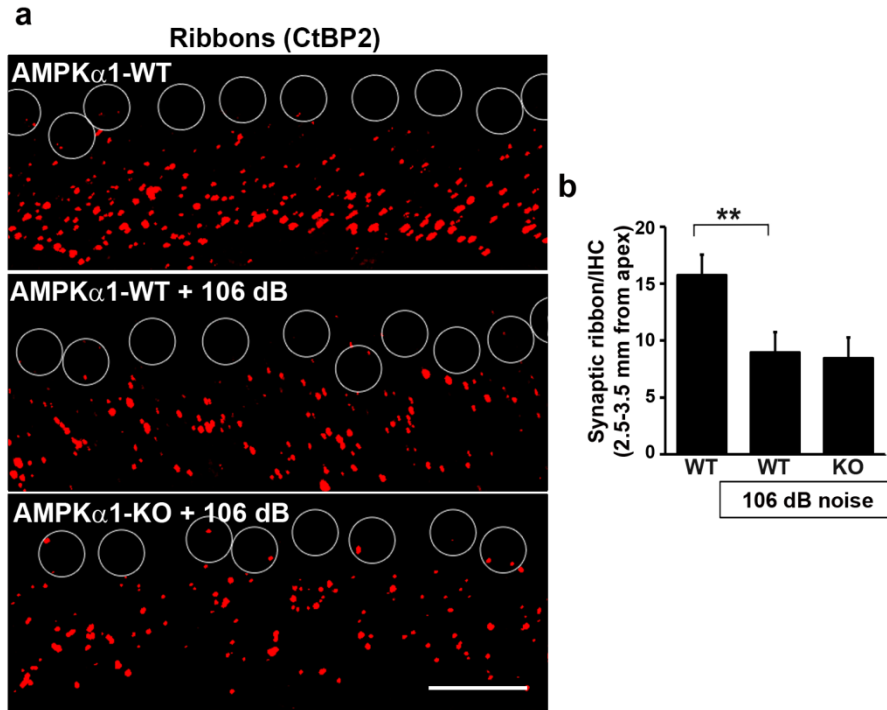


Figure 17. Noise-induced inner hair cell synaptic ribbon loss was not altered by AMPK α 1-KO. (a) The CtBP2-immunolabeled synaptic ribbons (red) in IHCs were reduced by 50% at 22.6 kHz 1 h after exposure to noise at 106 dB compared to unexposed cochlea. AMPK α 1-KO did not alter the synaptic ribbon number compared to WT mice under exposed or unexposed conditions. (b) CtBP2 immunolabeled ribbon particles in IHCs were decreased 1 h after 106 dB noise exposure, but remained unchanged by AMPK α 1-KO mice. AMPK α 1-WT: $n = 3$; 106 dB + AMPK α 1-WT: $n = 4$; 106 dB + AMPK α 1-KO: $n = 4$. Data are presented as means + SD, ** $p < 0.01$, * $p < 0.05$.

Discussion

Our results demonstrate for the first time that noise-induced phosphorylation of AMPK α in sensory hair cells mediates NIHL by increasing losses of synaptic ribbons and OHCs. Accordingly, agents that inhibit the activation of AMPK attenuated the loss of synaptic ribbons and OHC, and subsequently NIHL. The noise-intensity dependent increase of p-AMPK α 1 is in line with our previous reports (39, 40) and provides support for the concept of AMPK activation inducing hair cell death and NIHL. Additionally, total AMPK α 1 and AMPK α 2 increase with noise exposure and are predominantly localized in OHCs and IHCs as well as supporting cells such as Deiters and pillar cells, SGNs and stria vascularis. Noise-induced increases in total AMPK α 1 and α 2 may provide sufficient levels of kinase for phosphorylation; however, it is not clear if such an increase is due to overexpression of the AMPK α gene or a decrease in protein degradation. An earlier report detected expression of AMPK α 1 mRNA only in OHCs, but not IHCs (128), suggesting that noise-induced elevation of AMPK α 1 in IHCs may not be related with gene expression. AMPK α 1 was primarily localized in the cytosol, while AMPK α 2 was localized in both the cytosol and nuclei. This isoform specific subcellular localization implies potential alterations in function. Since AMPK α 2 is found localized in the nuclei, it is possible that this isoform is able to directly phosphorylate transcription factors and alter gene expression, while the α 1 isoform may have less of an impact on gene expression and more of an effect in short term changes, such as the alteration of protein activity.

Our evidence further supports the notion that AMPK activation leads to cell death. Since similar functional protection was achieved by both pharmacological inhibition and genetic silencing of AMPK α , we can conclude that treatment with siAMPK

or Compound C provides protection against noise-induced stimuli through its inhibition of AMPK. It is surprising that pretreatment with siAMPK α 1 reduces 98-dB thresholds shifts by 80% at 16 and 32 kHz with only 20% reduction of AMPK α 1 and 30% reduction of noise elevated p-AMPK α levels detected in OHCs. This indicates that a specific partial inhibition of AMPK α 1 in OHCs is sufficient for prevention of noise-induced outer hair cell loss and NIHL. Additionally, the activation of AMPK may alter multiple cellular targets that result in an augmented effect (116). It is also logical that treatment with compound C provides greater protection against noise-induced OHC losses compared to siAMPK α 1 pretreatment, which only targets the α 1 isoform. Still, Compound C and siAMPK α 1 treatment does not reduce 106 dB noise-induced IHC losses, highlighting the severe damaging effect of the noise intensity-dependent activation of AMPK and the potential influence of multiple cell death pathways that may circumvent AMPK activation. For example, we previously described the modulation of noise-induced OHC apoptosis and necrosis by caspases and RIP-kinases, respectively. Inhibition of either pathway shifts the prevalence of OHC death to the alternative pathway (39), supporting the concept that multiple targets are necessary to comprehensively alter cell fate, especially for the severe damage.

Our results are the first to implicate the activation of AMPK as a key initial mediator affecting synaptic ribbons and functional deficits. Inhibition of AMPK either via siAMPK α 1 or Compound C reduces the extent of 106 dB noise-induced IHC synaptic ribbon loss one hour and 14 days after exposures and protects against the decline of wave I amplitudes associated with IHC synaptic density (19). The protection of synaptic ribbons may contribute to the protection of auditory thresholds at 8 kHz without corresponding loss of OHCs and IHCs (132, 133). Additionally, noise-induced synaptic ribbon dispersion is in line with Liberman's study (130). Our results demonstrate that

such dispersion is also prevented by inhibition of AMPK by siRNA. This spatial disruption may have significant functional implications since functional synapses require the juxtaposition of pre-synaptic ribbons against post-synaptic terminals of auditory nerve fibers. Although the post-synaptic terminals were not detected in this study, it is likely that this synaptic ribbon dispersion is also associated with an increase in the number of “orphan” ribbons and post-synaptic terminals that are non-functional. Additionally, both 98 and 106 dB exposures result in IHC synaptic ribbon loss that partially recovers over time, suggesting that noise-induced synaptopathy is reversible at least to some extent with the moderate noise damage. This contrasts with a previous report which showed no significant recovery between 24 hours and 14 days post-exposure (130). This discrepancy may be due to the variability of mouse strain. All of this evidence suggests that AMPK may be a target for prevention of noise-induced synaptopathy.

Although pretreatment with siAMPK α 1 or the pharmacological inhibitor compound C attenuates noise-induced losses of synaptic ribbons and OHCs and NIHL in CBA/J mice, AMPK α 1-KO C57BL/6/J mice exacerbated NIHL at both 98 and 106 dB SPL, but not at noise conditions (90 - 94 dB SPL) that induces temporary or mild threshold shifts (less than 30 dB). This is in line with previous reports showing impairment of auditory threshold recovery after exposure to noise that causes temporary threshold shifts in AMPK α 1-KO mice compared to -WT mice (128). These differences in lack of protection against NIHL in C57BL/6 and the excellent protection elicited by siRNA and compound C are probably related to strain-dependent changes. The AMPK α 1-KO mice are on a C57BL/6 background and are thus not comparable to the CBA/J strain used for the siRNA and compound C studies. The C57BL/6 strain is characterized by an early onset age-related hearing loss that can develop as early as 1 – 6 months of age. This phenotype is caused by the presence of a homozygous recessive *ahl* mutation of

cadherin 23, which results in a splice variant that alters the stability and formation of stereocilia tip links necessary for mechanotransduction. To avoid the accelerated age-related hearing loss that is associated with this strain, the experiments with the C57BL/6 mice were conducted at a younger age of seven weeks, as opposed to three months of age for CBA/J mice. This modified noise model results in threshold shifts of 35 and 30 dB at 16 and 32 kHz two weeks after a 98-dB noise exposure, contrasting with the 50 dB threshold shifts induced in CBA/J mice at three months of age. Age-matched comparisons of responses to noise exposures between the two strains were not made; therefore, we cannot comment on the noise susceptibilities between the C57BL/6 versus CBA/J mice with our noise conditions. However, other groups demonstrate that C57BL/6 mice are more susceptible to NIHL compared to age-matched CBA/J at older ages of five to seven months due to the increased auditory degeneration associated with the accelerated age-related hearing loss of the C57BL/6 strain (134). Still, it is clear that the seven-week old C57BL/6 model used in this study induces a lower level of hearing loss compared to the three-month old CBA/J model. This was also accompanied by lower levels of hair cell losses.

The inconsistencies between the siRNA, compound C and knockout studies also point to the intrinsic differences between the two methods of inhibition, in which siRNA silencing transiently inhibits the expression of a gene, while a knockout eliminates gene function for the animal's entire lifespan. This fundamental difference is significant as it can affect the outcome of the gene knockdown or knockout. For example, the outcome of prolonged versus acute exposure to AMPK inhibition is different. A partial reduction of AMPK, modeled by silencing and pharmacological inhibition, may prevent the noise-induced imbalance of AMPK α 1 signaling, whereas abolishment of cellular AMPK by knockout of AMPK α 1 alters other molecular events as well. Since AMPK is traditionally

considered a protective enzyme that maintains cellular energy levels, we speculate that noise insults initially trigger a protective response which may convert into a pathological response with a hyper-elevated activation of AMPK. In line with this hypothesis, the knockout of AMPK α 1 would eliminate all functions, including initial protective responses of AMPK, which may contribute to the deterioration of auditory sensitivity. The efficiency of our protection strategies support this premise, with Compound C, a drug that targets both AMPK α isoforms acutely, being the most effective, followed by AMPK α 1 siRNA, which targets the α 1 isoform acutely and finally no protection elicited by the elimination of the α 1 isoform in AMPK α 1-KO mice.

Despite the worsening of hearing function, the knockout of AMPK α 1 does not alter noise-induced losses of OHCs and synaptic ribbons. In fact, noise-induced OHC loss is minimal at less than 10% loss, even at the very basal regions of the cochlea, implying that sensory hair cell deficits may play a minor role in the pathology induced by AMPK α 1-KO mice and suggesting alteration of other molecular events, such as the abundance of BK channels in OHCs, in exacerbating NIHL (128). Alternatively, we speculate that the absence of protection by AMPK α 1-KO mice may be caused by an overcompensation of the other AMPK α 2 isoform. Since compound C is not specific for a particular AMPK α isoform, this overcompensation effect could be tested by pharmacological treatment of AMPK α 1-KO mice. If our hypothesis is true, treatment with compound C should protect against NIHL in AMPK α 1-KO mice due to its ability to decrease AMPK α 2 activity. Furthermore, the separate isoforms may also differ in subcellular localization, targets and/or sensitivity to AMP, thus altering the response of AMPK α 1-KO mice to noise insults. Sections show AMPK α 1 predominantly localized in the cytosol of the cells of the cochlea, while the AMPK α 2 isoform is found in both the nucleus and cytoplasm. This difference in distribution implies potential alterations in

function. Since AMPK α 2 is found localized in the nuclei, it is possible that this isoform is able to directly phosphorylate transcription factors and alter gene expression, while the α 1 isoform may have less of an impact on gene expression and more of an effect in short term changes, such as the alteration of short term protein activity.

In agreement with the literature, AMPK α 1 and 2 is also localized in the exposed stria vascularis, mainly in the marginal cells and basal cells, where p-AMPK α has been strongly detected post noise exposure in previous studies (47). The marginal cells of the stria vascularis have high energy requirements due to the abundant expression of sodium-potassium-ATPase (Na⁺-K⁺-ATPase) (135). To drive the active transport of ions across the membranes, these cells contain a large number of mitochondria to generate the necessary ATP (136). A transient cochlear ischemia inhibits the expression of Na⁺-K⁺-ATPase and connexin 26, a marker for gap junctions through which K⁺ ions are cycled, and subsequently reduces the endocochlear potential (137).

AMPK α 1 and α 2 are also strongly increased within the SGNs, which is accompanied by swelling of the neuronal bodies. This is in line with reports in the literature which demonstrate the swelling of afferent ribbon synapses, followed by degeneration of SGNs at later times. Pathological cellular swelling is commonly associated with an unregulated flux of cations, such as Na⁺, due to the failure of extrusion mechanisms that require ATP. Along with this influx of cations, anions are also driven into the cell, which subsequently drives the influx of water, causing the cell body to swell. The primary extrusion mechanism to maintain a cation balance in neuronal cells is Na⁺-K⁺-ATPase. Due to the energy-dependence of the extrusion pump, a depletion of ATP in spiral ganglion neurons would reduce the active transport of cations out of the cells and result in cellular swelling. Especially under noise-induced excitotoxic conditions, high levels of glutamate released at the ribbon synapses activate N-methyl-

D-aspartate (NMDA) receptors which trigger the opening of non-selective cation channels. The survival of the SGNs depends upon ATP to maintain the homeostatic balance of the ATP-dependent extrusion pumps and the influx of non-selective cations (138).

This evidence points to the stria vascularis, spiral ligament and spiral ganglion neurons as potential sites for AMPK-mediated pathology that we have not yet investigated since energy metabolism plays a critical role in the recycling of ions for the endolymph as well as the ionic balance of SGNs after excitotoxic injury. Overall, the results from this chapter point out a novel target for future development of drugs to prevent or ameliorate NIHL and noise-induced cochlear synaptopathy.

CHAPTER FOUR: AMPK ACTIVATION BY LKB1 VIA CELLULAR ATP REDUCTION

Introduction

Liver kinase B1 (LKB1) is an upstream serine/threonine kinase of AMPK which phosphorylates the enzyme under low energy levels (139). LKB1 activity is regulated by the adaptor protein Ste20 Related Adaptor (STRAD) and the scaffolding protein Mouse Protein 25 (MO25), which exist in a 1:1:1 intracellular ratio (140). STRAD is a pseudokinase which allosterically binds the kinase domain of LKB1, while MO25 stabilizes the LKB1 activation loop by interacting with both LKB1 and STRAD. This leaves the active site of LKB1 accessible, which is required for its kinase activity. The formation of a stable heterotrimeric LKB1/STRAD/MO25 complex translocates LKB1 from the nuclei to the cytosol, where it exerts its serine/threonine kinase activity on AMPK, when bound by AMP (141) (Fig. 18). A specific mechanism for the regulation of the activation and inactivation of this heterotrimeric complex is yet unknown. The C-terminal region of LKB1 contains several post-translational phosphorylation sites, including Serine 428 (S428). The phosphorylation of LKB1 at this site increased the phosphorylation of AMPK, while its mutation abolished AMPK activation (142). Moreover, the phosphorylation at S428 has been implicated as an important nucleotranslocation signal, for LKB1 to be actively exported out of the nucleus (142, 143). In addition to AMPK, LKB1 directly phosphorylates a family of 14 various AMPK-related kinases, such as the microtubule affinity regulating kinases (MARKs) (144).

Currently, no research in the field has examined LKB1 in the inner ear or its role in NIHL or other inner ear disorders. In this chapter, the localization of LKB1 was examined and its role in the pathogenesis of NIHL and the noise-induced activation of AMPK was investigated.

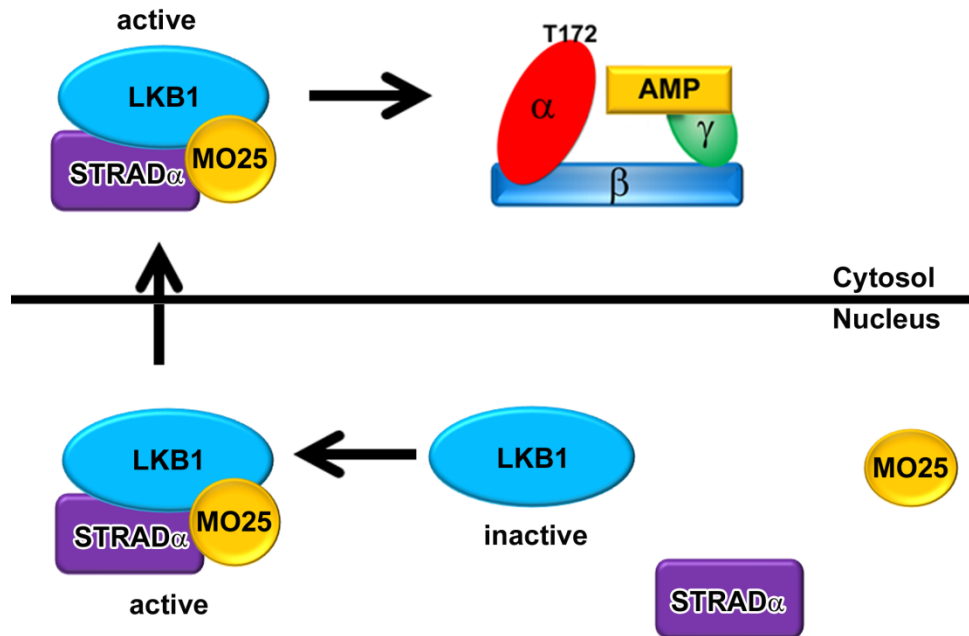


Figure 18. LKB1 activates AMPK. Inactive LKB1 is present in the nucleus and becomes active when bound by its pseudokinase STRAD α and adaptor protein MO25. The stable, active LKB1-STRAD-MO25 complex can receive a phosphorylating nucleotranslocation signal, which allows it to be exported to the cytosol where LKB1 phosphorylates AMPK on threonine 172 of the α -subunit, in the presence of AMP binding of the AMPK γ subunit, increasing the activity of AMPK by about 1000-fold.

Results

Noise exposure increased the phosphorylation of LKB1 in the organ of Corti.

Since liver kinase B1 (LKB1) serves as the primary upstream kinase of AMPK, we examined the phosphorylation of LKB1 (p-LKB1) levels in the cochlea in response to noise insults. Immunoblots of total cochlear homogenates showed a single band for p-LKB1 at the molecular weight of 54 kDa, which was robustly increased 1 h after the exposure (Fig. 19c). No change was detected in total LKB1 levels (Fig. 19d). Increased immunolabeling for p-LKB1 was localized to the nuclei and cytosol of the organ of Corti, mainly in the OHCs, IHCs, Deiters and pillar cells 1 h following the exposure (Fig. 19a). The increased immunolabeling for p-LKB1 in OHC cytosol was quantified on surface preparations, which showed a greater than 2-fold increase in high-frequency OHCs 1 h after the 98 dB exposure compared with controls (Fig. 19b). No increases were detected in low-frequency OHCs. Furthermore, the p-LKB1 was also increased in the spiral ganglion neurons, the basal cells of the stria vascularis and the fibrocytes of the spiral ligament after the exposure (Fig. 19a).

Noise exposure increased the colocalization of LKB1-STRAD α in outer hair cells.

In addition to the phosphorylation of LKB1 at serine 428, the activity of LKB1 can be assessed by colocalization of LKB1 and STRAD α in OHCs since LKB1 is allosterically activated by binding to the pseudokinase STRAD α . Immunolabeling for total LKB1 and total STRAD α in OHCs was increased by over 2-fold and almost 4-fold, respectively, 1 h after 98-dB noise exposure compared to controls (Fig. 20a). The overlap coefficient for LKB1-STRAD α colocalization in OHCs was quantified and displayed a 2-fold increase in 1 h after noise exposure (Fig. 20b).

Pretreatment with LKB1 siRNA reduced noise-induced p-LKB1 in outer hair cells, noise-induced outer hair cells loss and auditory threshold shifts.

Since noise exposure resulted in activation of LKB1 in cochlear tissue, we evaluated the role of LKB1 in NIHL using siRNA silencing techniques. First, pretreatment with 0.6 µg siLKB1 resulted in a 20% reduction of total LKB1 specifically within OHCs and also reduced the phosphorylation of LKB1 caused by 98-dB noise exposure by 25%, compared to scrambled siRNA (siControl) treated groups (Fig. 21a). The siLKB1 pretreatment prevented the extent of noise-induced OHC loss to baseline levels at 3.5 – 4 mm and significantly reduced OHC loss by 50% at 4.5 – 5 mm from the apex (Fig. 21c). This correlated with the reduction of noise-induced auditory threshold shifts from 15 dB to baseline levels at 8 kHz and from 40-50 dB to 5 dB at both 16 and 32 kHz two weeks after the exposure (Fig. 21b).

Pretreatment with LKB1 siRNA attenuated noise-induced losses of inner hair cell synaptic ribbons and ABR wave I amplitudes.

To determine if inhibition of LKB1 activation by siRNA can attenuate noise-induced loss of IHC synaptic ribbons, ribbon particles were counted 1 h after, or wave I amplitude was measured 2 weeks after 106 dB noise exposure. For comparison with the protection of synaptic ribbons by inhibition of AMPK, the 106 dB noise condition was used. Noise exposure decreased CtBP2-labeled IHC synaptic ribbons from the 22 kHz region (corresponding to 3 mm from the apex) by 70% compared to unexposed controls. Pretreatment of siLKB1 prevented noise-induced synaptic ribbon loss. The ribbon count increased from 5 to 8 ribbons per IHC (Fig. 21a, b). ABR wave I amplitudes were examined at 8 (1 mm from apex) and 16 kHz (2.4 mm from apex) to avoid regions where hair cell loss occurred (132). Pretreatment with siLKB1 recovered the noise-reduced

ABR wave I amplitude at 70 and 80 dB at 8 kHz to baseline levels, and elevated the wave I amplitudes by at least 3-fold at 16 kHz (Fig. 22c, d).

Silencing LKB1 reduced the noise-induced activation of AMPK in basal outer hair cells.

To examine whether noise-induced phosphorylation of AMPK α 1 is mediated by LKB1, CBA/J mice were pretreated with siLKB1 72 h prior to noise exposure at 98 dB SPL. Pretreatment with siLKB1 significantly reduced the 98 dB noise-induced immunolabeling of p-AMPK α in basal OHCs by 20% (Fig. 23a, a'), indicating that LKB1 phosphorylates AMPK α 1.

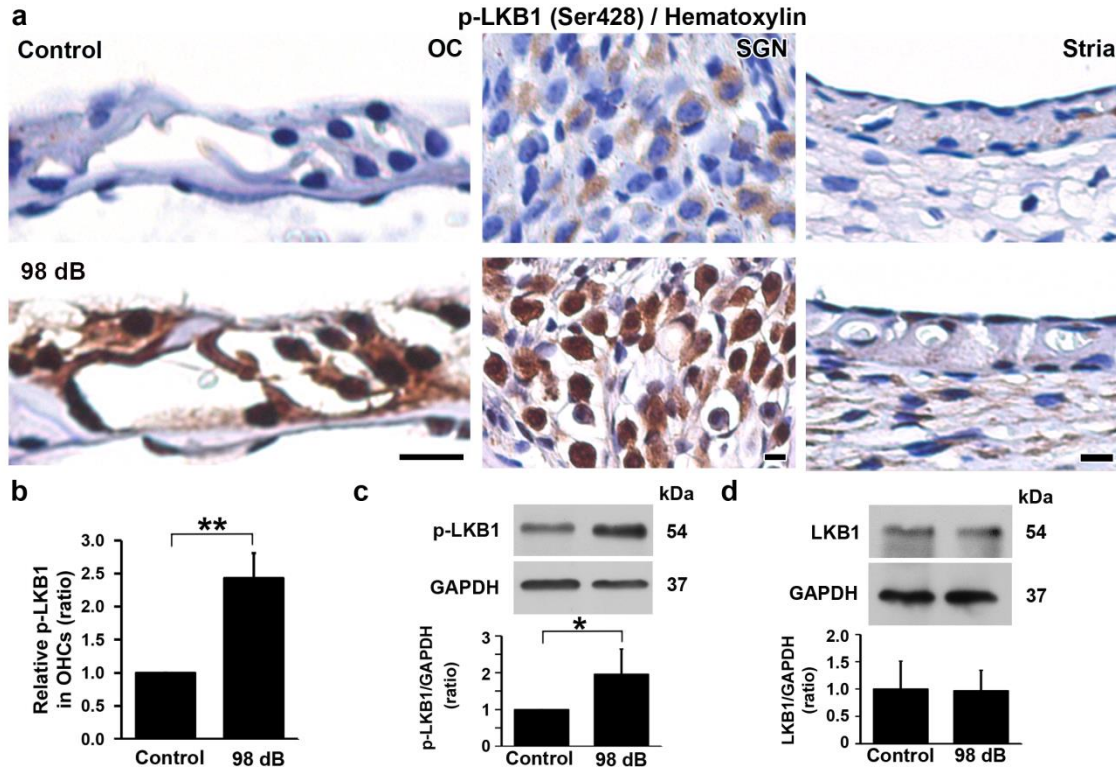


Figure 19. Noise exposure increased p-LKB1 in the organ of Corti, spiral ganglion neurons and spiral ligament. (a) Cochlear sections showed increased DAB-stained immunolabeling of p-LKB1 (brown) in the cytosol and nuclei of OHCs, IHCs, supporting cells, spiral ganglion neurons, basal cells of the stria vascularis and fibrocytes of the spiral ligament 1 h after 98-dB noise exposure compared to unexposed controls. Representative images were taken from the basal turn, scale bar = 10 μ m, $n = 5$. **(b)** Quantification of p-LKB1 immunolabeling in OHCs of surface preparations show increases 1 h after the exposure. $n = 4$. **(c)** Western blot using total cochlear homogenates showed increased p-LKB1 1 h after the exposure compared to controls. GAPDH served as the sample loading control. $n = 5$. **(d)** The levels of total LKB1 were not changed with noise exposure by Western analysis. $n = 3$. Data **(b, c, d)** are presented as mean + SD, * $p < 0.05$, ** $p < 0.01$.

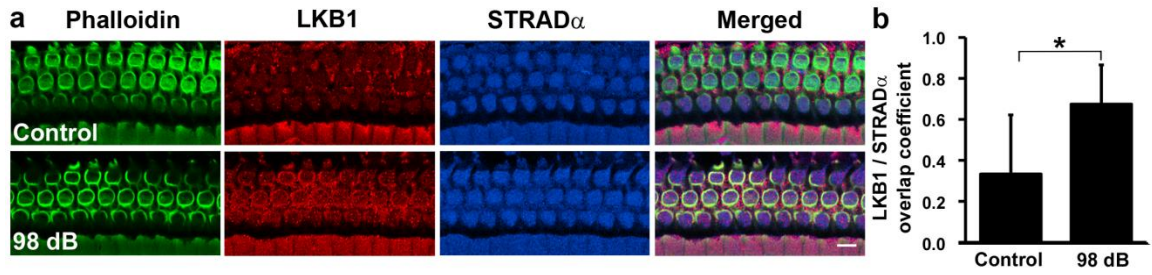


Figure 20. Noise exposure increased LKB1-STRAD α colocalization in outer hair cells. (a) The LKB1 (red) and STRAD α (blue) colocalization was stronger in OHCs (green) 1 h after 98 dB SPL exposure. (b) Quantification of LKB1 and STRAD α overlap coefficient in OHCs displayed a significant increase after the noise exposure. $n = 3$. Data (a, b) are presented as mean + SD, * $p < 0.05$.

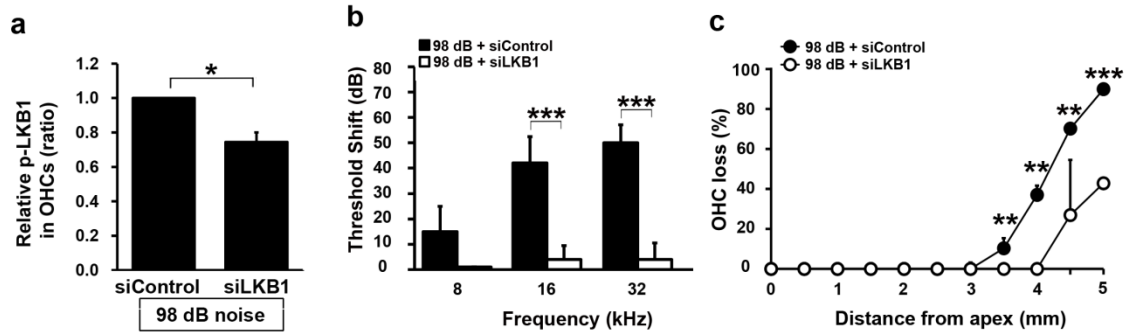


Figure 21. Inhibition of LKB1 reduced noise-induced p-LKB1 in outer hair cells, loss of outer hair cell loss and ABR threshold shifts. (a) Pretreatment with siLKB1 significantly decreased p-LKB1 immunolabeling in OHCs 1 h after the exposure. $n = 5$. **(b)** Pretreatment with siLKB1 reduced 98 dB noise-induced threshold shifts at 16 and 32 kHz 14 days after the exposure. $n = 5$. **(c)** Quantitative analysis of OHCs revealed significant protection with siLKB1 pretreatment 14 d after the exposure. 98 dB + siControl: $n = 12$; 98 dB + siLKB1: $n = 3$. Data **(a, b, c)** are presented as means + SD, *** $p < 0.001$, ** $p < 0.01$, * $p < 0.05$.

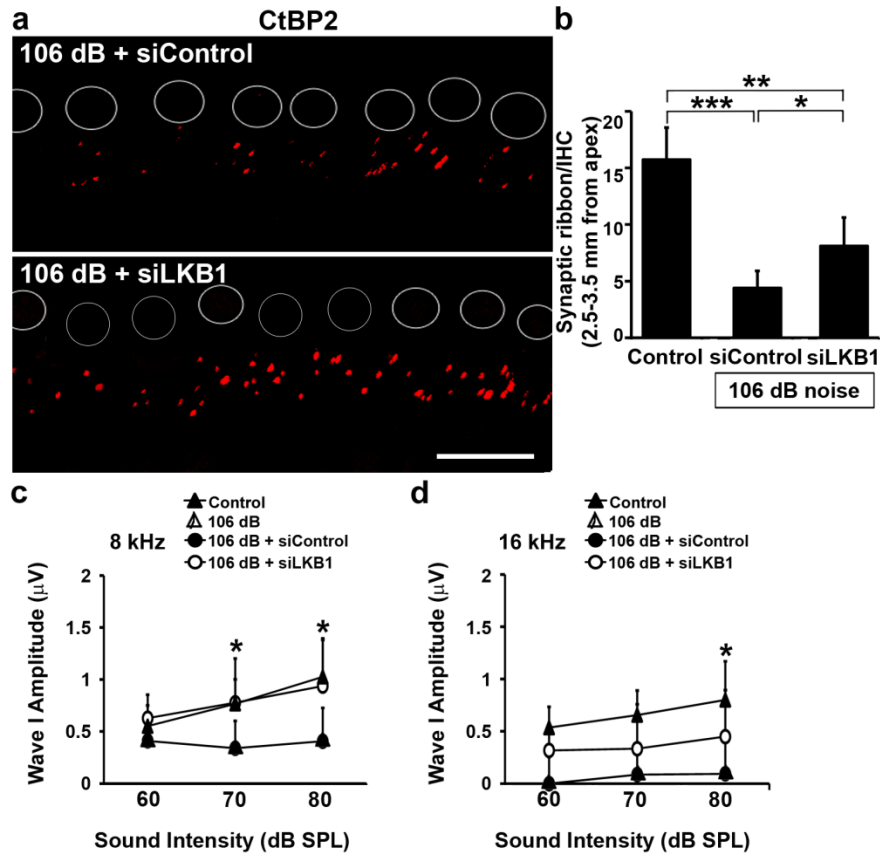


Figure 22. Inhibition of LKB1 partially prevented noise-induced inner hair cell synaptic ribbon loss at 22 kHz and decline of ABR wave I amplitude. (a) Pretreatment with siLKB1 increased the CtBP2 (red) immunolabeled synaptic ribbons in IHCs 1 h after 106-dB noise exposure. Representative images were taken from the middle turn, $n = 4$, scale bar = 10 μm. Dashed circles show the outline of IHC nuclei. **(b)** CtBP2 immunolabeled ribbon particles in IHCs increased with siLKB1 pretreatment. $n = 4$. **(c, d)** Pretreatment with siLKB1 recovered wave I amplitudes to baseline levels at 8 kHz **(c)** and attenuated the decline of wave I amplitudes at 16 kHz **(d)**. Control: $n = 10$; 106 dB + siControl: $n = 11$; 106 dB + siLKB1: $n = 6$; *: 106 dB + siControl vs 106 dB + siLKB1. Data **(b, c, d)** are presented as means + SD, *** $p < 0.001$, ** $p < 0.01$, * $p < 0.05$.

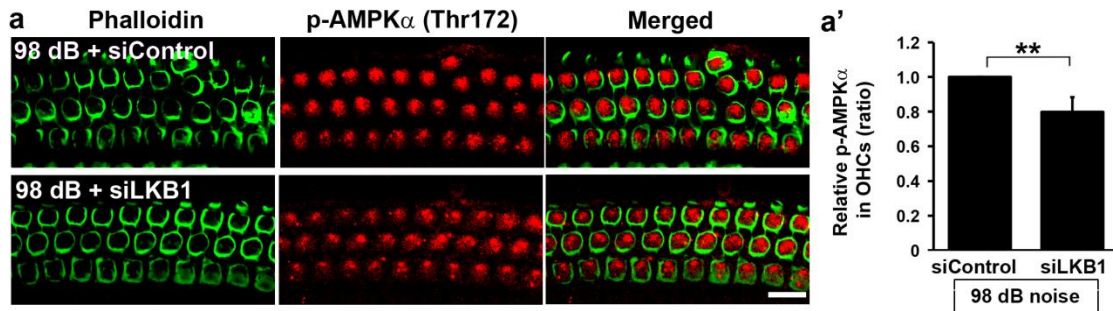


Figure 23. Noise-induced phosphorylation of AMPK α is reduced in outer hair cells of siLKB1 pretreatment mice. (a) Pretreatment with siLKB1 decreased p-AMPK α immunolabeling (red) in OHCs (labeled with phalloidin staining green) of CBA/J mice 1 h after 98-dB exposure. $n = 3$. (a') Quantification of p-AMPK α immunolabeling in OHCs displays significant decreases. $n = 3$. Data are presented as means + SD; ** $p < 0.01$.

Discussion

Our results are in agreement with the concept that LKB1 is an AMPK kinase. This conclusion is supported by data demonstrating that inhibition of LKB1 by siRNA reduced 98 dB noise-induced auditory thresholds to near baseline levels similar to that achieved by pretreatment with siAMPK α 1 or Compound C. Despite the excellent functional protection, the reduction of OHC and synaptic ribbon loss by pretreatment with siLKB1 was not as great compared to that achieved by siAMPK α 1 or Compound C. This implies the involvement of other players that may be affecting noise-induced auditory thresholds which may include the disruption of hair cell stereocilia stiffness or structure or an alteration in the neurotransmission of SGNs, since robust p-LKB1 levels were detected in all cell types in the cochlea. The pretreatment of siLKB1 reduced p-AMPK α by about 20%, similar to the 30% reduction detected with siAMPK α 1 treatment, making a strong case for the direct phosphorylation of AMPK by LKB1 following noise exposure.

The activation of LKB1 in the organ of Corti, including in the nuclei and cytosol of OHCs, IHCs, supporting cells, SGNs, stria vascularis and total cochlear tissue homogenates, after noise exposure indicates reduction of intracellular ATP levels in the cochlea, which is in line with our previous publication (40). The discrepancy between increased levels of p-LKB1 in Deiters cells and other supporting cell types with minimal AMPK activation after noise exposure may be owed to an effect of intrinsic differences in homeostatic defense systems against metabolic stress as supporting cells are resistant to inner ear insults, while sensory hair cells are vulnerable (145-147). Alternatively, it is plausible that off-target effects of LKB1 activity play divergent roles in cochlear sensory cells versus supporting cells since LKB1 is known to phosphorylate a total of 14 AMPK-

related kinases including the microtubule affinity regulating kinases (MARKs), which are involved in cellular polarity and cytoskeleton regulation (144, 148).

The detailed molecular mechanisms by which LKB1 is activated and transported to the cytosol remain unclear. The phosphorylation of LKB1 was localized partially within the cytosol and nuclei of sensory and supporting cell types in the organ of Corti, SGNs and stria vascularis (143). This high level of nuclear and cytosolic localization suggests that serine 428 (Ser428) phosphorylation is a necessary site for LKB1 translocation. The activation of LKB1 after noise exposure is further reinforced by the increased colocalization of LKB1 with the pseudokinase STRAD α within OHCs (142, 149-151).

In summary, we provide evidence that noise increased the phosphorylation of LKB1 and its colocalization with the pseudokinase STRAD in sensory hair cells and supporting cells. LKB1 mediated the loss of IHC synaptic ribbons, OHCs and auditory function after noise exposure. Silencing of LKB1 reduced the loss of OHCs and synaptic ribbons and decreased auditory threshold shifts. Similar to the protection by siAMPK α 1, we detected a disproportional effect of LKB1 siRNA treatment, which reduced LKB1 by 20% in OHCs specifically, and reduced the functional deficits by over 80%. This suggests that the activity of LKB1 also likely alters multiple cellular targets, one of which is AMPK, which may then also induce several of its own signaling pathways, causing this amplified functional protection. Still, inhibition of AMPK (Chapter 3) was more effective in protecting against noise-induced auditory deficits than the inhibition of LKB1, which was not able to completely diminish AMPK phosphorylation. This suggests that the inhibition of the LKB1 pathway is only one mechanism to abolish AMPK activity and alternative sources such as direct allosteric binding by AMP may contribute to NIHL.

**CHAPTER FIVE: AMPK ACTIVATION BY CAMKK β VIA
INTRACELLULAR CALCIUM INFLUX**

Introduction

As described in Chapter 1, the disruption of calcium homeostasis by calcium influx has been involved in NIHL. As the level of intracellular calcium increases, calcium-binding messenger protein calmodulin (CaM) acts as a calcium buffer and sensor, binding free calcium via its two calcium-binding sites. This calcium/CaM complex changes the conformation of CaM, allowing it to interact with a variety of proteins, including calcium/calmodulin-dependent protein kinases (CaMKs), a group of serine/threonine protein kinases that are activated following increases in intracellular calcium levels (152). In particular, calcium/CaM can stimulate downstream calcium signaling via CaMKK.

CaMKK consists of 2 isoforms, CaMKK α and CaMKK β . CaMKK β is primarily expressed in the brain and neuronal tissues and plays a role in signaling neuronal processes (153). CaMKK β is an upstream kinase for calcium-calmodulin kinase (CaMK) I and IV. These two kinases require the formation of calcium/CaM complexes and phosphorylation of CaMKK to become functional. The binding of calcium/CaM exposes a loop on CaMKI and CaMKIV that can be phosphorylated by CaMKK (154). Following its phosphorylation, CaMKIV can translocate to the nucleus to stimulate downstream targets, such as the transcription factor cAMP response element-binding protein (CREB). CaMKI primarily promotes cytosolic signaling pathways that regulate the cytoskeleton and neuronal plasticity through the phosphorylation of mitogen-activated protein (MAP) kinases. In addition, CaMKK β can phosphorylate AMP-activated protein kinase (AMPK), a cellular energy sensor that regulates the energy balance of the cell (155) (refer to Chapter 3). The CaMKK β -AMPK pathway requires calcium/CaM binding in addition to phosphorylation by CaMKK β (155) (Fig. 24).

Calcium overload and disruption of intracellular calcium homeostasis can trigger apoptotic or necrotic cell death through the activation of calcium dependent enzymes, such as calcineurin, caspases, calpain proteases and endonucleases (156, 157). These calcium-dependent enzymes can cleave cell survival proteins such as Bcl-2 or dephosphorylate pro-apoptotic proteins such as BAD, promoting cell death (158, 159). Moreover, CaM levels are elevated after noise trauma in the guinea pig cochlea, increasing the activation of downstream calcium signaling pathways (85). On the other hand, the inhibition of calcium signaling pathways prevented apoptosis in a variety of cell types. Treatment with W7, an inhibitor of CaM, prevented apoptosis in the presence of apoptotic bioprobes (160). Treatment with the calcium chelator, BAPTA-AM blocked apoptosis by buffering intracellular calcium levels. Additionally, calcium influx can also cause synaptopathy by stimulating the excessive release of glutamate neurotransmitters at the synapse. The resulting overactivation of glutamate receptors on the post-synaptic terminals can cause excitotoxicity and swelling of the nerve terminals, resulting in functional deficits.

In this chapter, the expression of CaMKK β in the inner ear was characterized in detail. The role of noise-induced calcium influx and subsequent CaMKK β signaling in the pathogenesis of NIHL and the noise-induced activation of AMPK was examined using CaMKK β siRNA silencing and CaMKK β -knockout mice. In addition, we also used the pharmacological inhibitor of calcium channels Verapamil. Verapamil is a non-selective, L-type, high-voltage activated calcium channel blocker (161). It is a FDA-approved drug commonly used for its antihypertensive and antianginal effects due to its potent vasodilation activity (162). The drug plasma concentrations peak at 1-2 hours after administration and it has a half-life of 2.8 – 7.4 h, but the half-life increases even further after repetitive dosing. Verapamil has the ability to transverse the blood brain barrier

(163). Generally, a low dosage is necessary to elicit protective responses in several tissue types, including the murine cochlea (98, 164-167). Specifically, in the murine noise model, of four L-type voltage-gated calcium channel (VGCC) blockers that decreased the ABR threshold shift, verapamil had a significantly lower dose (98).

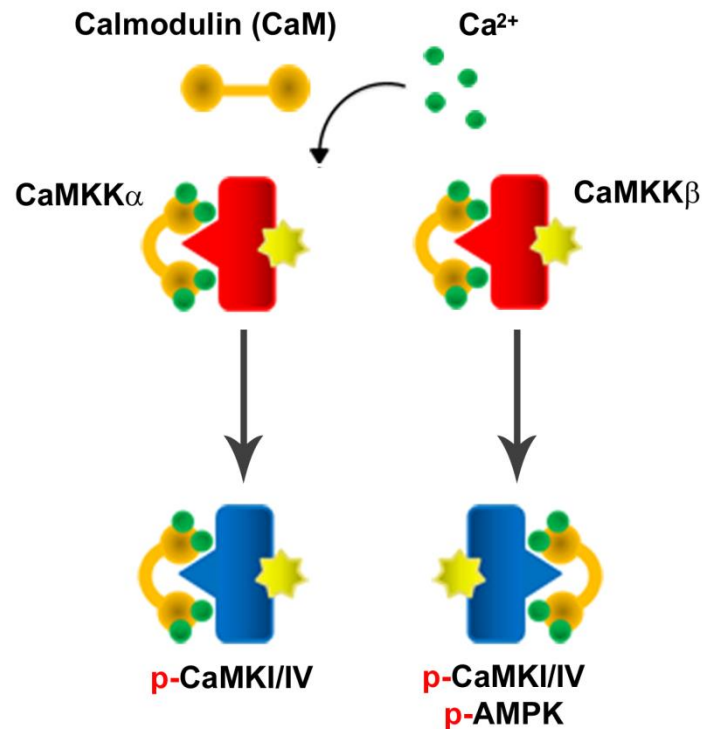


Figure 24. CaMKK signaling. Calcium binding protein calmodulin (dark yellow) is activated by the binding of 4 calcium ions (green). The active complex activates CaMKKs (red), which, when active, phosphorylate downstream kinases including CaMKI and CaMKIV (blue). The β isoform of CaMKK also activates AMPK.

Results

Treatment with the calcium channel blocker verapamil reduced noise-induced hearing loss and outer hair cell death.

We first examined the contribution of calcium influx into OHCs via L-type, high voltage-gated calcium channels (VGCCs) to NIHL by administering IP injections of the calcium channel blocker verapamil and assessing the protection against NIHL. Two weeks after 98 dB SPL BBN exposure, measurement of auditory thresholds displayed a reduction of noise-induced PTS in the verapamil-treated group compared to vehicle-treated groups at 16 and 32 kHz (Fig 25a). After 106 dB SPL, verapamil treatment reduced thresholds shifts at 8 kHz, but was unable to alleviate NIHL at 16 and 32 kHz (Fig. 25b).

Next, OHC losses were quantified along the entire length of the cochlear epithelium 14 days after 98 dB SPL BBN exposure. The OHC loss was decreased in the verapamil-treated group compared to the vehicle-treated group (Fig. 25c, d). The loss of OHCs with verapamil treatment began at 3.5 mm instead of at 3.0 mm from the apex as detected with vehicle treatment. OHC loss was reduced from 40% to 5% at 4 mm, and 80% to 40% at 4.5 mm from the apex with verapamil treatment. In contrast, treatment of verapamil did not alter the number of IHC synaptic ribbons at the 22 kHz region of the sensory epithelium (3 mm from the apex) which were reduced 1 h after 106 dB noise exposure (Fig. 26a, a').

Noise increased CaMKK β activity in basal outer hair cells and other cochlear cell types.

Since CaMKK β is a central kinase in calcium signaling cascades, the level of CaMKK β was examined after noise exposure at 98 dB SPL. In the unexposed animal, CaMKK β was weakly localized in all cell types in the organ of Corti, spiral ganglion neurons, and

stria vascularis, but strongly expressed in the fibrocytes of the spiral ligament. One hour after the noise exposure, CaMKK β was increased in the organ of Corti, including in IHCs, OHCs, pillar and Deiters cells, spiral ganglion neurons, stria vascularis, including marginal and basal cells, and spiral ligament (Fig. 27a). Western blot of total cochlear homogenates detected a single band for CaMKK β at 55 kDa without alteration after noise exposure (Fig. 27b).

We then detected CaMKK β activity by assessing the phosphorylation of its downstream targets, CaMKI (p-CaMKI) at threonine 177 and CaMKIV (p-CaMKIV) at threonine 196. To quantify the intensity of p-CaMKI and p-CaMKIV staining specifically within OHCs, surface preparations were immunolabeled. Surface preparations showed punctate increases in the immunolabeling for p-CaMKI (Fig. 28a, a') by 73% and p-CaMKIV (Fig. 28b, b') by 95% across basal OHCs 1 h after 98 dB exposure compared to unexposed controls. Severe 106 dB noise exposure resulted in changes in the immunolabeling pattern of p-CaMKI from broad punctate increases across basal OHCs to robust increases in the cuticular plate of select basal OHCs 1 h after the exposure (Fig. 28c). The p-CaMKI-labeled OHCs followed a gradient in which the lower basal region (5 mm from the apex) of the epithelium displayed the majority of p-CaMKI positive OHCs and only a few were present in the upper basal region (4 mm from the apex) (Fig. 28c'). Immunoblots of total cochlear homogenates detected a single band for p-CaMKI and p-CaMKIV at molecular weights of 45 and 60 kDa without alteration after noise exposure (Fig. 28d, e).

Pretreatment with CaMKK β siRNA reduced noise-induced CaMKK β activity and protected against noise-induced loss of outer hair cells and hearing function.

In order to determine the contribution of CaMKK β to NIHL, the effects of CaMKK β siRNA (siCaMKK β) pretreatment on noise-induced loss of hair cells and NIHL was examined.

Seventy-two hours after the delivery of 0.6 μg siCaMKK β , CaMKK β immunolabeling was significantly reduced by 47% in basal OHCs (Fig. 29a, a'). Immunolabeling of its downstream target p-CaMKI was not altered in unexposed cochlea, but the 98-dB noise-induced increases in p-CaMKI were reduced by 20% with siCaMKK β pretreatment. Finally, pretreatment with siCaMKK β attenuated 98-dB noise-induced threshold shifts by 35 and 30 dB at 16 and 32 kHz measured at two weeks after the exposure (Fig. 29b). Noise-induced OHC loss was also completely prevented at 3.5 – 4 mm and reduced by 50 – 40% at 4.5 - 5.5 mm from the apex (Fig. 29c, d).

Noise induced hearing loss and outer hair cell loss were reduced in CaMKK β -KO mice.

Finally, CaMKK β -knockout (CaMKK β -KO) mice were utilized to explore the pathological function of CaMKK β in NIHL. We first detected an 84% decrease in CaMKK β mRNA copy number within the cochlea of CaMKK β -KO mice compared to their WT counterparts (Fig. 30e). No differences were detected for the CaMKK α isoform (Fig. 30f). Despite these changes in CaMKK β expression, CaMKK β -WT, -KO and heterozygous mice showed similar baseline auditory function (Fig. 30g)

We then assessed the effect of noise of 92, 94 and 98 dB SPL in CaMKK β -WT, -KO and -heterozygous mice. The 92 and 94 dB SPL noise exposures induced an average of 30 dB PTS only at 32 kHz that remained unchanged between CaMKK β -KO and -WT littermates 2 weeks after the exposure (Fig. 30a, b). Exposures to noise at 98-dB noise resulted in PTS of 30 dB at both 16 and 32 kHz. CaMKK β -KO mice showed a significant 10 dB reduction of PTS at 16 kHz compared to their WT littermates (Fig. 30c). Furthermore, OHC loss was significantly decreased in the cochlea of CaMKK β -KO mice 2 weeks after 98 dB noise exposure. Some OHC loss began at 2 mm from the apex in

CaMKK β -WT mice, while OHC loss was delayed to 5 mm in KO mice. There were significant differences in OHC loss at 4.5 and 5.0 mm from the apex (Fig. 30d).

Noise-induced synaptopathy was not altered between CaMKK β -KO and –WT mice

In order to determine if the reduced CaMKK β activity within knockout mice can attenuate noise-induced loss of IHC synaptic ribbons, ribbon particles were counted 1 h after 98-dB noise exposure. IHCs of surface preparations from the 22 kHz region (3 mm from the apex) of CaMKK β -KO mice showed similar numbers of CtBP2-labeled synaptic ribbons compared to WT mice after the exposure (Fig. 31a, b).

Noise-induced p-AMPK α is reduced in CaMKK β -KO mice

To explore the noise-induced phosphorylation of AMPK α by CaMKK β , CaMKK β -KO mice were utilized. The levels of p-AMPK α were not altered in unexposed CaMKK β -KO mice as detected by Western blot and immunolabeling of surface preparations. Western blot using total cochlear homogenates showed an average of 30% reduction of p-AMPK α in CaMKK β -KO mice exposed to 98 dB noise compared to their WT littermates (Fig. 32b). Immunolabeling for p-AMPK α in basal OHCs of surface preparations was significantly reduced by 28% in CaMKK β -KO mice 1 h after the exposure (Fig. 32a, a').

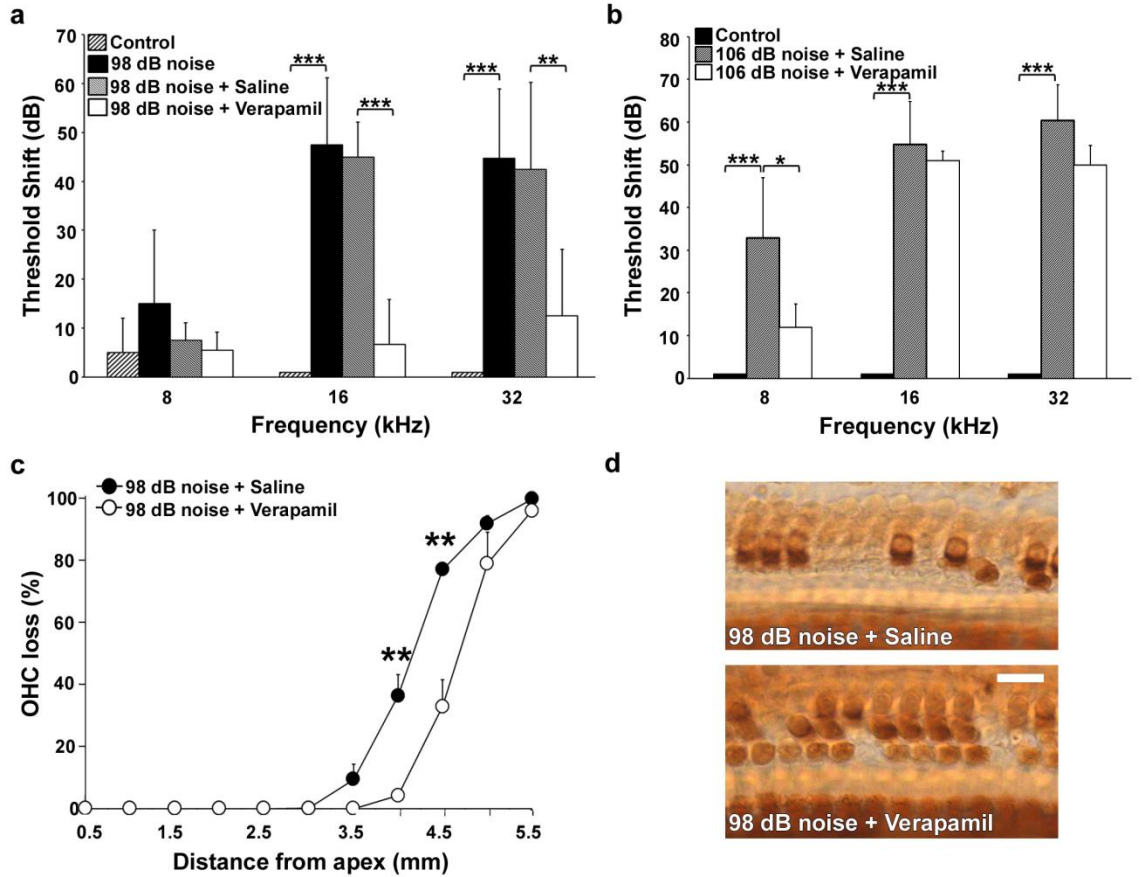


Figure 25. Verapamil treatment reduced noise-induced hearing loss and outer hair cell loss. (a) Verapamil treatment reduces 98-dB noise-induced auditory threshold shifts at 16 and 32 kHz. Control: $n = 14$, 98 dB noise: $n = 12$, 98 dB noise + Saline: $n = 3$, 98 dB noise + Verapamil: $n = 10$. (b) Verapamil treatment reduces 106-dB noise-induced auditory thresholds shifts at 8 kHz. $n = 6$. (c) Quantitative analysis of OHCs revealed significant protection with verapamil treatment 14 d after the exposure. 98 dB + saline: $n = 5$; 98 dB + verapamil: $n = 9$. (c') Representative images of OHC loss were taken from the basal turn at 4.5 mm from the apex, scale bar = 10 μm . Data (a, b, c) are presented as means + SD, *** $p < 0.001$, ** $p < 0.01$, * $p < 0.05$.

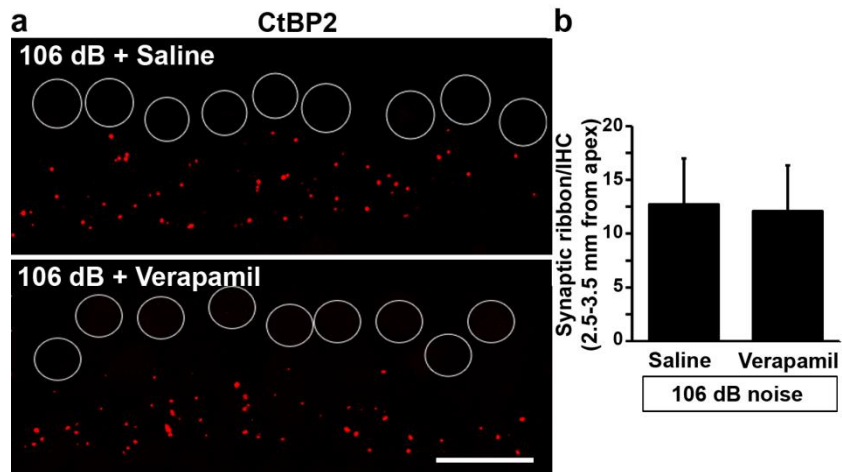


Figure 26. Verapamil treatment did not alter noise-induced inner hair cell synaptic ribbon loss.

(a) Verapamil treatment did not alter the CtBP2 (red) immunolabeled synaptic ribbons in IHCs 1 h after 106 dB SPL BBN exposure. Representative images were taken from the 22.6 kHz region of the middle turn, $n = 4$, scale bar = 10 μm . Dashed circles represent the outline of IHC nuclei. **(b)** CtBP2 immunolabeled ribbon particles in IHCs were unchanged. Data are presented as means + SD, $n = 4$.

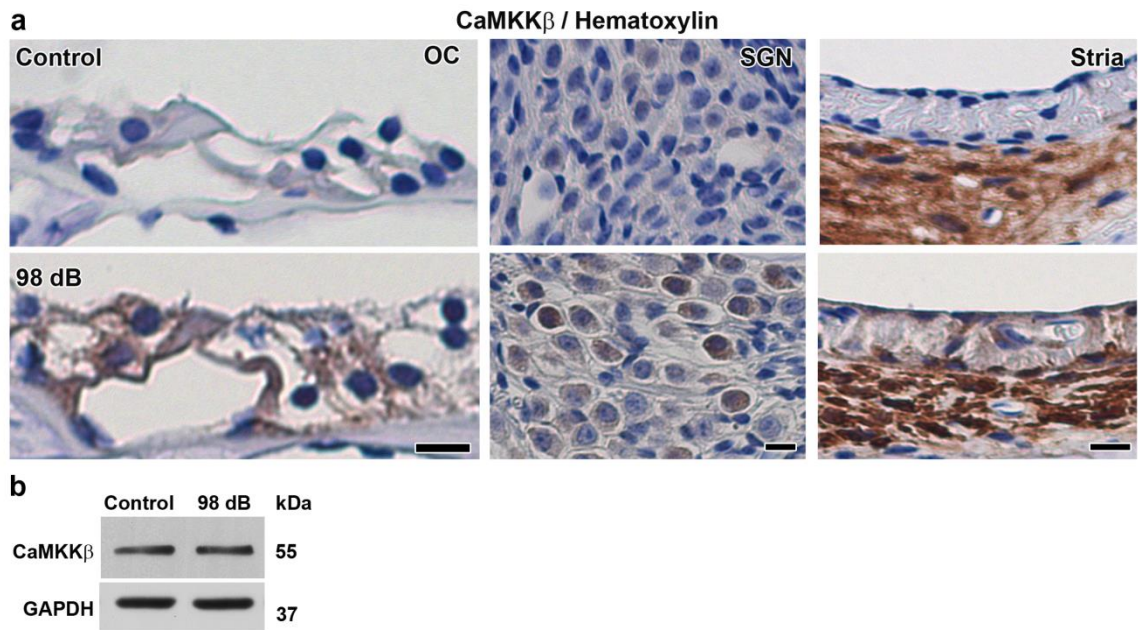


Figure 27. Noise exposure increased CaMKK β in the organ of Corti, spiral ganglion neurons and spiral ligament. (a) Sections display increased localization of CaMKK β immunolabeling (brown) in the organ of Corti, including OHCs and IHCs, pillar cells and Deiters cells, spiral ganglion neurons, stria vascularis and spiral ligament. Representative images were taken from the basal turn, scale bar = 10 μ m, $n = 3$. **(b)** Western blotting of total cochlear homogenates detected no change in the levels of CaMKK β with 98 dB noise exposures. GAPDH served as the sample loading control. $n = 3$.

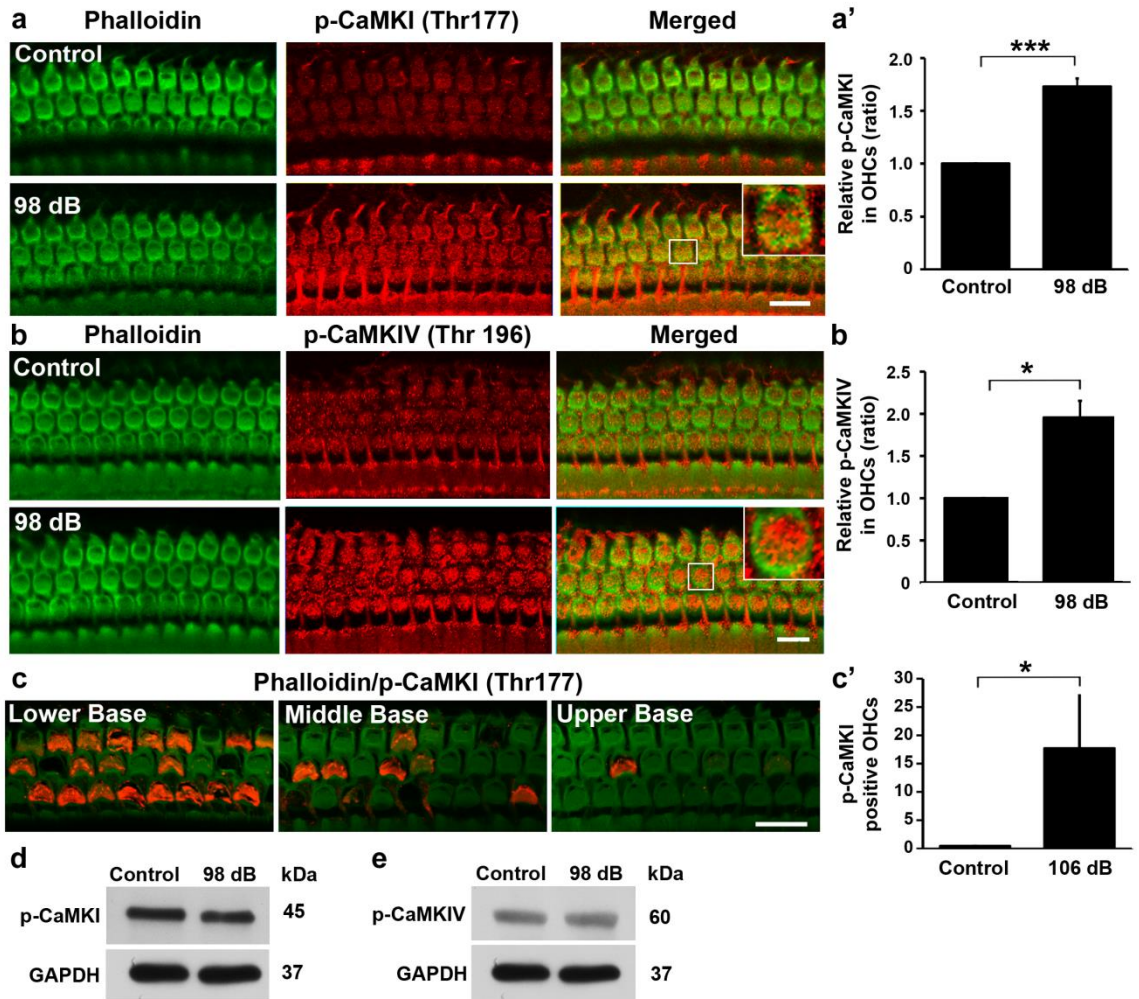


Figure 28. Noise exposure induced p-CaMKI and p-CaMKIV in basal outer hair cells. (a, b) The p-CaMKI (red) (a) p-CaMKIV (red) (b) immunolabeling was stronger in basal OHCs with phalloidin staining (green) 1 h after 98 dB SPL exposure. (a', b') Quantification of p-CaMKI (a') and p-CaMKIV (b') immunolabeling in OHCs displayed a significant increase after the noise exposure. (c) The basal region of the sensory epithelium displayed a tonotopic gradient of OHCs positive for p-CaMKI (red) immunolabeling 1 h after exposure to 106 dB SPL. (c') Quantification of the number of p-CaMKI positive OHCs along the basal turn (4-5 mm from the apex) confirmed a significant increase. $n = 4$. (d, e) Western blot of total cochlear homogenates showed no

change in the levels of p-CaMKI **(d)** and p-CaMKIV **(e)** between 98 dB noise and controls. GAPDH served as the sample loading control. $n = 3$. Data are presented as means + SD, * $p < 0.05$, $n = 6$. Representative images **(a, b, c)** were taken from the basal turn, scale bar = 10 μm .

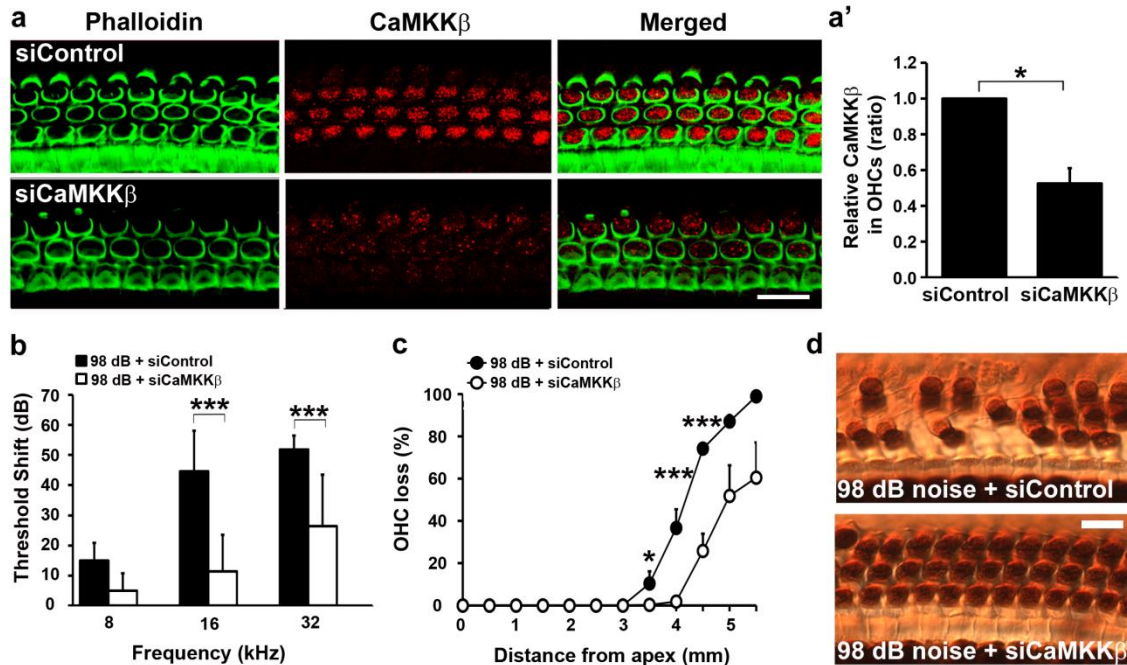


Figure 29. Inhibition of CaMKK β via siRNA reduced CaMKK β activity, noise-induced hearing loss and outer hair cell loss. (a) Treatment with siCaMKK β decreased CaMKK β immunolabeling (red) in OHCs with phalloidin staining (green) in unexposed mice 72 h after silencing. Representative images were taken from the basal turn, scale bar = 10 μ m. **(a')** Quantification of CaMKK β levels verified significant decrease in OHCs. $n = 3$. **(b)** Pretreatment with siCaMKK β reduced 98 dB SPL noise-induced threshold shifts at 16 and 32 kHz 14 days after the exposure. 98 dB + siControl: $n = 11$; 98 dB + siCaMKK β : $n = 7$. **(c)** Quantitative analysis of OHCs showed significant protection with siCaMKK β pretreatment 14 d after the exposure. 98 dB + siControl: $n = 5$; 98 dB + siCaMKK β : $n = 7$. **(d)** Representative images show DAB stained myosin VIIa immunolabeled OHCs at 4 mm from the apex of siControl or siCaMKK β treated cochlea. Data **(a', b, c)** are presented as means + SD, *** $p < 0.001$, * $p < 0.05$.

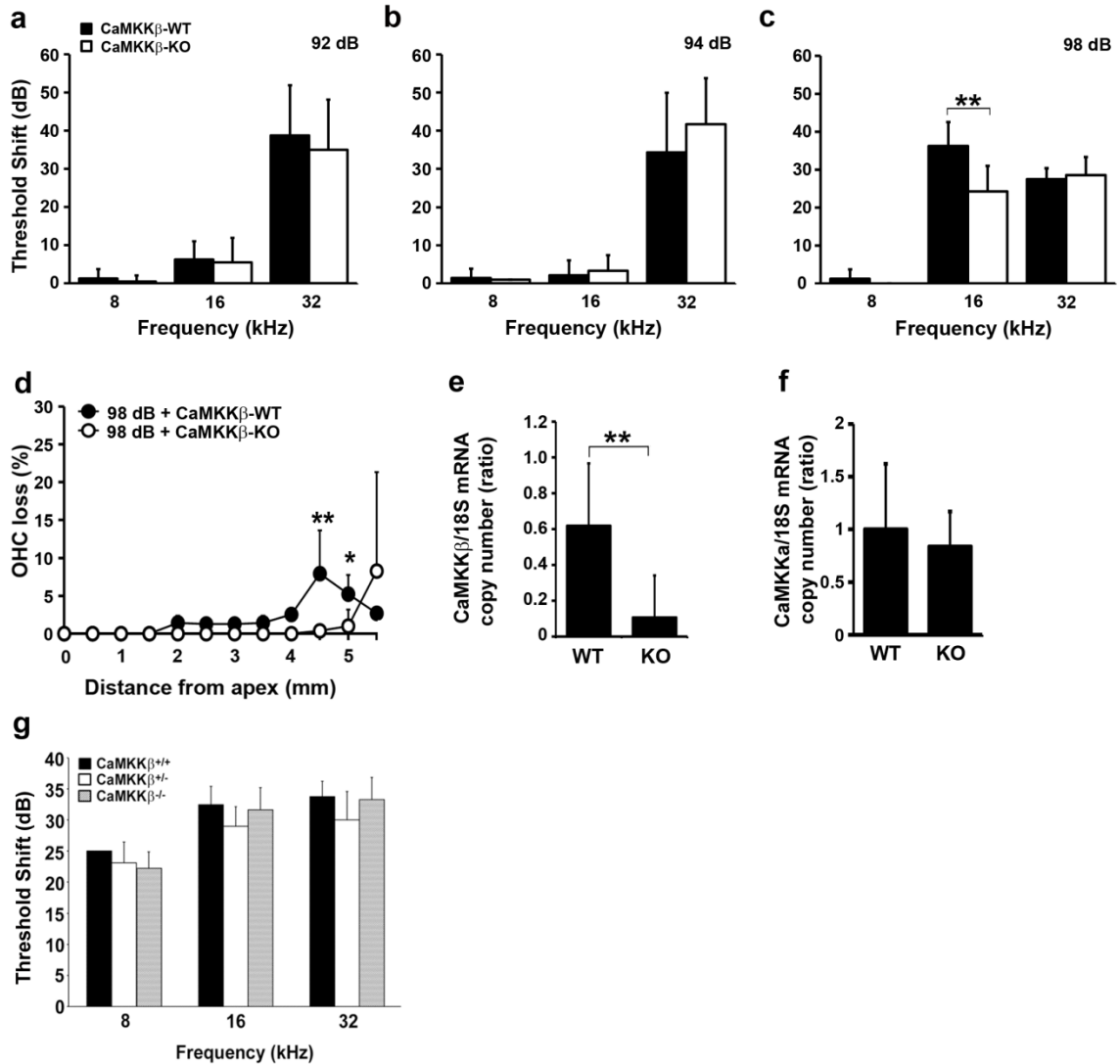


Figure 30. Noise-induced hearing loss and outer hair cell loss is reduced by CaMKK β -knockout. (a, b) The 92 (a) and 94 (b) dB SPL noise-induced permanent threshold shifts remained unchanged between CaMKK β -KO and -WT mice 14 days after the exposure. 92 dB + CaMKK β -KO: $n = 10$; 92 dB + CaMKK β -WT: $n = 4$; 94 dB + CaMKK β -KO: $n = 6$; 94 dB + CaMKK β -WT: $n = 7$. (c) The 98 dB SPL noise-induced threshold shifts were decreased by 10 dB at 16 kHz by CaMKK β -KO mice 14 days after the exposure. $n = 6$. (d) Quantitative analysis of OHCs showed significant protection by CaMKK β -KO mice at 4.5 and 5 mm from the apex 14 d after the exposure. $n = 6$. (e)

CaMKK β mRNA copy number in total cochlear tissue homogenates was reduced in CaMKK β -KO compared to WT mice. 18S served as loading control. $n = 7$. **(f)** CaMKK α mRNA copy number was unchanged in total cochlear tissue homogenates of CaMKK β -KO compared to WT littermates. 18S served as loading control. $n = 7$. **(g)** Baseline auditory thresholds remain unchanged between CaMKK β -KO, -WT, and -heterozygous mice at 8, 16, and 32 kHz. $n = 3$. Data are presented as means + SD, * $p < 0.05$, ** $p < 0.01$.

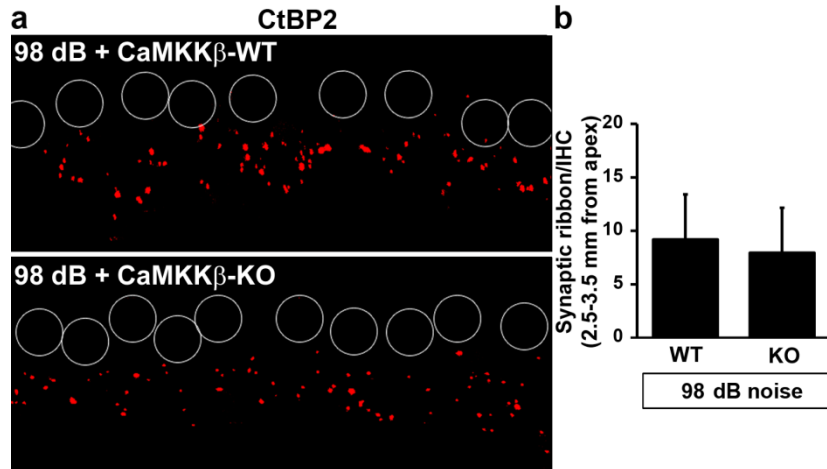


Figure 31. Noise-attenuated inner hair cell synaptic ribbons were not altered by CaMKK β -knockout. (a) CaMKK β -KO mice did not alter the CtBP2 (red) immunolabeled synaptic ribbons in IHCs at 22.6 kHz 1 h after 98 dB SPL BBN exposure. Representative images were taken from the middle turn, $n = 4$, scale bar = 10 μ m. Dashed circles show the outline of IHC nuclei. **(b)** Quantification of CtBP2 immunolabeled ribbon particles in IHCs were unchanged. Data are presented as means + SD, $n = 4$.

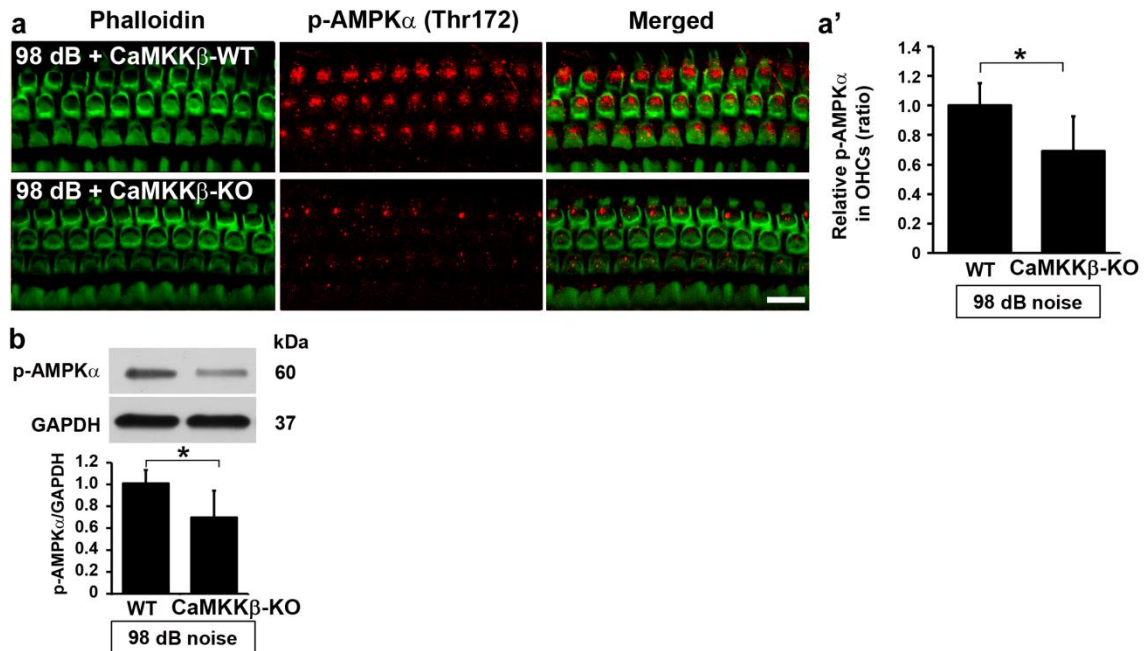


Figure 32. Noise-induced phosphorylation of AMPK α is reduced in outer hair cells of CaMKK β -knockout mice. (a) p-AMPK α (red) immunolabeling was reduced in OHCs with phalloidin staining (green) 1 h after exposure (98 dB SPL) of CaMKK β -KO mice compared to wild-type littermates. $n = 4$. Representative images were taken from the basal turn, Scale bar = 10 μ m. **(a')** Quantification of p-AMPK α immunolabeling in OHCs confirmed a significant decrease. $n = 4$. **(b)** Immunoblot of total cochlear homogenates shows reduction of p-AMPK α 1 h after exposure (98 dB SPL BBN) of CaMKK β -KO mice compared to wild-type littermates. GAPDH served as loading control. $n = 3$. Data **(a', b)** are presented as means + SD; ** $p < 0.01$, * $p < 0.05$.

Discussion

Concomitant with AMPK phosphorylation, CaMKK β activity, as indicated by the phosphorylation of the CaMKK β targets, CaMKI and CaMKIV, is increased by noise exposure in basal OHCs. Interestingly, the patterning associated with p-CaMKI is altered in a noise-intensity-dependent manner. One hour after 98 dB SPL, p-CaMKI-associated immunofluorescence forms a punctate pattern, the intensity of which increased in OHCs throughout the basal region of the sensory epithelium. One hour after 106 dB exposure, the p-CaMKI-immunolabeling is robustly increased in the cuticular plate of select OHCs in a gradient along the basal region of the sensory epithelium with the greatest number of p-CaMKI-positive OHCs located in the lower base where OHC death is initially observed (28). Such changes imply progressive overloading of calcium and calcium-associated signaling pathways in OHCs that are undergoing and/or very near to death (168), as apoptotic and necrotic OHC death occurs 1 h after 106 dB SPL BBN, but not after 98 dB noise exposure (39). Supporting cells and IHCs, which do not undergo cell death at this time point, display no p-CaMKI immunolabeling.

This notion of noise intensity dependent changes in insults is further supported by the protection against noise-induced auditory threshold shifts by the inhibition of calcium channels via verapamil treatment. Verapamil treatment is able to effectively reduce the extent of NIHL induced by 98 dB noise exposure, but does not provide any protection from the 106 dB noise exposure, pointing to the changes in calcium-associated signaling observed in the immunohistochemistry studies. The variations in p-CaMKI immunolabeling pattern may be explained by intensity-dependent changes in calcium overloading. After the 98-dB exposure, the extent of calcium influx via mechanotransduction (MET) channels and VGCCs is probably limited at least in part by

calcium binding proteins including calmodulin that restrict intracellular free calcium diffusion and incite calcium-associated signaling responses (169). After the 106-dB exposure, the increased vibratory stimulus increases the influx of ions through both of the channels, overwhelming calcium chelators and elevating the intracellular free calcium level within OHCs. It is possible that calcium influx via MET channels (0.2 – 10% of MET current) may be taken up by the mitochondria and endoplasmic reticulum of the Hensen's body located at the cuticular plate, which acts as a calcium store (170). The noise-induced release of ATP into the endolymph can activate purinergic receptors which promote inositol triphosphate (IP₃) mediated calcium release at the Hensen's body. Furthermore, the plasma membrane calcium ATPase (PMCA), the primary mechanism by which calcium is extruded from hair cells, is densely localized in outer hair cell stereocilia region (171). The sum of these activities provide an explanation for the robust increase of p-CaMKI specifically localized at the cuticular plate under this condition (61).

The possible explanation for the lack of protection of auditory thresholds and synaptic elements by verapamil treatment at the 106-dB condition is that the accumulation of free calcium at the synaptic ribbon active zone overwhelms our protective strategies. Calcium influx primarily enters through VGCCs (>90%) at the basolateral surface and functions to trigger neurotransmitter release at the ribbon synapse. Thus, after the 106-dB exposure, the influx of calcium through VGCCs can lead to a surge of neurotransmitter release, resulting in excitotoxicity of the synapse. This introduces a two-hit pathological effect of calcium-associated pathologies at both the apical and basal poles of hair cells, which may overwhelm protective responses elicited by verapamil treatment.

CaMKK β appears to mediate AMPK's contribution to the progression of NIHL. Inhibition of CaMKK β by siRNA reduces 98 dB noise-induced auditory thresholds,

although the protection is not as great as that of siAMPK α 1, Compound C, or siLKB1. Considering the robust reduction of CaMKK β mRNA and p-AMPK α protein in the knockout mice, the 10 dB degree of protection against auditory threshold shifts and OHCs after noise exposure seems inadequate compared to the 30 dB protection elicited by CaMKK β siRNA. Since the activation of AMPK is noise intensity-dependent, the relatively lower permanent threshold shift induced by the 98 dB exposure in the CaMKK β knockout of C57B6/J mice may be a plausible explanation. Furthermore, studies have shown that the two strains differ in noise-induced cochlear pathology. The CBA/J strains show significant reductions in the endocochlear potential, abnormal stria vascularis and spiral ligament pathology acutely after noise trauma compared to the C57B6/J strains (172). In addition, mRNA levels of CaMKK α are not altered in the knockout mice. Although the activity of CaMKK α from isolated rat brain is 7-fold lower than that of CaMKK β in phosphorylating AMPK (173), it does not exclude the possibility that CaMKK α activity is able to phosphorylate AMPK more efficiently in the absence of CaMKK β , therefore, masking the effect of CaMKK β -KO.

Despite the partial protection of auditory thresholds observed with verapamil treatment and by CaMKK β -KO mice, these therapies were unable to protect against the loss of synaptic ribbons. This contrasts with the evidence in Chapters 3 and 4 showing protection of noise-induced synaptic ribbon loss when either LKB1 or AMPK are targeted. It is likely that our protective strategies were overwhelmed by calcium influx within hair cells. This is especially likely in the case of synaptopathy, since calcium stimulates the excessive release of the neurotransmitter glutamate, which causes excitotoxicity. The activation of only a few VGCCs at the synaptic active zone is sufficient in eliciting both functional and pathological effects. In fact, a previous study has estimated that less than ten Ca_v1.3 VGCCs are open at a time to induce a high calcium

concentration nanodomain near the synaptic ribbon active zone compared to the 80 channels localized per active zone (174). It is likely that verapamil treatment was unable to completely eliminate calcium influx through all 80 channels and thus, we were unable to protect against the overloading of calcium. Still, we cannot exclude the possibility that a sub-optimal verapamil dose was utilized. Furthermore, since synaptopathy is primarily caused by increased calcium levels at the synaptic ribbon, rather than calcium signaling through CaMKKs, it is reasonable that a lack of protection was exhibited by the CaMKK β -KO mice.

Finally, the discrepancy in CaMKK β , p-CaMKI and p-CaMKIV levels between immunolabeled OHCs or paraffin sections and immunoblots is possibly due to the fact that the cochlear tissue homogenates includes multiple cell types, including a variety of supporting cells, spiral ganglion neurons, and stria fibrocytes, masking changes occurring only in OHCs. In summary, our results demonstrate changes in calcium signaling in a noise intensity-dependent manner. Additionally, we demonstrate that inhibition of CaMKK β either via silencing or knockout mice reduce the phosphorylation of AMPK α and the extent of OHC loss and NIHL. These results suggest that calcium influx after noise exposure is another source in addition to intracellular ATP reduction which contributes to NIHL.

CHAPTER SIX: SUMMARY AND FUTURE DIRECTIONS

SUMMARY AND FUTURE DIRECTIONS

In summary, these results present for the first time that noise-intensity dependent phosphorylation of AMPK α in sensory hair cells facilitates NIHL by mediating loss of IHC synaptic ribbons and OHCs. This noise-induced activation of AMPK α 1 is facilitated by two pathways which converge upon AMPK α 1: one initiated by changes in the intracellular ATP levels of the cell and activated by LKB1, and the other by CaMKK β , triggered by increases in intracellular calcium. Agents that inhibit either of these pathways reduce the extent of AMPK phosphorylation and, subsequently, NIHL and OHC or synaptic ribbon loss (Fig. 33).

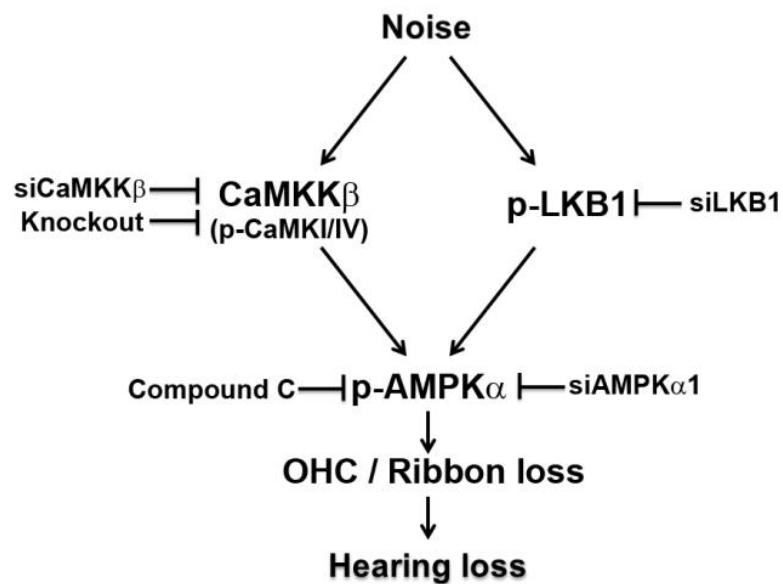


Figure 33. Summary. Noise trauma, which induces permanent threshold shifts and outer hair cell loss, increases the phosphorylation of AMPK α , hair cell loss and subsequently hearing loss in a noise intensity-dependent fashion. Reduction of AMPK α by AMPK inhibitors, Compound C or AMPK α 1 siRNA, decreases p-AMPK α and protects from noise-induced losses of OHC and synaptic ribbons and hearing loss.

Concomitantly, noise trauma induces the phosphorylation of LKB1 and the CaMKK β targets, p-CaMKI and p-CaMKIV. Inhibition of CaMKK β by siRNA and knockout decreases the level of CaMKK β , alleviating NIHL. Reduction of LKB1 by siRNA reduces the level of p-LKB1 and, subsequently, promotes the protection of noise-induced hair cell loss and NIHL. Finally, either inhibition of LKB1 via siRNA or knockout of CaMKK β diminishes the expression of p-AMPK α , suggesting noise-induced activation of AMPK is mediated through both intracellular ATP reduction and calcium influx.

This conclusion is supported by evidence demonstrating that the inhibition of AMPK activity with the selective AMPK inhibitor Compound C or through pretreatment with siAMPK α 1 reduces p-AMPK α and NIHL via protection from losses of IHC synaptic ribbons and OHCs. Concomitant with the phosphorylation of AMPK, the activities of LKB1 (p-LKB1) and CaMKK β (p-CaMKI/IV), significantly increases after noise exposure. Inhibition of LKB1 by siRNA and CaMKK β via siRNA or genetic knockout reduces p-AMPK α and the extent of NIHL, suggesting that the activation of AMPK via LKB1 and CaMKK β following noise exposure contributes to the pathogenesis of NIHL. Moreover, the efficiency of systemic pharmacological treatment with compound C implicates a novel therapeutic target in prevention and amelioration of NIHL.

The expression of total levels of AMPK α 1, AMPK α 2, LKB1 and CaMKK β significantly increases within sensory cells and supporting cells of the organ of Corti, SGNs and the spiral ligament at an acute time point 1 h after 98-dB noise exposure. This acute and rapid change in gene expression suggests that these key homeostasis molecules may be primary or secondary response genes that are activated rapidly in response to noise insults. Immediate early genes or primary response genes are genes that are induced following an extracellular signal in a rapid manner (within 30 min) that does not require an initial round of protein synthesis. On the other hand, secondary

response genes are activated at later times (2 h) in response to the initial primary response genes, which typically encode transcription factors such as c-fos, c-jun, and AP-1, which increase in the organ of Corti and lateral wall tissues of the noise-exposed guinea pig cochlea (175).

The current study implies that noise-induced pathological signaling events may vary with intensity of the noise exposure. Protection of auditory threshold shifts and OHCs by inhibiting AMPK (siAMPK α 1, Compound C and AMPK α 1-KO) and calcium-CaMKK β (verapamil) is significantly less effective for the more severe 106 dB noise condition compared to the 98 dB noise conditions. This discrepancy was most obvious with verapamil treatment, which does not provide protection from 106 dB noise-induced auditory threshold shifts, while inhibition of AMPK reduces protection. However, one cannot rule out that this may be an effect of a less-than-optimal concentration or drug treatment to target VGCCs. The noise-intensity dependent changes in signaling pathways is also emphasized by the alteration of the immunolabeling pattern of p-CaMKI, between 98 and 106 dB noise conditions. As discussed in Chapter 5, the localization of p-CaMKI from the cytosol to the cuticular plate is suggestive of an IP₃-mediated calcium release at the Hensen's body and implicate an initial protective response (mitochondrial and ER calcium uptake) or calcium extrusion via PMCA pumps, followed by a pathological reaction (calcium release). This evidence alludes to the ineffectiveness of protective cellular responses under increasing noise severities.

Several hypotheses may explain these findings: 1) Severe noise exposure at 106 dB might induce multiple cell death events in addition to the activation of AMPK, such as receptor-interacting protein kinases (39) which may bypass calcium or ATP-initiated pathways, 2) Since inhibition of LKB1 or AMPK was able to provide greater protection than the blockade of calcium influx against 106 dB noise exposure, energy

homeostasis may contribute initially to noise-induced cochlear pathology, and the dysregulation of calcium homeostasis may be a secondary effect of ATP depletion, 3) Excessive overloading of calcium and calcium-associated cell death signaling pathways are more quickly activated under the 106 dB noise condition, accelerating cell death pathways and, thus, making therapies less effective in preventing or protecting against death. The third hypothesis is supported by evidence in Chapter 5 showing a lack of protection against noise-induced synaptopathy by inhibition of calcium influx through VGCCs via verapamil or inhibition of CaMKK β via knockout mice.

Overall, this study identifies AMPK α as a novel therapeutic target to prevent NIHL. Current studies have yet to establish a comprehensive target for NIHL and have only addressed therapies that play partial roles in protection. Because it is likely that NIHL is an effect of multiple pathological processes, a key goal is to identify an inclusive therapy. AMPK provides a prospective target that addresses many intertwining pathways from multiple pathological stimuli and thus delivers a promising approach. As described in detail in Chapter 1, several phenomena including calcium influx, ATP depletion and generation of ROS likely plays a role in initiating and exacerbating the pathological responses of sensory cells that lead to NIHL. AMPK sits at a crossroads between these 3 events and thus may more effectively address the complexities of NIHL signaling pathways as a therapeutic target. However, further investigations are necessary to advance the current study and to address the unanswered questions. Of particular importance is the need to assess differences in the signaling pathways between sensory hair cells, which are injured by noise exposure, and supporting cells that are resistant to noise insults.

As demonstrated in Chapter 3 – 5, noise-induced changes in sensory hair cells, such as increases in expression of total AMPK α 1, AMPK α 2, p-LKB1 and CaMKK β were

also present in supporting cell types, despite the inconsistency in noise-induced cell fate. Addressing the fundamental differences in downstream signaling pathways associated with the activation of these molecules is necessary in order to determine key therapeutic targets, while limiting off-target effects. It is possible that the maintenance of homeostasis and ion imbalances is more effective and efficient due to the present of gap junctions between supporting cell types that allow for diffusion and flux of ions and second messengers. The buffering of calcium and potassium ions among supporting cells have been reported. Supporting cells take up potassium ions from the perilymph fluid surrounding the basolateral pole of hair cells. These potassium ions are recycled back to the endolymph through a series of gap junctions between supporting cells, fibrocytes and the cells of the stria vascularis. Dysfunction of these gap junctions can reduce the endocochlear potential and alter auditory function (176, 177). Additionally, intercellular calcium waves have been detected among Deiter's cells in response to damage and extracellular ATP signals, and these calcium waves are propagated through connexin gap junction channels (62, 178, 179). The cell-cell communication of supporting cells provide increased buffering capacity compared to the sensory hair cells and may significantly contribute to an altered cellular response to the activities of AMPK, LKB1 and CaMKK β . The increased aptitude of supporting cells to recover from a metabolic disruption may prevent a chronic activation of these signaling molecules that could cause the upregulation of pro-apoptotic genes, such as Bim, the activities of pro-apoptotic kinases such as JNK and may increase ROS and RNS through increased nitric oxide synthase activity. Alternatively, AMPK activity may more quickly resolve cellular imbalances in supporting cells by upregulating mitochondrial biogenesis genes such as peroxisome proliferator-activated receptor gamma coactivator 1-alpha (PGC1 α) or stimulating autophagy.

Moreover, changes in noise-induced signaling pathways are also apparent in the stria vascularis, spiral ligament, and SGNs. Chapter 3 and 4, highlight the potential involvement of the stria vascularis in the regulation of noise-induced energy homeostasis. The Na⁺-K⁺-ATPase within marginal cells of the stria vascularis transports potassium ions inward from the intrastrial space in order to maintain the low sodium, high potassium content of the endolymph. After noise insults, it is probable that potassium recycling is increased in order to sustain the endocochlear potential and maintain appropriate ionic balances, necessitating an increased demand for ATP production to drive these energy-consuming processes. Additionally, the release of ATP by marginal cells occurs after noise exposure. Extracellular ATP within the endolymph fluid can act upon purinergic receptors on the plasma membrane of marginal cells to stimulate inositol triphosphate (IP₃)-mediated calcium release. This effect may in turn increase ATP expenditure through the activity of calcium-ATPases, which serve to remove the intracellular calcium from the cytosol into the ER. Altogether, these various mechanisms of energy expenditure may result in energy failure and ionic imbalances of these cell types and of the endolymph. The reduction of ATP levels probably upregulates the expression of p-LKB1 and AMPK as a protective response, while CaMKKβ expression may also increase in response to the secondary intracellular calcium release in the stria vascularis. Our results showing increases in expression of AMPKα1/2, p-LKB1 and CaMKKβ support this hypothesis. Thus, reductions in auditory function as assessed by auditory thresholds without changes in hair cell death may be a result of underlying pathologies in the ionic imbalances specific to the stria vascularis.

The pharmacological agents, Compound C and Verapamil, protect against noise-induced damage of hearing function and hair cells, particularly in the case of Compound C. Despite the efficiency of this systemic treatment, advanced investigations are

necessary in order to examine the effectiveness of these pharmacological treatments. In this study, both pharmacological agents are delivered systemically to mimic a clinically paradigm of an oral medication. However, because both drugs are delivered at time points before and after the noise exposure, it is not clear whether the effects were a result of a protection effect, a rescue effect, or a combination of both. Further investigations are necessary to distinguish the functional effects of pharmacological treatments at time point only prior to noise exposure and only after noise exposure. These studies would provide information on the most effective drug delivery system for a clinical application. Additionally, we would better understand the protection from a mechanistic standpoint by determining key timing of pathological responses.

The use of knockout mice models in the study reveals a complex relationship between the activation of AMPK signaling and its outcome, whether protective or pathological. Inhibition of AMPK via siRNA (siAMPK α 1) or the use of a pharmacological inhibitor (Compound C) was able to reduce the extent of noise-induced cochlear deficits, contrasting with the worsening of cochlear deficits detected in AMPK α 1-KO mice. This highlights the need to address the differences between a reduction in the activity of AMPK versus the knockout of the gene and its function. The inconsistencies may point to differences in the degree and timing of gene inhibition. In this study, siRNA silencing partially reduces AMPK α 1 expression by 20% in OHCs and subsequently reduces its activity by 30% as determined by AMPK α phosphorylation. This partial reduction still allows for 70% activity of AMPK within OHCs to maintain the necessary AMPK cellular functions. The partial 30% reduction of its activity may be sufficient to reduce the pathological response AMPK may have on the cell at least to some extent. This contrasts with the knockout study which eliminates the AMPK gene, including its potentially protective function. Furthermore, the siRNA silencing acutely and transiently

inhibited AMPK activity. This acute expression prevents any overcompensation that the cell may adapt to in the knockout mouse.

In order to more clearly understand the pathological or pro-survival function of AMPK in the noise-exposed cochlea, further studies are necessary to examine the duration of AMPK activation to identify the key timing or circumstance in which AMPK activation converts from a protective to pathological function. We suspect that its role depends on noise intensity, where exposures to noise levels that cause temporary hearing losses may promote cell preservation through the energy conserving activity of AMPK's downstream targets, such as autophagy (71). On the other hand, exposure to noise that causes permanent hearing losses may lead to a sustained activation of AMPK as part of the cell's protective response to the increased level of stress. Under this condition, the chronic activation of AMPK may alter cellular events, which may include the upregulation of pro-apoptotic genes as the cell prepares to eliminate the damaged cell. If this hypothesis is true, treatment with an AMPK activator, such as metformin, under temporary hearing loss noise conditions may worsen recovery from NIHL. Determining a balance for AMPK activation and inhibition may be a key strategy for designing future therapies.

REFERENCES

1. Hibino, H., Nin, F., Tsuzuki, C., and Kurachi, Y. 2010. How is the highly positive endocochlear potential formed? The specific architecture of the stria vascularis and the roles of the ion-transport apparatus. *Pflugers Arch* 459:521-533.
2. Cody, A.R., and Russell, I.J. 1985. Outer hair cells in the mammalian cochlea and noise-induced hearing loss. *Nature* 315:662-665.

3. 2012. WHO global estimates on the prevalence of hearing loss. WHO Media Centre.
4. Oishi, N., and Schacht, J. 2011. Emerging treatments for noise-induced hearing loss. *Expert Opin Emerg Drugs* 16:235-245.
5. Seidman, M.D., and Strandberg, R.T. 2010. Noise and quality of life. *Int J Environ Res Public Health* 7:3730-3738.
6. Helfer, T.M., Canham-Chervak, M., Canada, S., and Mitchener, T.A. 2010. Epidemiology of hearing impairment and noise-induced hearing injury among U.S. military personnel, 2003-2005. *Am J Prev Med* 38:S71-77.
7. Humes, L., Joellenbeck, L.M., and Durch, J. 2005. Noise and military service implications for hearing loss and tinnitus. In *National Academies Press, Washington, DC*.
8. 2009. Hearing Loss Prevention for Veterans (HLPP). Washington, DC: Department of Veteran Affairs.
9. Saunders, G.H., and Griest, S.E. 2009. Hearing loss in veterans and the need for hearing loss prevention programs. *Noise Health* 11:14-21.
10. Mostafapour, S.P., Lahargoue, K., and Gates, G.A. 1998. Noise-induced hearing loss in young adults: the role of personal listening devices and other sources of leisure noise. *Laryngoscope* 108:1832-1839.
11. 2007. Noise Induced Hearing Loss. N.I.o.D.a.O.C. Disorders, editor. Bethesda: NIH.
12. 1998. Occupational Noise Exposure: Criteria for a Recommended Standard. U.S.D.o.H.a.H. Services, editor. Cincinnati: DHHS National Institute for Occupational Safety and Health.
13. Yamasoba, T., Pourbakht, A., Sakamoto, T., and Suzuki, M. 2005. Ebselen prevents noise-induced excitotoxicity and temporary threshold shift. *Neurosci Lett* 380:234-238.
14. Canlon, B. 1988. The effect of acoustic trauma on the tectorial membrane, stereocilia, and hearing sensitivity: possible mechanisms underlying damage, recovery, and protection. *Scand Audiol Suppl* 27:1-45.

15. Canlon, B., Miller, J., Flock, A., and Borg, E. 1987. Pure tone overstimulation changes the micromechanical properties of the inner hair cell stereocilia. *Hear Res* 30:65-72.
16. Spoendlin, H. 1971. Primary structural changes in the organ of Corti after acoustic overstimulation. *Acta Otolaryngol* 71:166-176.
17. Puel, J.L., Ruel, J., Gervais d'Aldin, C., and Pujol, R. 1998. Excitotoxicity and repair of cochlear synapses after noise-trauma induced hearing loss. *Neuroreport* 9:2109-2114.
18. Pujol, R., Rebillard, G., Puel, J.L., Lenoir, M., Eybalin, M., and Recasens, M. 1990. Glutamate neurotoxicity in the cochlea: a possible consequence of ischaemic or anoxic conditions occurring in ageing. *Acta Otolaryngol Suppl* 476:32-36.
19. Kujawa, S.G., and Liberman, M.C. 2009. Adding insult to injury: cochlear nerve degeneration after "temporary" noise-induced hearing loss. *J Neurosci* 29:14077-14085.
20. Liberman, L.D., Suzuki, J., and Liberman, M.C. 2015. Dynamics of cochlear synaptopathy after acoustic overexposure. *J Assoc Res Otolaryngol* 16:205-219.
21. Liberman, L.D., Suzuki, J., and Liberman, M.C. 2015. Erratum to: dynamics of cochlear synaptopathy after acoustic overexposure. *J Assoc Res Otolaryngol* 16:221.
22. Wan, G., Gomez-Casati, M.E., Gigliello, A.R., Liberman, M.C., and Corfas, G. 2014. Neurotrophin-3 regulates ribbon synapse density in the cochlea and induces synapse regeneration after acoustic trauma. *Elife* 3.
23. Kujawa, S.G., and Liberman, M.C. 2006. Acceleration of age-related hearing loss by early noise exposure: evidence of a misspent youth. *J Neurosci* 26:2115-2123.
24. Robertson, D., and Johnstone, B.M. 1980. Acoustic trauma in the guinea pig cochlea: early changes in ultrastructure and neural threshold. *Hear Res* 3:167-179.
25. Liberman, M.C. 1987. Chronic ultrastructural changes in acoustic trauma: serial-section reconstruction of stereocilia and cuticular plates. *Hear Res* 26:65-88.

26. Liberman, M.C., and Dodds, L.W. 1987. Acute ultrastructural changes in acoustic trauma: serial-section reconstruction of stereocilia and cuticular plates. *Hear Res* 26:45-64.
27. Gao, W.Y., Ding, D.L., Zheng, X.Y., Ruan, F.M., and Liu, Y.J. 1992. A comparison of changes in the stereocilia between temporary and permanent hearing losses in acoustic trauma. *Hear Res* 62:27-41.
28. Wang, Y., Hirose, K., and Liberman, M.C. 2002. Dynamics of noise-induced cellular injury and repair in the mouse cochlea. *J Assoc Res Otolaryngol* 3:248-268.
29. Yamane, H., Nakai, Y., Takayama, M., Konishi, K., Iguchi, H., Nakagawa, T., Shibata, S., Kato, A., Sunami, K., and Kawakatsu, C. 1995. The emergence of free radicals after acoustic trauma and strial blood flow. *Acta Otolaryngol Suppl* 519:87-92.
30. Hawkins, J.E., Jr. 1971. The role of vasoconstriction in noise-induced hearing loss. *Ann Otol Rhinol Laryngol* 80:903-913.
31. Miller, J.M., and Dengerink, H. 1988. Control of inner ear blood flow. *Am J Otolaryngol* 9:302-316.
32. Hu, B.H., Henderson, D., and Nicotera, T.M. 2006. Extremely rapid induction of outer hair cell apoptosis in the chinchilla cochlea following exposure to impulse noise. *Hear Res* 211:16-25.
33. Henderson, D., and Hamernik, R.P. 1986. Impulse noise: critical review. *J Acoust Soc Am* 80:569-584.
34. van Loo, G., Saelens, X., van Gorp, M., MacFarlane, M., Martin, S.J., and Vandenabeele, P. 2002. The role of mitochondrial factors in apoptosis: a Russian roulette with more than one bullet. *Cell Death Differ* 9:1031-1042.
35. Galluzzi, L., Vitale, I., Abrams, J.M., Alnemri, E.S., Baehrecke, E.H., Blagosklonny, M.V., Dawson, T.M., Dawson, V.L., El-Deiry, W.S., Fulda, S., et al. 2012. Molecular definitions of cell death subroutines: recommendations of the Nomenclature Committee on Cell Death 2012. *Cell Death Differ* 19:107-120.
36. Vanlangenakker, N., Vanden Berghe, T., Krysko, D.V., Festjens, N., and Vandenabeele, P. 2008. Molecular mechanisms and pathophysiology of necrotic cell death. *Curr Mol Med* 8:207-220.

37. Vandenabeele, P., Galluzzi, L., Vanden Berghe, T., and Kroemer, G. 2010. Molecular mechanisms of necroptosis: an ordered cellular explosion. *Nat Rev Mol Cell Biol* 11:700-714.
38. Trichonas, G., Murakami, Y., Thanos, A., Morizane, Y., Kayama, M., Debouck, C.M., Hisatomi, T., Miller, J.W., and Vavvas, D.G. 2010. Receptor interacting protein kinases mediate retinal detachment-induced photoreceptor necrosis and compensate for inhibition of apoptosis. *Proc Natl Acad Sci U S A* 107:21695-21700.
39. Zheng, H.W., Chen, J., and Sha, S.H. 2014. Receptor-interacting protein kinases modulate noise-induced sensory hair cell death. *Cell Death Dis* 5:e1262.
40. Chen, F.Q., Zheng, H.W., Hill, K., and Sha, S.H. 2012. Traumatic noise activates Rho-family GTPases through transient cellular energy depletion. *Journal of Neuroscience*.
41. Yang, W.P., Henderson, D., Hu, B.H., and Nicotera, T.M. 2004. Quantitative analysis of apoptotic and necrotic outer hair cells after exposure to different levels of continuous noise. *Hear Res* 196:69-76.
42. Nicotera, T.M., Hu, B.H., and Henderson, D. 2003. The caspase pathway in noise-induced apoptosis of the chinchilla cochlea. *J Assoc Res Otolaryngol* 4:466-477.
43. Yamashita, D., Miller, J.M., Jiang, H.Y., Minami, S.B., and Schacht, J. 2004. AIF and EndoG in noise-induced hearing loss. *Neuroreport* 15:2719-2722.
44. Han, W., Shi, X., and Nuttall, A.L. 2006. AIF and endoG translocation in noise exposure induced hair cell death. *Hear Res* 211:85-95.
45. Thalmann, R., Miyoshi, T., and Thalmann, I. 1972. The influence of ischemia upon the energy reserves of inner ear tissues. *Laryngoscope* 82:2249-2272.
46. Vlajkovic, S.M., Housley, G.D., Munoz, D.J., Robson, S.C., Sevigny, J., Wang, C.J., and Thorne, P.R. 2004. Noise exposure induces up-regulation of ecto-nucleoside triphosphate diphosphohydrolases 1 and 2 in rat cochlea. *Neuroscience* 126:763-773.
47. Nagashima, R., Yamaguchi, T., Kuramoto, N., and Ogita, K. 2011. Acoustic overstimulation activates 5'-AMP-activated protein kinase through a temporary

- decrease in ATP level in the cochlear spiral ligament prior to permanent hearing loss in mice. *Neurochem Int* 59:812-820.
48. Thalmann, R., Miyoshi, T., Kusakari, J., and Ise, I. 1975. Normal and abnormal energy metabolism of the inner ear. *Otolaryngol Clin North Am* 8:313-333.
 49. Quirk, W.S., and Seidman, M.D. 1995. Cochlear vascular changes in response to loud noise. *Am J Otol* 16:322-325.
 50. Miller, J.M., Brown, J.N., and Schacht, J. 2003. 8-iso-prostaglandin F(2alpha), a product of noise exposure, reduces inner ear blood flow. *Audiol Neurootol* 8:207-221.
 51. Chen, F.Q., Zheng, H.W., Hill, K., and Sha, S.H. 2012. Traumatic noise activates Rho-family GTPases through transient cellular energy depletion. *J Neurosci* 32:12421-12430.
 52. Minami, S.B., Yamashita, D., Ogawa, K., Schacht, J., and Miller, J.M. 2007. Creatine and tempol attenuate noise-induced hearing loss. *Brain Res* 1148:83-89.
 53. Spicer, S.S., and Schulte, B.A. 1992. Creatine kinase in epithelium of the inner ear. *J Histochem Cytochem* 40:185-192.
 54. Hirose, K., and Liberman, M.C. 2003. Lateral wall histopathology and endocochlear potential in the noise-damaged mouse cochlea. *J Assoc Res Otolaryngol* 4:339-352.
 55. Munoz, D.J., Kendrick, I.S., Rassam, M., and Thorne, P.R. 2001. Vesicular storage of adenosine triphosphate in the guinea-pig cochlear lateral wall and concentrations of ATP in the endolymph during sound exposure and hypoxia. *Acta Otolaryngol* 121:10-15.
 56. Peng, Y., Chen, J., He, S., Yang, J., and Wu, H. 2012. Release of ATP from marginal cells in the cochlea of neonatal rats can be induced by changes in extracellular and intracellular ion concentrations. *PLoS One* 7:e47124.
 57. Zhao, H.B., Yu, N., and Fleming, C.R. 2005. Gap junctional hemichannel-mediated ATP release and hearing controls in the inner ear. *Proc Natl Acad Sci U S A* 102:18724-18729.

58. Bobbin, R.P., Chu, S.H., Skellett, R.A., Campbell, J., and Fallon, M. 1997. Cytotoxicity and mitogenicity of adenosine triphosphate in the cochlea. *Hear Res* 113:155-164.
59. Yan, D., Zhu, Y., Walsh, T., Xie, D., Yuan, H., Sirmaci, A., Fujikawa, T., Wong, A.C., Loh, T.L., Du, L., et al. 2013. Mutation of the ATP-gated P2X(2) receptor leads to progressive hearing loss and increased susceptibility to noise. *Proc Natl Acad Sci U S A* 110:2228-2233.
60. Sugahara, K., Shimogori, H., Okuda, T., Takemoto, T., Hashimoto, M., and Yamashita, H. 2004. Cochlear administration of adenosine triphosphate facilitates recovery from acoustic trauma (temporary threshold shift). *ORL J Otorhinolaryngol Relat Spec* 66:80-84.
61. Mammano, F., Frolenkov, G.I., Lagostena, L., Belyantseva, I.A., Kurc, M., Dodane, V., Colavita, A., and Kachar, B. 1999. ATP-Induced Ca(2+) release in cochlear outer hair cells: localization of an inositol triphosphate-gated Ca(2+) store to the base of the sensory hair bundle. *J Neurosci* 19:6918-6929.
62. Lahne, M., and Gale, J.E. 2010. Damage-induced cell-cell communication in different cochlear cell types via two distinct ATP-dependent Ca waves. *Purinergic Signal* 6:189-200.
63. Munoz, D.J., Thorne, P.R., Housley, G.D., Billett, T.E., and Battersby, J.M. 1995. Extracellular adenosine 5'-triphosphate (ATP) in the endolymphatic compartment influences cochlear function. *Hear Res* 90:106-118.
64. Chance, B., Schoener, B., Oshino, R., Itshak, F., and Nakase, Y. 1979. Oxidation-reduction ratio studies of mitochondria in freeze-trapped samples. NADH and flavoprotein fluorescence signals. *J Biol Chem* 254:4764-4771.
65. Turrens, J.F., Freeman, B.A., Levitt, J.G., and Crapo, J.D. 1982. The effect of hyperoxia on superoxide production by lung submitochondrial particles. *Arch Biochem Biophys* 217:401-410.
66. Hu, B.H., Henderson, D., and Nicotera, T.M. 2002. Involvement of apoptosis in progression of cochlear lesion following exposure to intense noise. *Hear Res* 166:62-71.
67. Yamashita, D., Jiang, H.Y., Schacht, J., and Miller, J.M. 2004. Delayed production of free radicals following noise exposure. *Brain Res* 1019:201-209.

68. Ohlemiller, K.K., Wright, J.S., and Dugan, L.L. 1999. Early elevation of cochlear reactive oxygen species following noise exposure. *Audiol Neurootol* 4:229-236.
69. Yamane, H., Nakai, Y., Takayama, M., Iguchi, H., Nakagawa, T., and Kojima, A. 1995. Appearance of free radicals in the guinea pig inner ear after noise-induced acoustic trauma. *Eur Arch Otorhinolaryngol* 252:504-508.
70. Ohinata, Y., Miller, J.M., Altschuler, R.A., and Schacht, J. 2000. Intense noise induces formation of vasoactive lipid peroxidation products in the cochlea. *Brain Res* 878:163-173.
71. Yuan, H., Wang, X., Hill, K., Chen, J., Lemasters, J., Yang, S.M., and Sha, S.H. 2015. Autophagy attenuates noise-induced hearing loss by reducing oxidative stress. *Antioxid Redox Signal* 22:1308-1324.
72. Bielefeld, E.C., Hu, B.H., Harris, K.C., and Henderson, D. 2005. Damage and threshold shift resulting from cochlear exposure to paraquat-generated superoxide. *Hear Res* 207:35-42.
73. Yamashita, D., Jiang, H.Y., Le Prell, C.G., Schacht, J., and Miller, J.M. 2005. Post-exposure treatment attenuates noise-induced hearing loss. *Neuroscience* 134:633-642.
74. Yamasoba, T., Nuttall, A.L., Harris, C., Raphael, Y., and Miller, J.M. 1998. Role of glutathione in protection against noise-induced hearing loss. *Brain Res* 784:82-90.
75. Fetoni, A.R., De Bartolo, P., Eramo, S.L., Rolesi, R., Paciello, F., Bergamini, C., Fato, R., Paludetti, G., Petrosini, L., and Troiani, D. 2013. Noise-induced hearing loss (NIHL) as a target of oxidative stress -mediated damage: cochlear and cortical responses after an increase in antioxidant defense. *J Neurosci* 33:4011-4023.
76. Ohinata, Y., Yamasoba, T., Schacht, J., and Miller, J.M. 2000. Glutathione limits noise-induced hearing loss. *Hear Res* 146:28-34.
77. Le Prell, C.G., Hughes, L.F., and Miller, J.M. 2007. Free radical scavengers vitamins A, C, and E plus magnesium reduce noise trauma. *Free Radic Biol Med* 42:1454-1463.

78. Sha, S.H., Taylor, R., Forge, A., and Schacht, J. 2001. Differential vulnerability of basal and apical hair cells is based on intrinsic susceptibility to free radicals. *Hear Res* 155:1-8.
79. Liu, Y.M., Li, X.D., Guo, X., Liu, B., Lin, A.H., Ding, Y.L., and Rao, S.Q. 2010. SOD2 V16A SNP in the mitochondrial targeting sequence is associated with noise induced hearing loss in Chinese workers. *Dis Markers* 28:137-147.
80. Ohlemiller, K.K., McFadden, S.L., Ding, D.L., Lear, P.M., and Ho, Y.S. 2000. Targeted mutation of the gene for cellular glutathione peroxidase (Gpx1) increases noise-induced hearing loss in mice. *J Assoc Res Otolaryngol* 1:243-254.
81. McFadden, S.L., Ohlemiller, K.K., Ding, D., Shero, M., and Salvi, R.J. 2001. The Influence of Superoxide Dismutase and Glutathione Peroxidase Deficiencies on Noise-Induced Hearing Loss in Mice. *Noise Health* 3:49-64.
82. Bottger, E.C., and Schacht, J. 2013. The mitochondrion: a perpetrator of acquired hearing loss. *Hear Res* 303:12-19.
83. Park, J.S., Kim, S.W., Park, K., Choung, Y.H., Jou, I., and Park, S.M. 2012. Pravastatin attenuates noise-induced cochlear injury in mice. *Neuroscience* 208:123-132.
84. Fridberger, A., Flock, A., Ulfendahl, M., and Flock, B. 1998. Acoustic overstimulation increases outer hair cell Ca²⁺ concentrations and causes dynamic contractions of the hearing organ. *Proc Natl Acad Sci U S A* 95:7127-7132.
85. Zuo, H., Cui, B., She, X., and Wu, M. 2008. Changes in Guinea pig cochlear hair cells after sound conditioning and noise exposure. *J Occup Health* 50:373-379.
86. Maurer, J., Heinrich, U.R., and Mann, W. 1993. Morphologic damage and changes of intracellular calcium-binding sites after acute noise trauma in the organ of Corti of the guinea pig. *ORL J Otorhinolaryngol Relat Spec* 55:7-12.
87. Yamoah, E.N., Lumpkin, E.A., Dumont, R.A., Smith, P.J., Hudspeth, A.J., and Gillespie, P.G. 1998. Plasma membrane Ca²⁺-ATPase extrudes Ca²⁺ from hair cell stereocilia. *J Neurosci* 18:610-624.
88. Kozel, P.J., Friedman, R.A., Erway, L.C., Yamoah, E.N., Liu, L.H., Riddle, T., Duffy, J.J., Doetschman, T., Miller, M.L., Cardell, E.L., et al. 1998. Balance and

- hearing deficits in mice with a null mutation in the gene encoding plasma membrane Ca²⁺-ATPase isoform 2. *J Biol Chem* 273:18693-18696.
89. Minami, S.B., Yamashita, D., Schacht, J., and Miller, J.M. 2004. Calcineurin activation contributes to noise-induced hearing loss. *J Neurosci Res* 78:383-392.
 90. Ikeda, K., Kusakari, J., and Takasaka, T. 1988. Ionic changes in cochlear endolymph of the guinea pig induced by acoustic injury. *Hear Res* 32:103-110.
 91. Lopez, I., Ishiyama, G., Acuna, D., Ishiyama, A., and Baloh, R.W. 2003. Immunolocalization of voltage-gated calcium channel alpha1 subunits in the chinchilla cochlea. *Cell Tissue Res* 313:177-186.
 92. Hafidi, A., and Dulon, D. 2004. Developmental expression of Ca(v)1.3 (alpha1d) calcium channels in the mouse inner ear. *Brain Res Dev Brain Res* 150:167-175.
 93. Layton, M.G., Robertson, D., Everett, A.W., Mulders, W.H., and Yates, G.K. 2005. Cellular localization of voltage-gated calcium channels and synaptic vesicle-associated proteins in the guinea pig cochlea. *J Mol Neurosci* 27:225-244.
 94. Platzer, J., Engel, J., Schrott-Fischer, A., Stephan, K., Bova, S., Chen, H., Zheng, H., and Striessnig, J. 2000. Congenital deafness and sinoatrial node dysfunction in mice lacking class D L-type Ca²⁺ channels. *Cell* 102:89-97.
 95. Engel, J., Michna, M., Platzer, J., and Striessnig, J. 2002. Calcium channels in mouse hair cells: function, properties and pharmacology. *Adv Otorhinolaryngol* 59:35-41.
 96. Triggle, D.J. 2006. L-type calcium channels. *Curr Pharm Des* 12:443-457.
 97. Brandt, A., Striessnig, J., and Moser, T. 2003. CaV1.3 channels are essential for development and presynaptic activity of cochlear inner hair cells. *J Neurosci* 23:10832-10840.
 98. Uemaetomari, I., Tabuchi, K., Nakamagoe, M., Tanaka, S., Murashita, H., and Hara, A. 2009. L-type voltage-gated calcium channel is involved in the pathogenesis of acoustic injury in the cochlea. *Tohoku J Exp Med* 218:41-47.
 99. Heinrich, U.R., Maurer, J., and Mann, W. 1999. Ultrastructural evidence for protection of the outer hair cells of the inner ear during intense noise exposure by

- application of the organic calcium channel blocker diltiazem. *ORL J Otorhinolaryngol Relat Spec* 61:321-327.
100. Heinrich, U.R., Maurer, J., and Mann, W. 1997. Alteration of loosely bound calcium in the guinea pig organ of Corti after treatment with diltiazem as calcium channel blocker. *Eur Arch Otorhinolaryngol* 254:223-229.
 101. Shen, H., Zhang, B., Shin, J.H., Lei, D., Du, Y., Gao, X., Wang, Q., Ohlemiller, K.K., Piccirillo, J., and Bao, J. 2007. Prophylactic and therapeutic functions of T-type calcium blockers against noise-induced hearing loss. *Hear Res* 226:52-60.
 102. Brini, M., Pinton, P., King, M.P., Davidson, M., Schon, E.A., and Rizzuto, R. 1999. A calcium signaling defect in the pathogenesis of a mitochondrial DNA inherited oxidative phosphorylation deficiency. *Nat Med* 5:951-954.
 103. Cardenas, C., Miller, R.A., Smith, I., Bui, T., Molgo, J., Muller, M., Vais, H., Cheung, K.H., Yang, J., Parker, I., et al. 2010. Essential regulation of cell bioenergetics by constitutive InsP3 receptor Ca²⁺ transfer to mitochondria. *Cell* 142:270-283.
 104. Sousa, S.C., Maciel, E.N., Vercesi, A.E., and Castilho, R.F. 2003. Ca²⁺-induced oxidative stress in brain mitochondria treated with the respiratory chain inhibitor rotenone. *FEBS Lett* 543:179-183.
 105. Echtay, K.S., Murphy, M.P., Smith, R.A., Talbot, D.A., and Brand, M.D. 2002. Superoxide activates mitochondrial uncoupling protein 2 from the matrix side. Studies using targeted antioxidants. *J Biol Chem* 277:47129-47135.
 106. Okuda, M., Lee, H.C., Kumar, C., and Chance, B. 1992. Comparison of the effect of a mitochondrial uncoupler, 2,4-dinitrophenol and adrenaline on oxygen radical production in the isolated perfused rat liver. *Acta Physiol Scand* 145:159-168.
 107. Negre-Salvayre, A., Hirtz, C., Carrera, G., Cazenave, R., Trolly, M., Salvayre, R., Penicaud, L., and Casteilla, L. 1997. A role for uncoupling protein-2 as a regulator of mitochondrial hydrogen peroxide generation. *FASEB J* 11:809-815.
 108. Brookes, P.S., Yoon, Y., Robotham, J.L., Anders, M.W., and Sheu, S.S. 2004. Calcium, ATP, and ROS: a mitochondrial love-hate triangle. *Am J Physiol Cell Physiol* 287:C817-833.

109. Boehning, D., Patterson, R.L., Sedaghat, L., Glebova, N.O., Kurosaki, T., and Snyder, S.H. 2003. Cytochrome c binds to inositol (1,4,5) trisphosphate receptors, amplifying calcium-dependent apoptosis. *Nat Cell Biol* 5:1051-1061.
110. Miwa, S., and Brand, M.D. 2003. Mitochondrial matrix reactive oxygen species production is very sensitive to mild uncoupling. *Biochem Soc Trans* 31:1300-1301.
111. Oishi, N., Chen, F.Q., Zheng, H.W., and Sha, S.H. 2013. Intra-tympanic delivery of short interfering RNA into the adult mouse cochlea. *Hear Res* 296:36-41.
112. Chen, F.Q., Zheng, H.W., Schacht, J., and Sha, S.H. 2013. Mitochondrial peroxiredoxin 3 regulates sensory cell survival in the cochlea. *PLoS One* 8:e61999.
113. Viollet, B., Horman, S., Leclerc, J., Lantier, L., Foretz, M., Billaud, M., Giri, S., and Andreelli, F. 2010. AMPK inhibition in health and disease. *Crit Rev Biochem Mol Biol* 45:276-295.
114. Winder, W.W., and Thomson, D.M. 2007. Cellular energy sensing and signaling by AMP-activated protein kinase. *Cell Biochem Biophys* 47:332-347.
115. Hardie, D.G., Scott, J.W., Pan, D.A., and Hudson, E.R. 2003. Management of cellular energy by the AMP-activated protein kinase system. *FEBS Lett* 546:113-120.
116. Hardie, D.G. 2003. Minireview: the AMP-activated protein kinase cascade: the key sensor of cellular energy status. *Endocrinology* 144:5179-5183.
117. Hardie, D.G., Salt, I.P., Hawley, S.A., and Davies, S.P. 1999. AMP-activated protein kinase: an ultrasensitive system for monitoring cellular energy charge. *Biochem J* 338 (Pt 3):717 -722.
118. Riek, U., Scholz, R., Konarev, P., Rufer, A., Suter, M., Nazabal, A., Ringler, P., Chami, M., Muller, S.A., Neumann, D., et al. 2008. Structural properties of AMP-activated protein kinase: dimerization, molecular shape, and changes upon ligand binding. *J Biol Chem* 283:18331-18343.
119. Suter, M., Riek, U., Tuerk, R., Schlattner, U., Wallimann, T., and Neumann, D. 2006. Dissecting the role of 5'-AMP for allosteric stimulation, activation, and deactivation of AMP-activated protein kinase. *J Biol Chem* 281:32207-32216.

120. Weisova, P., Davila, D., Tuffy, L.P., Ward, M.W., Concannon, C.G., and Prehn, J.H. 2011. Role of 5'-adenosine monophosphate-activated protein kinase in cell survival and death responses in neurons. *Antioxid Redox Signal* 14:1863-1876.
121. McCullough, L.D., Zeng, Z., Li, H., Landree, L.E., McFadden, J., and Ronnett, G.V. 2005. Pharmacological inhibition of AMP-activated protein kinase provides neuroprotection in stroke. *J Biol Chem* 280:20493-20502.
122. Li, J., Zeng, Z., Viollet, B., Ronnett, G.V., and McCullough, L.D. 2007. Neuroprotective effects of adenosine monophosphate-activated protein kinase inhibition and gene deletion in stroke. *Stroke* 38:2992-2999.
123. Kefas, B.A., Cai, Y., Kerckhofs, K., Ling, Z., Martens, G., Heimberg, H., Pipeleers, D., and Van de Casteele, M. 2004. Metformin-induced stimulation of AMP-activated protein kinase in beta-cells impairs their glucose responsiveness and can lead to apoptosis. *Biochem Pharmacol* 68:409-416.
124. Yun, H., Lee, M., Kim, S.S., and Ha, J. 2005. Glucose deprivation increases mRNA stability of vascular endothelial growth factor through activation of AMP-activated protein kinase in DU145 prostate carcinoma. *J Biol Chem* 280:9963-9972.
125. Schulz, E., Dopheide, J., Schuhmacher, S., Thomas, S.R., Chen, K., Daiber, A., Wenzel, P., Munzel, T., and Keaney, J.F., Jr. 2008. Suppression of the JNK pathway by induction of a metabolic stress response prevents vascular injury and dysfunction. *Circulation* 118:1347-1357.
126. Yun, H., Kim, H.S., Lee, S., Kang, I., Kim, S.S., Choe, W., and Ha, J. 2009. AMP kinase signaling determines whether c-Jun N-terminal kinase promotes survival or apoptosis during glucose deprivation. *Carcinogenesis* 30:529-537.
127. Zhou, G., Myers, R., Li, Y., Chen, Y., Shen, X., Fenyk-Melody, J., Wu, M., Ventre, J., Doebber, T., Fujii, N., et al. 2001. Role of AMP-activated protein kinase in mechanism of metformin action. *J Clin Invest* 108:1167-1174.
128. Foller, M., Jaumann, M., Dettling, J., Saxena, A., Pakladok, T., Munoz, C., Ruth, P., Sopjani, M., Seebohm, G., Ruttiger, L., et al. 2012. AMP-activated protein kinase in BK-channel regulation and protection against hearing loss following acoustic overstimulation. *FASEB J* 26:4243-4253.

129. Raimundo, N., Song, L., Shutt, T.E., McKay, S.E., Cotney, J., Guan, M.X., Gilliland, T.C., Hohuan, D., Santos-Sacchi, J., and Shadel, G.S. 2012. Mitochondrial stress engages E2F1 apoptotic signaling to cause deafness. *Cell* 148:716-726.
130. Liberman, L.D., and Liberman, M.C. 2015. Dynamics of cochlear synaptopathy after acoustic overexposure. *J Assoc Res Otolaryngol* 16:205-219.
131. Shen, Q.W., Gerrard, D.E., and Du, M. 2008. Compound C, an inhibitor of AMP-activated protein kinase, inhibits glycolysis in mouse longissimus dorsi postmortem. *Meat Sci* 78:323-330.
132. Muller, M., von Hunerbein, K., Hoidis, S., and Smolders, J.W. 2005. A physiological place-frequency map of the cochlea in the CBA/J mouse. *Hear Res* 202:63-73.
133. Chen, G.D., and Fechter, L.D. 2003. The relationship between noise-induced hearing loss and hair cell loss in rats. *Hear Res* 177:81-90.
134. Ohlemiller, K.K., Wright, J.S., and Heidbreder, A.F. 2000. Vulnerability to noise-induced hearing loss in 'middle-aged' and young adult mice: a dose-response approach in CBA, C57BL, and BALB inbred strains. *Hear Res* 149:239-247.
135. Schulte, B.A., and Adams, J.C. 1989. Distribution of immunoreactive Na⁺,K⁺-ATPase in gerbil cochlea. *J Histochem Cytochem* 37:127-134.
136. Crawley, B.K., and Keithley, E.M. 2011. Effects of mitochondrial mutations on hearing and cochlear pathology with age. *Hear Res* 280:201-208.
137. Morizane, I., Hakuba, N., Shimizu, Y., Shinomori, Y., Fujita, K., Yoshida, T., Shudou, M., and Gyo, K. 2005. Transient cochlear ischemia and its effects on the stria vascularis. *Neuroreport* 16:799-802.
138. Furukawa, H., and Gouaux, E. 2003. Mechanisms of activation, inhibition and specificity: crystal structures of the NMDA receptor NR1 ligand-binding core. *EMBO J* 22:2873-2885.
139. Shaw, R.J., Kosmatka, M., Bardeesy, N., Hurley, R.L., Witters, L.A., DePinho, R.A., and Cantley, L.C. 2004. The tumor suppressor LKB1 kinase directly activates AMP-activated kinase and regulates apoptosis in response to energy stress. *Proc Natl Acad Sci U S A* 101:3329-3335.

140. Zeqiraj, E., Filippi, B.M., Deak, M., Alessi, D.R., and van Aalten, D.M. 2009. Structure of the LKB1-STRAD-MO25 complex reveals an allosteric mechanism of kinase activation. *Science* 326:1707-1711.
141. Boudeau, J., Baas, A.F., Deak, M., Morrice, N.A., Kieloch, A., Schutkowski, M., Prescott, A.R., Clevers, H.C., and Alessi, D.R. 2003. MO25alpha/beta interact with STRADalpha/beta enhancing their ability to bind, activate and localize LKB1 in the cytoplasm. *EMBO J* 22:5102-5114.
142. Xie, Z., Dong, Y., Zhang, M., Cui, M.Z., Cohen, R.A., Riek, U., Neumann, D., Schlattner, U., and Zou, M.H. 2006. Activation of protein kinase C zeta by peroxynitrite regulates LKB1-dependent AMP-activated protein kinase in cultured endothelial cells. *J Biol Chem* 281:6366-6375.
143. Song, P., Xie, Z., Wu, Y., Xu, J., Dong, Y., and Zou, M.H. 2008. Protein kinase Czeta-dependent LKB1 serine 428 phosphorylation increases LKB1 nucleus export and apoptosis in endothelial cells. *J Biol Chem* 283:12446-12455.
144. Lizcano, J.M., Goransson, O., Toth, R., Deak, M., Morrice, N.A., Boudeau, J., Hawley, S.A., Udd, L., Makela, T.P., Hardie, D.G., et al. 2004. LKB1 is a master kinase that activates 13 kinases of the AMPK subfamily, including MARK/PAR-1. *EMBO J* 23:833-843.
145. Tiede, L., Steyger, P.S., Nichols, M.G., and Hallworth, R. 2009. Metabolic imaging of the organ of corti--a window on cochlea bioenergetics. *Brain Res* 1277:37-41.
146. Jensen-Smith, H.C., Hallworth, R., and Nichols, M.G. 2012. Gentamicin rapidly inhibits mitochondrial metabolism in high-frequency cochlear outer hair cells. *PLoS One* 7:e38471.
147. May, L.A., Kramarenko, II, Brandon, C.S., Voelkel-Johnson, C., Roy, S., Truong, K., Francis, S.P., Monzack, E.L., Lee, F.S., and Cunningham, L.L. 2013. Inner ear supporting cells protect hair cells by secreting HSP70. *J Clin Invest* 123:3577-3587.
148. Jansen, M., Ten Klooster, J.P., Offerhaus, G.J., and Clevers, H. 2009. LKB1 and AMPK family signaling: the intimate link between cell polarity and energy metabolism. *Physiol Rev* 89:777-798.

149. Dorfman, J., and Macara, I.G. 2008. STRADalpha regulates LKB1 localization by blocking access to importin-alpha, and by association with Crm1 and exportin-7. *Mol Biol Cell* 19:1614-1626.
150. Xie, Z., Dong, Y., Zhang, J., Scholz, R., Neumann, D., and Zou, M.H. 2009. Identification of the serine 307 of LKB1 as a novel phosphorylation site essential for its nucleocytoplasmic transport and endothelial cell angiogenesis. *Mol Cell Biol* 29:3582-3596.
151. Zhu, H., Moriasi, C.M., Zhang, M., Zhao, Y., and Zou, M.H. 2013. Phosphorylation of serine 399 in LKB1 protein short form by protein kinase Czeta is required for its nucleocytoplasmic transport and consequent AMP-activated protein kinase (AMPK) activation. *J Biol Chem* 288:16495-16505.
152. Means, A.R. 2000. Regulatory cascades involving calmodulin-dependent protein kinases. *Mol Endocrinol* 14:4-13.
153. Skelding, K.A., and Rostas, J.A. 2012. The role of molecular regulation and targeting in regulating calcium/calmodulin stimulated protein kinases. *Adv Exp Med Biol* 740:703-730.
154. Selbert, M.A., Anderson, K.A., Huang, Q.H., Goldstein, E.G., Means, A.R., and Edelman, A.M. 1995. Phosphorylation and activation of Ca(2+) -calmodulin-dependent protein kinase IV by Ca(2+) -calmodulin-dependent protein kinase la kinase. Phosphorylation of threonine 196 is essential for activation. *J Biol Chem* 270:17616-17621.
155. Hurley, R.L., Anderson, K.A., Franzone, J.M., Kemp, B.E., Means, A.R., and Witters, L.A. 2005. The Ca²⁺/calmodulin-dependent protein kinase kinases are AMP-activated protein kinase kinases. *J Biol Chem* 280:29060-29066.
156. Wyllie, A.H. 1980. Glucocorticoid-induced thymocyte apoptosis is associated with endogenous endonuclease activation. *Nature* 284:555-556.
157. Kim, M.J., Jo, D.G., Hong, G.S., Kim, B.J., Lai, M., Cho, D.H., Kim, K.W., Bandyopadhyay, A., Hong, Y.M., Kim, D.H., et al. 2002. Calpain-dependent cleavage of cain/cabin1 activates calcineurin to mediate calcium-triggered cell death. *Proc Natl Acad Sci U S A* 99:9870-9875.
158. Choi, W.S., Lee, E.H., Chung, C.W., Jung, Y.K., Jin, B.K., Kim, S.U., Oh, T.H., Saido, T.C., and Oh, Y.J. 2001. Cleavage of Bax is mediated by caspase-

- dependent or -independent calpain activation in dopaminergic neuronal cells: protective role of Bcl-2. *J Neurochem* 77:1531-1541.
159. Wang, H.G., Pathan, N., Ethell, I.M., Krajewski, S., Yamaguchi, Y., Shibasaki, F., McKeon, F., Bobo, T., Franke, T.F., and Reed, J.C. 1999. Ca²⁺-induced apoptosis through calcineurin dephosphorylation of BAD. *Science* 284:339-343.
160. Olofsson, M.H., Havelka, A.M., Brnjic, S., Shoshan, M.C., and Linder, S. 2008. Charting calcium-regulated apoptosis pathways using chemical biology: role of calmodulin kinase II. *BMC Chem Biol* 8:2.
161. Singh, B.N. 1986. The mechanism of action of calcium antagonists relative to their clinical applications. *Br J Clin Pharmacol* 21 Suppl 2:109S-121S.
162. 2009. Calan (Verapamil hydrochloride) tablets. F.a.D. Administration, editor.
163. Uchida, S., Yamada, S., Nagai, K., Deguchi, Y., and Kimura, R. 1997. Brain pharmacokinetics and in vivo receptor binding of 1,4-dihydropyridine calcium channel antagonists. *Life Sci* 61:2083-2090.
164. Ritz, B., Rhodes, S.L., Qian, L., Schernhammer, E., Olsen, J.H., and Friis, S. 2010. L-type calcium channel blockers and Parkinson disease in Denmark. *Ann Neurol* 67:600-606.
165. Matsumura, C.Y., Pertille, A., Albuquerque, T.C., Santo Neto, H., and Marques, M.J. 2009. Diltiazem and verapamil protect dystrophin-deficient muscle fibers of MDX mice from degeneration: a potential role in calcium buffering and sarcolemmal stability. *Muscle Nerve* 39:167-176.
166. Freir, D.B., Costello, D.A., and Herron, C.E. 2003. A beta 25-35-induced depression of long-term potentiation in area CA1 in vivo and in vitro is attenuated by verapamil. *J Neurophysiol* 89:3061-3069.
167. Liang, J.H., Li, J.X., Wang, X.H., Chen, B., Lu, Y., Zhang, P., Han, R., and Ye, X.F. 2004. L-type calcium channel blockers enhance 5-HTP-induced antinociception in mice. *Acta Pharmacol Sin* 25:644-650.
168. Esterberg, R., Hailey, D.W., Rubel, E.W., and Raible, D.W. 2014. ER-mitochondrial calcium flow underlies vulnerability of mechanosensory hair cells to damage. *J Neurosci* 34:9703-9719.

169. Hackney, C.M., Mahendrasingam, S., Penn, A., and Fettiplace, R. 2005. The concentrations of calcium buffering proteins in mammalian cochlear hair cells. *J Neurosci* 25:7867-7875.
170. Spicer, S.S., Thomopoulos, G.N., and Schulte, B.A. 1999. Novel membranous structures in apical and basal compartments of inner hair cells. *J Comp Neurol* 409:424-437.
171. Dumont, R.A., Lins, U., Filoteo, A.G., Penniston, J.T., Kachar, B., and Gillespie, P.G. 2001. Plasma membrane Ca²⁺-ATPase isoform 2a is the PMCA of hair bundles. *J Neurosci* 21:5066-5078.
172. Ohlemiller, K.K. 2006. Contributions of mouse models to understanding of age- and noise-related hearing loss. *Brain Res* 1091:89-102.
173. Hawley, S.A., Pan, D.A., Mustard, K.J., Ross, L., Bain, J., Edelman, A.M., Frenguelli, B.G., and Hardie, D.G. 2005. Calmodulin-dependent protein kinase kinase-beta is an alternative upstream kinase for AMP-activated protein kinase. *Cell Metab* 2:9-19.
174. Brandt, A., Khimich, D., and Moser, T. 2005. Few CaV1.3 channels regulate the exocytosis of a synaptic vesicle at the hair cell ribbon synapse. *J Neurosci* 25:11577-11585.
175. Matsunobu, T., Ogita, K., and Schacht, J. 2004. Modulation of activator protein 1/DNA binding activity by acoustic overstimulation in the guinea-pig cochlea. *Neuroscience* 123:1037-1043.
176. Xia, J.H., Liu, C.Y., Tang, B.S., Pan, Q., Huang, L., Dai, H.P., Zhang, B.R., Xie, W., Hu, D.X., Zheng, D., et al. 1998. Mutations in the gene encoding gap junction protein beta-3 associated with autosomal dominant hearing impairment. *Nat Genet* 20:370-373.
177. Denoyelle, F., Lina-Granade, G., Plauchu, H., Bruzzone, R., Chaib, H., Levi-Acobas, F., Weil, D., and Petit, C. 1998. Connexin 26 gene linked to a dominant deafness. *Nature* 393:319-320.
178. Anselmi, F., Hernandez, V.H., Crispino, G., Seydel, A., Ortolano, S., Roper, S.D., Kessar, N., Richardson, W., Rickheit, G., Filippov, M.A., et al. 2008. ATP release through connexin hemichannels and gap junction transfer of second

messengers propagate Ca²⁺ signals across the inner ear. *Proc Natl Acad Sci U S A* 105:18770-18775.

179. Zhang, Y., Tang, W., Ahmad, S., Sipp, J.A., Chen, P., and Lin, X. 2005. Gap junction-mediated intercellular biochemical coupling in cochlear supporting cells is required for normal cochlear functions. *Proc Natl Acad Sci U S A* 102:15201-15206.